Provenance of siliclastic sedimentary rocks in the eastern portion of the North Caribou Greenstone Belt

A Thesis Submitted in Partial Fulfillment of the Requirements

for the degree of

Masters of Science

in Earth Sciences

University of Ottawa, Canada

By

Acknowledgements

First and foremost, I would like to thank Goldcorp Inc. for its contribution to the extensive research of the North Caribou greenstone belt in and around the Musselwhite Mine. Furthermore, I would like to thank John Biczok for leading and inspiring field teams. Without his enthusiasm and interest, much of this research and funding would not have taken place. I would also like to thank NSERC for funding through Collaborative Research Development program to Keiko Hattori and the MITACS-Accelerate internship program to the author for their support of this project and many others.

Next, I would like to thank for supervisor Dr. Keiko Hattori. She is an inspiration to all female scientists and helped me reach my potential by inspiring me to work hard and see beyond the scope of what has been done before. I would also like to thank all the other staff at the University of Ottawa and beyond including Dave Schneider, Glen Milne, and George Mrazek, and Chris McFarlane at UNB for their patience and who helped guide me through many stages of my data collection. I am also very grateful to the support staff at the University of Ottawa including Helene De Gouffe, Caroline Bisson and Lisa-Robin Murphy for all they have done for the department and me.

Many students had come before me and contributed to the research and understanding of the geological history of the North Caribou greenstone belt. I would like to acknowledge them for their hard work and contribution to this thesis, my interpretations, and understanding of the complicated history of the region. Thank you, Jason Duff, Amanda Van Lankvelt, Tash Kalbfleisch and Emilie Gagnon.

A special shout-out to all my friends and office mates at the University of Ottawa. Especially Erin Adlakha, David Diekrup, Adam Sookdeo, and Mary Devine whom I wouldn't have survived my first year as a grad student without. Thank you for all the late night chats, encouragement and advice. Marion 225 is missed.

Last but not least I would like to thank my husband, Chris Bell. Without his guidance, support, inspiration, and love I am sure this thesis would never have been completed. I am very lucky to have such a smart, beautiful person in my life.

List of Contents

List of Figures

List of Tables

Abstract

The Zeemal Heaton Lake metasedimentary assemblage comprises ~50% of the eastern limb of the North Caribou greenstone belt, which hosts the Musselwhite gold deposit (~ 5.4 Moz Au). The metasedimentary assemblage is divided into two based on their distribution: the Central-belt and North-rim of the belt. The Zeemal Heaton Lake metasedimentary rocks have been interpreted to represent a turbidite succession, consisting of pelite, arkose, wacke and conglomerate. Detrital U-Pb zircon age populations from this study indicate variable sources in the Central-belt metasediments with a maximum age of deposition of 2798.8 ± 29 Ma, while metasediments along the North portion of the limb display a maximum age of deposition of 2696 ± 39 Ma. This indicates the likelihood of two discrete basins with the Zeemal Heaton Lake assemblage.

Neodymium isotopic values for the sedimentary rocks along the North-rim of the belt display εNd^{2680Ma} ranging from -1.2 to -0.9. An overlapping but slightly more evolved signature shown in the Central portion with values of εNd^{2800Ma} -1.6 to 0.1. This indicates detritus for the Central-belt was likely sourced from the older (~2850 Ma), (tonalite-granodiorite) surrounding intrusions. The North-rim sediments were sourced (in part) from the younger (~2700 Ma) granitic intrusions and rhyolites. The surrounding batholiths display εNd^{t} overlapping with North-rim sedimentary rocks, however, indicate significant contribution beyond these immediate surrounding batholiths, which may include older mafic (2982 ± 0.8, 2870 ±2 Ma), younger rhyolitic unit (2723 ± 2 Ma) or more distal sources than the intrusions immediately adjacent to the belt.

Peak metamorphic mineral assemblages indicate a minimum of amphibolite facies-garnet zone or greater across the Central-belt portion of the greenstone belt. The North-rim metasediments display evidence for aureole metamorphism which may overprint earlier regional metamorphism. Nitrogen abundance and $\delta^{15}N$ values of biotite of the Zeemal Heaton Lake metasedimentary assemblage indicate variable values than those associated with mineralization at the Musselwhite Mine, which is reported by Isaacs (2008). Mineralizing fluids from the Musselwhite mine have been interpreted by Issacs (2008) to be related to both metamorphic and magmatic fluids. Fluids associated with the Eyapamikama and/or Zeemal Heaton Lake metasediments appear to be metamorphic with minor magmatic influence near regional shear zones, but not directly related to the auriferous fluids which formed the Musselwhite mine.

Sedimentation of the Zeemal Heaton Lake metasedimentary rocks in the eastern limb of the North Caribou greenstone belt is interpreted to have begun during 2720 to 2710 Ma and continue until 2680 Ma. Unconformable Timiskaming-type syn-tectonic sedimentation occurred during rapid erosion of Tonalite-Trondhjemite-Granodiorite intrusions, a younger rhyolitic unit and mafic volcanic rocks into the basin. Detrital zircon age populations of 2700 to 2730 ±8 Ma, 2828 ± 9 to 2886 ± 8 and 2928 ± 12 to 3132 ± 7 Ma indicate erosion of variable igneous sources surrounding sedimentary lithologies which all appear to have undergone a minimum of D_2 regional deformation.

Introduction

The North Caribou greenstone belt is located in the middle of the North Caribou superterrane of the Western Superior Province as defined by Percival et al. 2006a (**Figure 1**). This is one of five superterranes located in the Western Superior Province and is considered to be the core to which all other terranes accreted (Percival et al., 2006a). The North Caribou superterrane preserves evidence for an assembly event before 2870 Ma (Percival et al. 2006a) and has distinct isotopic and seismic characteristics that distinguish it from adjacent regions (Percival et al., 2006a). The North Caribou greenstone belt has been of geological interest for several decades since the discovery of the banded-iron formation hosted orogenic gold deposit which has subsequently become the Musselwhite mine. It includes the metasedimentary Eyapamikama and the Zeemal Heaton metasedimentary assemblages that lie respectively west and east of Opapimiskan Lake. The Zeemal Heaton Lake metasedimentary rocks comprise ~50 % on the surface of the supracrustal rocks in the eastern limb of the North Caribou greenstone belt (Breaks et al. 2001) and are the focus of this study. Clearly, to fully understand the complex tectonic history of the belt, a detailed investigation of these sedimentary basins was needed.

Duff (2014) discovered detrital zircon grains within the Zeemal Heaton Lake metasedimentary assemblage within the North Caribou greenstone belt, which are ~150 Ma younger than previously dated supracrustal units in the belt. These young sediments are of interest as they are similar in age to Timiskaming-type sediments which occur throughout the Abitibi and are associated with large orogenic gold deposits. This study will further delineate the occurrence of these relatively young sediments.

Objectives

This research sets out to evaluate the timing of deposition, provenance, metamorphic, and hydrothermal history of the young metasediments of the Zeemal Heaton Lake assemblage, and to confirm if they are in fact Timiskaming-type sediments. As well, contribute to the understanding of the complex tectonic history of the North Caribou greenstone belt. The sedimentary rocks in the eastern portion of the belt had seen little work until Duff (2014) discovered ~2698 Ma detrital zircons. Similarly, young sedimentary rocks called 'Timiskaming-type' rocks are known to be spatially associated with significant gold deposits elsewhere in the Archean Superior Province (Dubé and Gosselin, 2007; Bleeker, 2012; Bigot and Jebrak, 2015).

The provenance, depositional history, age, metamorphism, and hydrothermal alteration of these understudied Timiskaming-age sedimentary rocks in the North Caribou belt was determined using whole rock geochemistry, Nd isotope analysis, U-Pb zircon dating and trace element analysis and nitrogen isotope compositions of micas. The data are presented in this thesis.

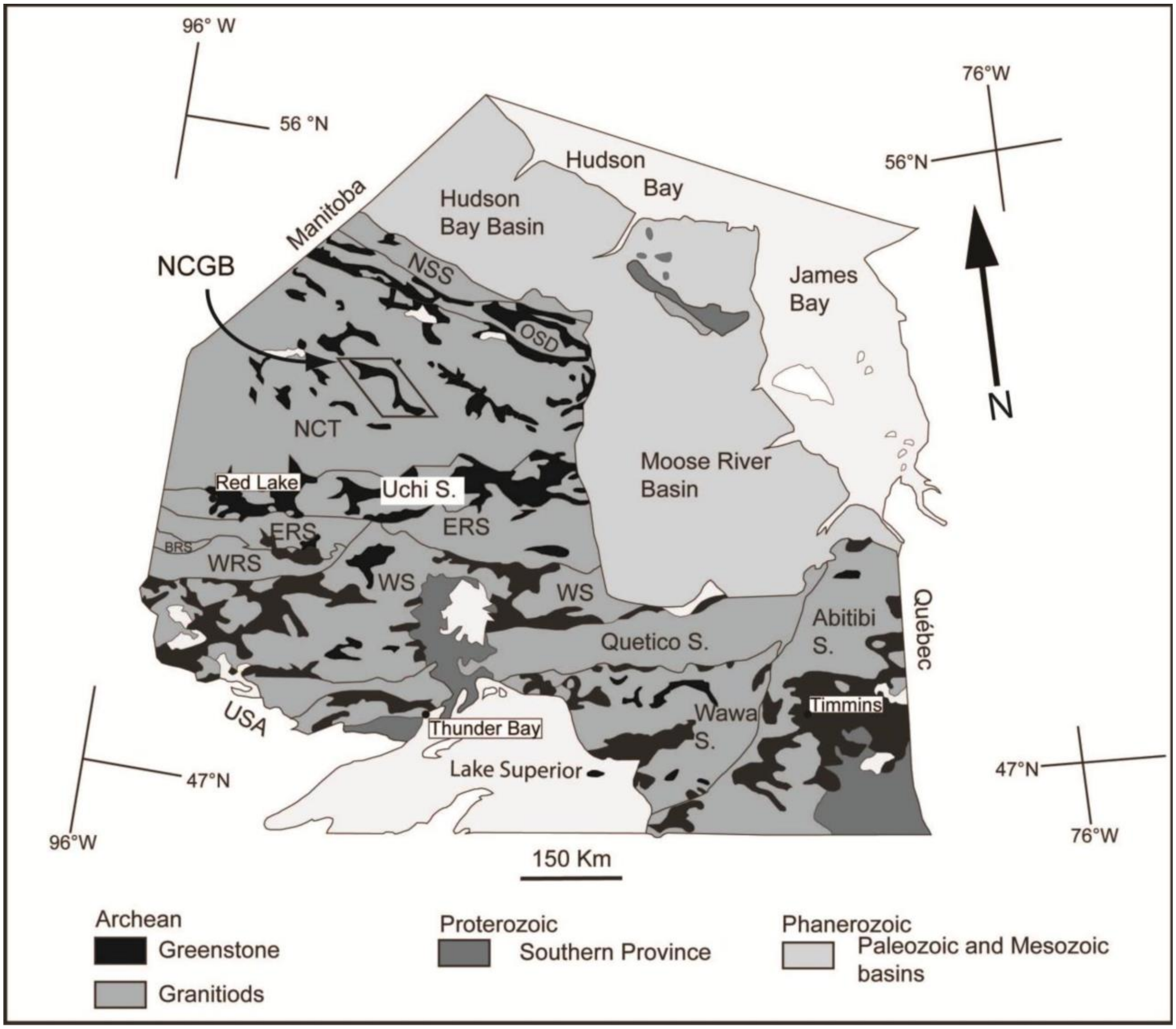

Figure 1: Simplified geologic map of the Western Superior Province (WSP). Outline with NCGB represents the location of Figure 2. Maps after Thurston et al. (1991), Stott et al. (2010), and Wyman et al. (2011) modified from Duff (2014). Other WSP subprovinces: BRS; Bird River Province, ERS; English River subprovince, NCGB: North Caribou greenstone belt, NSS: North Superior subprovince, OSD: Oxford-Stull domain, S: subprovince and WRS: Winnipeg River subprovince, WS; Wawa subprovince.

Previous Work

Geochronology

U-Pb zircon geochronological studies were first conducted by Donaldson and de Kemp (1998), in the western portion of the belt which included the Keeyask Lake (<2978 ± 3 Ma) and Agutua Arm assemblages (2981 ± 1.8 Ma) and the Weagamow batholith (2990 ± 1.8 Ma). Younger ages were also obtained by Donaldson and de Kemp (1987) and included the North Caribou batholith (2869 ± 3.6 Ma) and the Schade Lake Gneiss Complex (2856 ± 1.8 Ma). Later geochronological work by Davis and Stott (2001) documented high precision U-Pb zircon ages in and around the Musselwhite mine. They published ages for the North (2870 ± 2 Ma) and South Rim volcanic rocks (2981.9 ± 0.8 Ma), as well for the Eypamikama metasedimentary assemblage (< 2870 Ma). Biczok et al. (2012) report several ages for lithological unit within the Musselwhite mine and plutons around the mine. Deposition of the Au-bearing banded iron-formation has been bracketed by footwall (2982 ± 0.8 Ma) and hanging wall (2972 ± 1.6 Ma) felsic tuffs by Biczok et al. (2012).

Van Lankvelt (2013) completed a comprehensive geochronology study on intrusions including the internal and surrounding batholiths. These results show three main episodes of magmatism in the belt; a Mesoarchean (3100-2900 Ma) event, a large-scale magmatism from 2880-2830 Ma and hydrothermal event from 2760-2680 Ma (Van Lankvelt, 2013). She concluded that the latest stage of zircon overgrowth was hydrothermal because they display elevated LREE (Van Lankvelt, 2013).

Duff et al. (2012) presented U-Pb zircon ages of two samples from the Zeemal Heaton Lake assemblage. These zircon grains yielded ages ranging from 2674 ± 29 Ma to 3132 ± 36 Ma that differ from the ages younger than 2856 Ma returned for the same rock unit by Davis and Stott (2001). The Davis and Stott (2011) sample location was located in the Central-belt area of this study. Duff et al. (2012) also dated sediments within the North-rim of the Zeemal Heaton Lake assemblage. Duff et al. (2012) interpreted these sedimentary rocks to be "Timiskaming-type” and that the main provenances of Eyapamikama and Zeemal Heaton Lake assemblage basins were distinct and the depositional basin for the latter younger sandstones developed at ~2680-2700 Ma.

Nd Isotopes

Nd isotope work was conducted Duff (2014) to further delineate the source of the sedimentary rocks in the Zeemal Heaton Lake metasedimentary rocks and the Eyapamikama assemblage. Duff et al. (2012) were able to divide rocks in the eastern portion of the belt based on those with $\varepsilon Nd > 0$ and $\varepsilon Nd < 0$. North-rim sediments were calculated at 2700 Ma, while all other samples were calculated at 2850 Ma. Wyman et al. (2011) completed Nd isotope work on the surrounding batholiths and some volcanic rocks. Their results of batholiths and volcanic rocks show εNd(2850 Ma) values, between -6.8 and 0.2, which are similar to sedimentary rocks documented by Duff et al., (2012).

Nitrogen Isotopes

Nitrogen isotope compositions of biotite were determined from mineralized mine units within the Musselwhite mine, as well as on several regional (~20km east) mafic volcanic rocks, and one regional sedimentary rock sample (Issacs, 2008; Hollings et al., 2011). Issacs (2008) determined the nitrogen isotope values from biotite within the mine overlap with those found for granites (Jia and Kerrich, 2000), basalt (Marty and Zimmerman, 1999; Nishizawa et al., 2007) and sedimentary and metasedimentary rocks (Jia, 2006). The study inferred that a multiple source (metamorphic and magmatic) fluid phase mineralization had occurred in the Musselwhite mine.

Metamorphism

Most recently, extensive work by Kalbfleisch (2012) and Gagnon (2015) was conducted on deformation and metamorphism across the belt. Peak metamorphic conditions are recognized as amphibolite facies. Multiple events of regional metamorphism are coeval with widespread magmatism and correlated with accretion events in the Superior Province. Their interpretations suggest that following the cessation of magmatism, Abukuma-type (low P, intermediate T) regional metamorphism occurred plus a hydrothermal alteration pulse associated with an orogeny at 2750 to 2710 Ma.

Field Work

During the summer of 2013 and 2014, 46 samples (**Figure 2**) were collected across the eastern portion of the North Caribou greenstone belt. Many of the sample locations were collected with a helicopter because of the sites due to the lack of roads and rivers. Many of them are unknown previously due to heavy vegetation in the area, which was destroyed by a forest fire in 2012.

In 2013, 35 samples were collected between June 7^{th} and August 5^{th}. Metasedimentary outcrops were chosen based on previous mapping completed by the Ontario Geological Survey in 2001 that outlined outcrops with bedding measurements. Google Earth images were also used to identify possible outcrops. Outcrops were then accessed by helicopter for sampling. All rock types were sampled if discovered in the field.

In 2014, an additional 11 samples were collected between August 20^{th} and 27^{th}. These samples sites were chosen based on gaps in the previous sampling and outcrop findings by soil sampling teams and senior geologist, John Biczok at Goldcorp during the earlier exploration season of 2014. Sites were again accessed by helicopter.

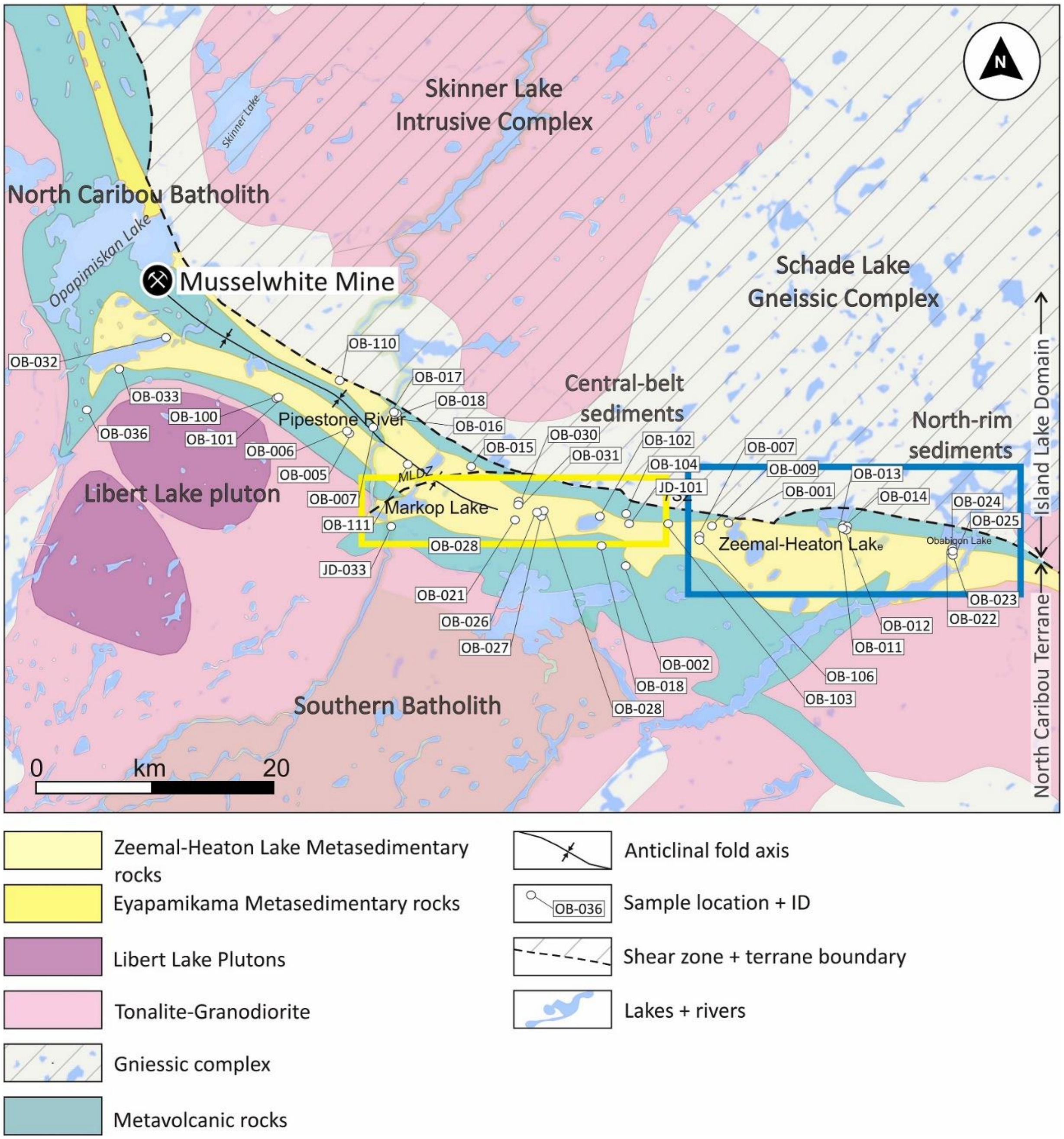

Figure 2: Simplified geologic map of the eastern portion of the North Caribou greenstone belt and Island Lake Domain. Modified after Ontario Geological Survey (2011). Samples (OB) collected by the author during 2013 and 2014. Samples with the prefix of JD were collected by Duff (2014) in 2010 and 2011. MLDZ: Markop Lake deformation zone. TSZ: Totogan shear zone.

Contributions from the author

This thesis provides new whole rock and mineral chemistry, U-Pb detrital zircon and trace element compositions, whole rock Nd isotope composition, nitrogen isotope composition of micas, and metamorphism from across the eastern portion of the belt. All samples were prepared by the author at the University of Ottawa and Carleton University. Multi-element analyses of the rocks were carried out at the Activation Laboratories in Ancaster, Ontario and ACME Labs in Vancouver, BC.

In the summer of 2010 and 2011, Jason Duff sampled mafic volcanic and metasedimentary rock from throughout the Northwestern and southeastern portions of the North Caribou greenstone belt. Duff (2014) completed U-Pb dating on two samples from the Zeemal Heaton Lake metasedimentary rocks which returned the relatively young "Timiskaming-type" ages. These zircons were further examined in this study for trace element compositions to evaluate possible provenance and possible metamorphic influences and fluid interaction. Petrographic observations, EMPA garnet analysis, and nitrogen isotope analysis of biotite using several of Duff's sedimentary samples were also utilized to increase the sample size for this study.

Regional Geology

Western Superior Province

The Superior Province, the largest Archean craton in the world, forms the core of the Canadian Shield and has been stable since ~2600 Ma (**Figure 1**). The Superior Province extends from Northwestern Quebec along the east side of Hudson Bay south through Ontario to the North shores of Lake Huron and Lake Superior. It also extends across western Ontario south of Hudson Bay and underlies most of southeastern Manitoba (Card et al., 1986). It consists primarily of gneissic Tonalite-Trondhjemite-Granodiorite (TTG), and volcanic-metasedimentary domains, striking east-west. These greenstone belts enveloping granitoid bodies are typical of classic granite–greenstone in many Archean terrains worldwide.

The subprovince nomenclature has been revised over time. Most recently, based on isotopic, zircon inheritance studies and aeromagnetic surveys to define superterranes and terranes within the Superior Province (Percival et al., 2006a, Stott et al., 2010). Superterranes preserve evidence of amalgamation events before assembly into their current configuration, as does the Superior Province at 2700 Ma.

The final amalgamation of the Western Superior Province was suggested as consisting of five discrete accretionary events which occurred during the Neoarchean until ~2680 Ma (Percival et al., 2006a). The included terranes are defined by Percival et al. (2006a) as having a tectonostratigraphic history independent of neighboring regions before amalgamation. The North Caribou superterrane is the largest of these Mesoarchean terranes within the Superior Province.

North Caribou Greenstone Belt

Geochronological Overview

The North Caribou greenstone belt is comprised of nine supracrustal units (**Table 1**). The Aguta Arm metavolcanic-rich assemblage occupies most of the Northwestern extremity of the North Caribou greenstone belt and lies in contact with the North Caribou Lake batholith and Weagamow and Round Lake batholiths (Breaks et al., 2001). A U-Pb zircon age by Donaldson and deKemp (1998) dates a lapilli tuff of this assemblage at 2980 ± 2 Ma. These rocks plausibly acted as a basement for succeeding supracrustal accumulations in the belt (Breaks et al. 2001). The Keeyask assemblage predominantly consists of east facing quartz arenite, mudstone and banded iron formation with minor quartz wacke, plagioclase-bearing arkosic arenite, and chert, while the Keeyask Lake metavolcanic unit consists of ultramafic to mafic rocks. The Keeyask assemblage unconformably overlies the Aguta Arm assemblage, and together these units are interpreted as a stable shelf platform volcano-sedimentary edifice (Breaks et al. 2001). The komatiitic rocks of the Keeyask Lake metavolcanic unit overly the Keeyask assemblage and to the southeast of the belt mark a change in greenstone development from a stable shelf to rift phase (Breaks et al. 2001). U-Pb zircon dating by deKemp (1987) of quartz arenite in the western arm of the North Caribou greenstone belt produced ages of 2990 Ma, indicating an older sedimentary assemblage.

The North Rim and South Rim volcanic rocks plus the Opapimiskan Lake and Forester Lake metavolcanic rocks were grouped as components of the McGruer Assemblage by Thurston et al. (1991) but were treated as separate units by Breaks et al. (2001). The North Rim volcanic rocks, which are dominated by mafic, mainly tholeiitic massive and pillowed flows, form the North to the eastern edge of the North Caribou Lake batholith and stretch for ~100 km from Atikomik Lake in the west to Opapimiskan Lake in the south Central (Breaks et al. 2001). Rocks of the North Caribou belt were intensely deformed at medium to high amphibolite facies producing metamorphic minerals such as biotite, garnet, and staurolite. The South Rim volcanic rocks are comprised of mafic to felsic rocks and can be traced for ~95 km from Wapikiskapia Lake to the Paseminon River, along the southern to the western edge of the North Caribou Lake batholith

(Breaks at el., 2001). The Mg-Fe tholeiites of the South Rim volcanic rocks characterized by a flat REE pattern (Duff, 2014), are interpreted by Hollings and Kerrich (1999) to be uncontaminated by crustal rocks and similar in chemical composition mid-ocean ridge basalts (MORB). Felsic volcanic rocks of the assemblage have geochemical characteristics of supra-subduction zone rocks and have been interpreted by Hollings et al. (1999) to represent the product of a plume-arc interaction. Little has been published on the geochemistry of the North Rim volcanics, however U-Pb zircon dates of 2981.9 Ma.

Table 1: U-Pb zircon dates of all units within the North Caribou greenstone belt

Unit	Major lithologies (dated unit)	Age (Ma)	Reference
Aguta Arm assemblage	tholeiitic basalt, lapilli tuff (dated)	2980	Donaldson & de Kemp, 1998
Keeyask Lake metavolcanic rocks	komatiite, basalt	2990	Donaldson & de Kemp, 1998
Keeyask Lake metasedimentary rocks	quartz arenite (dated) mudstone, banded iron formation.	<2978	Donaldson & de Kemp, 1998
Opapimiskan Lake metavolcanic rocks	komatiite, basalt, felsic tuff (dated), banded iron formation	2982-2972	Biczok et al., 2012
South Rim metavolcanic rocks	tholeiitic basalt to rhyolite (dated)	2980	Davis & Stott, 2001
North Rim metavolcanic	tholeiitic basalt to rhyolite (dated)	2870	Davis & Stott, 2001
Forester Lake metavolcanis	komatiite, basalt, rhyolite tuff (dated), banded iron formation	2982-2972	Davis & Stott, 2001
Eyapamikama Lake metasedimentary rocks	clastic metasedimentary rocks	<2856	Davis & Stott, 2001
Zeemal Heaton Lake metasedimentary rocks	clastic metasedimentary rocks	2674	Duff, 2014

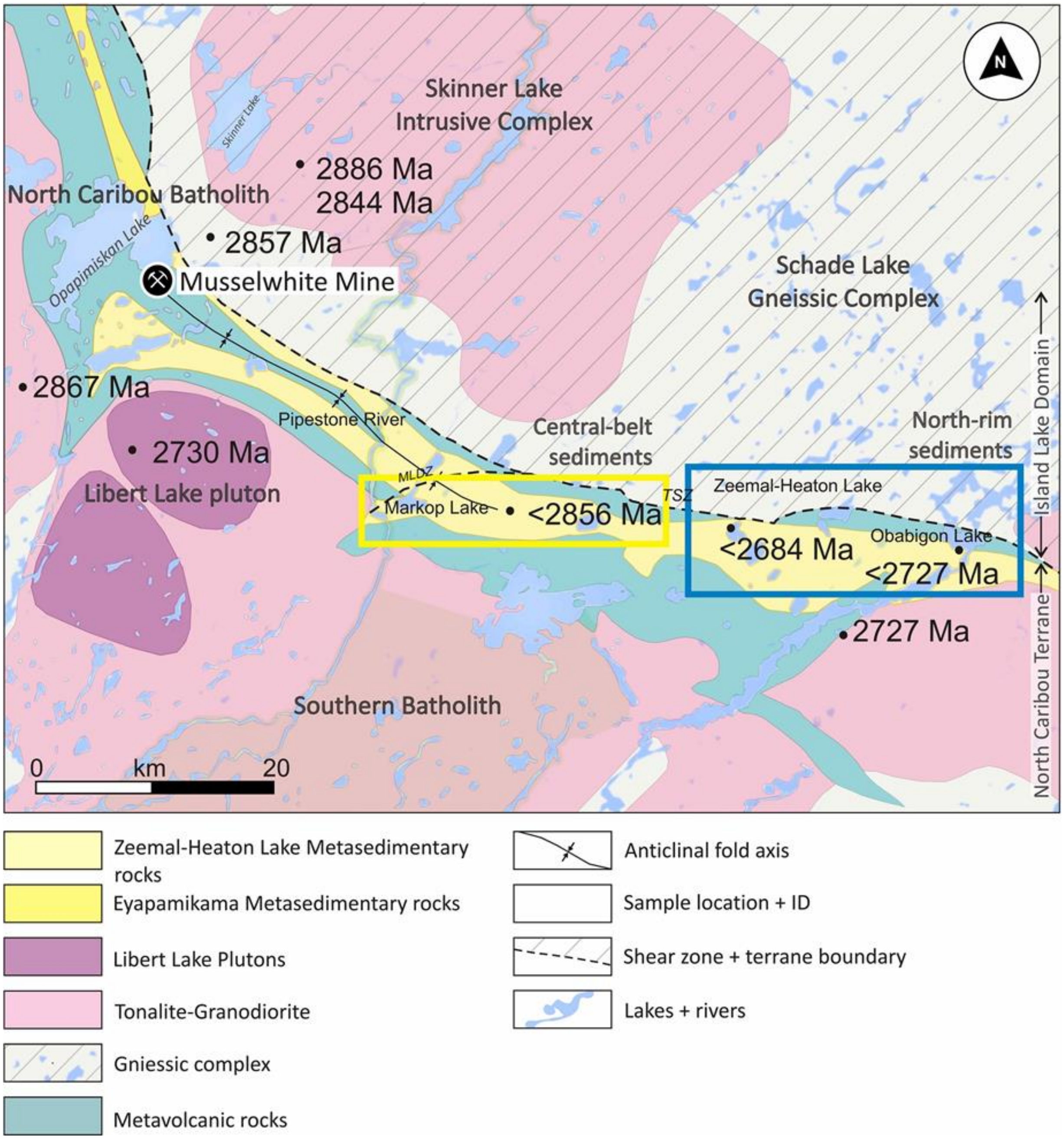

Figure 3: Simplified geologic map of the eastern portion of the North Caribou greenstone belt and Island Lake Domain with U-Pb zircon ages. Modified after Ontario Geological Survey (2011). Samples (OB) collected by the author during 2013 and 2014. Samples with the prefix of JD were collected by Duff (2014) in 2010 and 2011. MLDZ: Markop Lake deformation zone. TSZ: Totogan shear zone

from the South Rim rhyolitic tuff and 2870 Ma from the North Rim rhyolite (Davis and Stott, 2001) suggests that the North Rim volcanic rocks and South Rim volcanic rocks are not contemporaneous. To the south, near Opapipmiskan Lake, the North Rim volcanic rocks and South Rim volcanic rocks taper and the Opapimiskan assemblage begins to occur. The Opapimiskan assemblage consists primarily of mafic to ultramafic rocks with several horizons of banded iron formation that hosts the orogenic Musselwhite gold deposit. It is distributed within a roughly U-shaped regional unit, which is continuously traceable for 65 km Northwest from Markop Lake to Opapimiskan Lake and from there, south to Barrigar Lake before reversing to Zeemal Lake and finally, striking southeast to the Pipestone River (Breaks et al., 2001). The flat to moderately elevated light rare earth element (LREE) patterns of the Opapimiskan assemblage, in conjunction with the negative Nb and Ti anomalies of the komatiites and tholeiites, are interpreted to represent the product of mantle plume derived magmatism erupted through TTG crust (Hollings and Kerrich 1999). Together, the South Rim volcanic rocks and Opapimiskan assemblage likely represent the eruptive products of a single mantle plume that entrained tholeiitic melts from the upper mantle before erupting at ∼3000 Ma (Biczok et al., 2012).

The Eyapamikama and Zeemal Heaton Lake metasedimentary assemblages comprise the entire central portion of the belt, from the northwest to southeast. Breaks et al. (2001) have divided the Eyapamikama assemblage and Zeemal Heaton Lake metasedimentary rocks with a boundary occurring at Opapimiskan Lake. The Eyapamikama assemblage occurs to the North, and Zeemal Heaton Lake metasedimentary rocks lie to the south. For the purpose of this study, definition is used for these units. The Eyapamikama assemblage extends the entire medial portion of the greenstone belt to Opapimiskan Lake while the Zeemal Heaton Lake metasedimentary rocks comprise the medial portion to the south the lake.

The Zeemal Heaton Lake metasedimentary rocks comprise the youngest supracrustal unit in the belt and are the focus of this study. They are only postdated by peraluminous granitoid pegmatite, with the youngest dated at 2610 Ma (Bickzok et al., 2012; Van Lankvelt 2013). The structure noted in the Zeemal Heaton Lake metasedimentary rocks is a moderately to steeply dipping planar foliation that is parallel to the main E-W rend of the belt. The contact between the uppermost metavolcanic rocks of the Keeyask Lake volcanic rocks and the basal conglomerates of the Eyapamikama assemblage grades from conformable to unconformable and is exposed in several localities at low water level along the western shoreline of Eyapamikama Lake (Breaks et al., 2001). The latter consists of basal conglomerates, arkosic arenites, arkosic-subarkosic wackes, lithic wackes quartz wackes and metapelites, all of which have been metamorphosed from greenschist to prograde amphibolite conditions. Breaks et al. (2001) interpreted the Zeemal Heaton Lake metasedimentary rocks to have been deposited in an active volcanic environment that was surrounded by a rapidly rising granitoid terrane, as is evident from the intercalation of ultramafic flows with conglomerates, which contain a significant tonalite clasts. Previous U-Pb detrital zircon dating has been completed south of Opapimiskan Lake in the Zeemal Heaton Lake metasedimentary rocks. David and Stott (2001) dated a quartz arenite clast from the Central-belt area of this study at <2853 ± 1 Ma, and Duff (2014) dated a sublithic arenite and quartzofeldspathic arenite from the North-rim of the Zeemal Heaton Lake metasedimentary rocks at <2674 and <2712 Ma. The roughly 150 Ma age gap in detrital zircons of the immature Zeemal Heaton Lake metasedimentary rocks compared with the greenstone volcanic rocks are similar to those of other "Timiskaming-type" sedimentary rocks in the eastern and southern Superior Province. These occur in close, spatial relationship with large gold-deposits and shear zones. The youngest zircon population are comparable to monazite age (2666 Ma) in garnet which is interpreted to be coeval with gold mineralization (Oswald et al., 2015) and the accretionary age the North Caribou terrane (Duff, 2014). This may suggest that the deposition of the sedimentary rocks was broadly synchronous with the Totogon shear zone and the gold mineralization. The purpose of this study is to further define the provenance of the sedimentary rocks in the eastern portion of the belt and evaluate the ages of deposition in the area.

Deformation

The North Caribou greenstone belt has been intensely deformed and folded adjacent to the surrounding Island Lake domain. A Z-shape defines it with two E-W trending arms stretching outward from a roughly N-S trending regional and crustal-scale shear zone which follows lithological contacts in the Northern and Eastern margins. McNicoll et al. (2015) examined the tectonic history of the belt in detail and determined the earliest event, D_1, forms ENE-trending tight to isoclinal F_1 folds. These folds are preserved in areas of higher superimposed strain, such as the hinge zones of open F_2 folds, where a penetrative S_1 foliation is locally preserved. The main phase of penetrative ductile deformation in the North Caribou greenstone belt is regionally recognized as D_2 which has an SE-striking, steeply SW-dipping S_2 foliation axial planar to shallowly NW-plunging F_2 folds. D_3 deformation is a relatively weak folding event, characterized by minor warping/mesoscopic chevron folds characterized by axial-planar NE-trending crenulation cleavage. D_4 is characterized by late brittle fault zones associated with local pegmatite dykes (Breaks et al., 2001, McNicoll, et al., 2015).

Two main shear zones exist within the eastern portion of the North Caribou greenstone belt. This includes the right-lateral Markop Lake deformation zone and the dextral Totogan shear zone (Figure 2). The Markop Lake deformation zone is characterized by an increase in thickness of observed deformation and abundance of near-vertical metre scale shear zones in which foliation is thinly spaced, planar, and grain size is significantly reduced (Kalbfleisch, 2012). The Totogan shear zone follows the Northern margin of the eastern arm of the North Caribou greenstone belt and appears to merge with the Markop Lake deformation zone (Figure 2). While the zone is poorly exposed, both mafic volcanic rocks of the Opapimiskan assemblage, sedimentary rocks of the Zeemal Heaton Lake metasedimentary rocks experience an increased intensity of deformation towards the Northern margin of the belt (Kalbfleisch, 2012). Strike length varies between shear zones from 10-40 km, and the width of deformation is 200-300 m. However the Markop Lake deformation zone is not as discrete, as it may be as wide as 1500 m, and it may represent the westward termination of the extensive Totogan shear zone.

Metamorphism

Rocks on the southern margin near the North Caribou Batholith are predominately biotite grade greenschist facies (Gagnon et al. 2016), except an amphibolite grade contact aureole demarcating the intrusive contact of the North Caribou Batholith and associated with regional shear zones (Gagnon, 2015). Regional peak metamorphic conditions in the mine area have reached 550 °C and 3 kbars (Breaks et al., 2001, Otto, 2002, Oswald et al., 2015).

Surrounding Intrusive Complexes and Pegmatites

Numerous TTG batholiths surround the North Caribou greenstone belt (**Figure 2**). As with most TTG's in Archean terranes, they contain greater than 15 wt% Al_2O_3 at 70 wt% SiO_2 and are weakly peraluminous (Van Lankvelt, 2013). Van Lankvelt (2013) obtained U-Pb zircon ages from these intrusions and determined that the main period of granitoid magmatism occurred from 2880 to 2830 Ma. South of North Caribou greenstone belt, within the North Caribou Lake batholith, ages range from 2872 ± 12 Ma to 2829 ± 13 Ma. Younger granitoids (2844 ± 15 to 2828 ± 9 Ma) occur north of the North Caribou greenstone belt, and they include the Skinner Lake Intrusive Complex and Schade Lake Complex. Biczok et al. (2012) and Van Lankvelt (2013) obtained even younger ages for the small Libert Lake pluton 2730 ± 8 to 2700 ± 8 Ma, which occurs south of the North Caribou Lake batholith (Figure 2). Younger igneous rocks emplaced during this period are more evolved than the older rocks, with compositions between granodiorite and granite and were likely emplaced at depths around 20 km based on Al in hornblende geobarometry (Van Lanklvet, 2013). Magmatism from 2760 to 2680 Ma is likely related to a late Archean orogeny ~2720 to 2710 Ma (Percival et al. 2006b; Gangnon, 2015). The final felsic magmatic episode of the North Caribou greenstone belt occurs as S-type pegmatitic to aplitic dykes dated at 2666 to 2619 ± 14 Ma (Biczok et al., 2012; Van Lankvelt, 2013). The pegmatites are closest in age to the Libert Lake pluton (Biczok et al., 2012), and are interpreted to be sourced from this intrusion (Van Lankvelt, 2013). The ~300 Ma spread in ages of batholiths and pegmatites likely indicate that separate magmatic events occurred.

Pressure estimates based on Al-in-hornblende geobarometry by Van Lankvelt (2013) indicated two populations; those with the ages from 2880 to 2830 Ma show an increase in pressure from 5 to 8 kbar that she interpreted to represent crustal thickening. The second population based on metamorphic hornblende had a tight cluster of pressures from 5.5 to 6.5 kbar at circa 2700 Ma.

Mineralization at Musselwhite Mine

The Musselwhite gold mine is hosted within the North Caribou greenstone belt and is located on the south shore of Opapimiskan Lake. The deposit comprises multiple ore bodies within two banded iron formations, which are part of the Opapimiskan-Markop unit of the McGruer assemblage, and lies near the boundary between the North Caribou terrane and the Island Lake Domain to the North (**Figure 2**). These banded iron formations (deposited ~2980 Ma) are known as the Northern Iron formation which hosts the high-grade mineralization, and the Southern Iron Formation which also hosts mineralization (Biczok et al., 2012). The majority of mineralization is within the silicate facies of the banded iron formations characterized by abundant quartz veins, green amphibole (hornblende/ferri-tschermakite; Otto, 2002), replacement of the original grunerite, local chlorite patches, pyrrhotite as veinlets throughout the ore zone and as micro-fracture fillings within garnet (Biczok et al., 2012). Gold mineralization along axial planes is largely confined to subvertical high-strain zones in tightly folded areas, particularly where steeply dipping, isoclinal fold limbs transition into the crests or keels of antiformal and synformal structures (Bickzok et al., 2012). Gold mineralization in the mine area occurred under amphibolite conditions calculated at 540–600 °C by Otto (2002) and 530 to 550 °C at a pressure of 3 kbars. The nitrogen isotopic signatures of biotite suggest ore-forming fluids were from both magmatic and metamorphic fluids (Issacs, 2008). Duff (2014) interpreted based on garnet geochemistry from the mineralized zone in the mine, that fluid involved in Au mineralization was derived from, in part, metamorphic origin and mineralization may have occurred with multiple mineralizing events. Recently, Oswald et al., (2015) presented a new preliminary U-Pb age of 2666 Ma on late-M_2 monazite, which provides a minimum age for the regional D_2

metamorphic/deformation event with which most of the Au mineralization at Musselwhite is associated (Oswald et al., 2015).

Timiskaming-Type Sedimentary rocks

In 2013, Duff (2014) completed U-Pb detrital zircon dating on two samples taken from the Zeemal Heaton Lake metasedimentary rocks near the Northern border of the greenstone belt. Both samples yielded ages of 2674 Ma and 2723 Ma. These dates are ~150 Ma younger than <2856 Ma sedimentary rocks of the Eyapamikama assemblage in the western portion of the belt (Duff, 2014). Duff (2014) interpreted that these detrital zircon age distributions found in the Zeemal Heaton Lake metasedimentary rocks and Eyapamikama assemblages suggest different provenances and two basins that together record ~ 600 Ma of uplift and erosion of plutonic and volcanic rocks in the North Caribou greenstone belt. The younger Zeemal-Heaton Lake sedimentary rocks show similar age and tectonic relationship to that of "Timiskaming-type sedimentary rocks" elsewhere in the Superior Province (Thurston et al., 1991). Timiskaming-type sedimentary rocks represent the youngest supracrustal assemblage in greenstone belts and are deposited unconformably on older, volcanic arc successions (Shegelski, 1980; Corcoran and Mueller, 2007; Driese et al., 2011). Late-stage calc-alkaline to alkaline volcanic rocks can also be associated with Timiskaming successions. The sedimentary facies of Timiskaming-type sediments usually contain fluvial or shallow marine slump successions and includes conglomerate-sandstones with or without shales (Thurston et al., 1991). They usually contain locally derived detritus from the greenstone belt that they are commonly spatially associated with transpressional deformation and crustal-scale shear zones (Thurston et al. 1991; Leclair et al., 1993). Rapid lateral changes, stacking of the sedimentary lithofacies, and proximity to major basin-bounding faults support a tectonically induced sedimentary basin model (Mueller and Corcoran, 1998). However, there is some debate concerning the tectonic environments in which "Timiskaming-type" sedimentary rocks form (e.g., Lin et al., 2013).

Within the Wawa-Abitibi terrane of the Superior Province, which hosts many world-class orogenic gold deposits, shear zones are associated with Timiskaming-type sedimentary and volcanic rocks (Lodge et al., 2013). Most of the pre-D_1 volcanic construction along the margin of the Wawa subprovince occurred between 2722 and 2718 Ma. Subsequent deformation and accretion of the Wawa to the Superior Craton between 2695 and 2680 Ma (Corfu and Stott, 1998) culminated in the deposition of Timiskaming-type, calc-alkalic to alkalic metavolcanic and metasedimentary rocks (Lodge et al., 2013). Timiskaming-type assemblages in this terrane are comprised of syn-orogenic sedimentary and volcanic lithofacies and are deposited in localized pull-apart basins interpreted to be developed by transpressional shearing during terrane accretion or orogenic collapse interpreted to form unconformities during rapid deposition (Corcoran and Mueller, 2007). These sediments are considered to have deposited in pull-apart basins as they are elongate, narrow basins that are in close spatial association with strike-slip faulting where offsets or bends in strike-slip faults result in localized extension (Gürbüz, 2010).

Parmenter et al. (2006) and Lin et al. (2013) proposed that Timiskaming-type sedimentary rocks may be deposited in synclinal keels between granitoid domes during diapirism and sagduction (subsidence) based on recent data from the Northwestern Superior Province, rather than due to transpressional deformation and shearing. Lin et al. (2013) states, not all Timiskaming-type sedimentary rocks are associated with shear zones or in some cases have been documented as being older than proximal shear zones. For example, Parmenter et al. (2006) show that the Cross Lake Group in the Cross Lake greenstone belt in the Northwestern Superior experienced the entire post-regional D_1 deformation history along with the older supracrustal rocks in the belt. Therefore, the Timiskaming-type sedimentary rocks must have been deposited before D_4, and thus could not have been deposited during D_4 shear zones. Parmenter et al. (2006) demonstrated that basin development and sedimentation at Cross Lake, Manitoba was most likely contemporaneous with D_2 and the onset of diapirism and sagduction (vertical tectonism). They suggested that diapirism and uplift, concurrent with greenstone-belt subsidence (sagduction), were the mechanism for the development of a Timiskaming-type tectonic basin overlying the subsiding greenstone belt and between the surrounding domes. This sagduction related mechanism for sediment deposition has been observed in the Island Lake Domain within the North Caribou superterrane (Lin et al., 2013). Lin et al. (2013) showed that based on zircon populations through the stratigraphy that in the early stage of diapirism and sagduction, only the younger supracrustal rocks were exposed above the granitoid domes and supplied detritus into the sedimentary basin in the keel. As the process continued, the older supracrustal rocks became exposed and were the main source of detritus. Later during the process, the supracrustal rocks either became completely eroded away above the domes, or were buried below the sedimentary rocks in the keel, and the 2780 to 2700 Ma felsic intrusions in the domes were unroofed and became the main and eventually the only source of detritus to the basin. As diapirism and sagduction continued, the volcanic and the newly deposited sedimentary rocks were all strongly deformed and became steeply dipping. The synclinal keels, with steep contacts, were favorable locations for localized shearing and shear zones were developed, on one or both sides of the keel, explaining the common spatial association of shear zones with such sedimentary basins.

Regardless of the depositional setting of Timiskaming-type sedimentary rocks, their distribution is spatially associated with major deformation zones and spatially associated with orogenic and intrusion-related Au deposits (Leclair et al., 1993). Examples include the Timiskaming assemblage (turbidities dated <2674 Ma) along the Cadillac-Larder Lake Break shear zone (Corfu et al., 1991; Bleeker, 2012) which is spatially associated with the Kerr Addison, Kirkland Lake, and Sigma-Lamaque Au deposits (Dubé and Gosselin, 2007). As well, the Timmins mining camp along the Porcupine-Destor Fault Zone (Bleeker, 2012), and the syenite-hosted Beattie deposit (mineralization dated <2678.9 Ma; Bigot and Jebrak, 2015) are also associated with young Timiskaming-type rocks.

Sampling

Sample locations are listed in **Table 2** and **Figure 2**. Rock are named based on mineralogy and textures observed in hand sample and thin section. Protolith names are based on porphyroblast and feldspar mode. All rocks are metamorphosed, and metamorphic names are used when not describing protolith.

Jason Duff (2014) collected several metasedimentary samples from across the North Caribou Greenstone belt including both the Eyapamikama assemblage and Zeemal Heaton Lake metasedimentary rocks. Six of his samples from his collection were used in this study.

It should be noted all thin sections were cut perpendicular to foliation which was sub vertical. Interpretations of thin section structure were made based on this orientation.

Table 2: Analysis completed on each sample in this study

ID	Easting (m)	Northing (m)	Zone	Lithology	Whole Rock composition	Garnet EMPA	Zircon U-Pb Dating/Trace Element	Nd Isotope Whole Rock	Nδ15 of Biotite
JD-031	690548	5820459	15	two mica schist					x
JD-033	690553	5820452	15	garnet schist		x			
JD-071	312516	5819109	16	biotite garnet schist	x	x	x		x
JD-094	673810	5825668	15	two mica schist					x
JD-100	306991	5820283	16	biotite garnet schist	x	x	x		
JD-101	702814	5821125	15	muscovite quartz schist			x		x
OB-001	300911	5820933	16	amphibolite	x	x	x	x	x
OB-002	720900	5818973	15	mafic volcanic					
OB-003	689563	5825495	15	conglomerate	x			x	
OB-004	689528	5825491	15	conglomerate	x				
OB-005	688138	5825193	15	rhyolite	x				
OB-006	688263	5825115	15	conglomerate	x				x
OB-007	688321	5825120	15	conglomerate	x				
OB-008	307030	5820443	16	biotite garnet schist					
OB-009	307087	5820448	16	biotite garnet schist	x				x
OB-010	306977	5820421	16	biotite garnet schist	x	x			
OB-011	306863	5820459	16	biotite garnet schist					
OB-012	306830	5820438	16	biotite garnet schist	x		x		x
OB-013	307006	5820409	16	two mica schist	x				
OB-015	604690	5823570	15	staurolite-biotite schist					
OB-016	690661	5826164	15	mafic volcanoclastic	x			x	
OB-017	690636	5826154	15	mafic volcanic	x				
OB-018	690636	5826154	15	mafic volcanic	x				
OB-019	697088	5821037	15	gabbro					

OB-020	697088	5821037	15	rhyolite					
OB-021	697088	5821037	15	muscovite quartz schist	x			x	
OB-022	312491	5819049	15	meta-mafic volcanic	x				
OB-023	312523	5819102	16	biotite garnet schist	x	x			
OB-024	312453	5819147	16	biotite garnet schist	x				
OB-026	698291	5821335	15	muscovite quartz schist	x			x	
OB-027	698244	5821626	15	muscovite quartz schist	x				
OB-028	698406	5821626	15	muscovite quartz schist	x				
OB-030	697255	5821955	15	muscovite quartz schist					
OB-031	697201	5821901	15	muscovite quartz schist	x		x	x	
OB-032	678649	5829634	15	rhyolite	x				
OB-033	676289	5827940	15	volcanoclastic	x				
OB-034	681396	583147	15	garnet biotite schist	x	x		x	
OB-035	681396	583147	15	garnet biotite schist	x	x			
OB-036	674671	5825796	15	conglomerate	x				
OB-100	684442	5826595	15	muscovite quartz schist	x			x	
OB-101	684427	5826587	15	two mica schist	x				
OB-102	701290	5821459	15	andalusite garnet schist	x				
OB-103	704836	5821205	15	two mica schist	x				
OB-104	702659	5821642	15	two mica schist	x			x	
OB-106	299177	5820224	16	two mica schist	x			x	
OB-107	299188	5820362	16	two mica schist	x			x	
OB-108	701449	5819974	15	rhyolite	x				
OB-109	299846	5820924	16	two mica schist	x				
OB-110	687665	5827681	15	andalusite schist	x			x	
OB-111	691318	5823659	15	conglomerate	x			x	x

* Coordinates in UTM NAD83

Sample Petrography

Near-mine metasediments

Two garnet-biotite schists (metapelite) samples (OB-034, OB-035) were taken from the bank of Zeemal Lake in the vicinity (~2km) of the Musselwhite Mine. The matrix in thin section is mainly K and plagioclase feldspar (~200 µm in size) with minor to moderately foliated metamorphic biotite, and abundant poikiloblastic garnet ranging in size from 100-3000 µm (**Figure 10a**). Peak metamorphic minerals include garnet, biotite and K feldspar (garnet zone). Minor calcite is disseminated throughout the sample. Moderate chlorite retrogression of biotite is present. Abundant (~5 vol.%) accessory ilmenite helps define the foliation throughout the sample.

One staurolite-biotite schist (OB-015) and one andalusite-garnet schist (OB-102) sample were taken along the Northern margin of the Zeemal Heaton Lake metasedimentary rocks to the east of Markop Lake (**Figure 3**). Both samples are biotite (~ 25 vol%) and muscovite-rich (10 vol%) and the foliation strikes WNW. Quartz veins (>1 cm) both crosscut and parallel the foliation. In thin section, OB-015 contains abundant staurolite (5 vol%; 0.5 mm) with slight variation in Fe content (observed using a SEM). Staurolite contains inclusion trail foliation pitching to the left of the photomicrograph and a curved steep rim foliation (**Figure 5a**). OB-102, ~6 km to the east of OB-015, contains primarily coarse blocky andalusite (~1-3 mm), minor Fe-poor staurolite (~0.2-0.5 mm), almandine-rich garnet (~1 mm), biotite and quartz. Peak metamorphic minerals include biotite, garnet, andalusite, and staurolite. No significant retrogression was noted.

Figure 4: Field photographs. A) Gabbroic intrusion in contact with conglomerate unit. Note cooling contact on gabbro. Location 689563E 5825495N B) Deformed conglomerate unit in contact with metamorphosed mafic volcanic rocks. Clast occurrence and deformation decrease away from contact. Location 688138E 5825193N C) North-rim biotite garnet schist of Heaton Lake. Foliation defined by biotite. Location 307030E 5820443N D) Biotite garnet schist taken ~60m west of OB-008. Note increased strain. Location 307087E 5820448N E) Intensely deformed Central-belt muscovite quartz schist with abundant quartz veining. Location 698406E 5821626N F) Central-belt muscovite quartz schist taken 350m south-west of OB-028. Note variable strain and veining between samples. Location 698244E 5821626N.

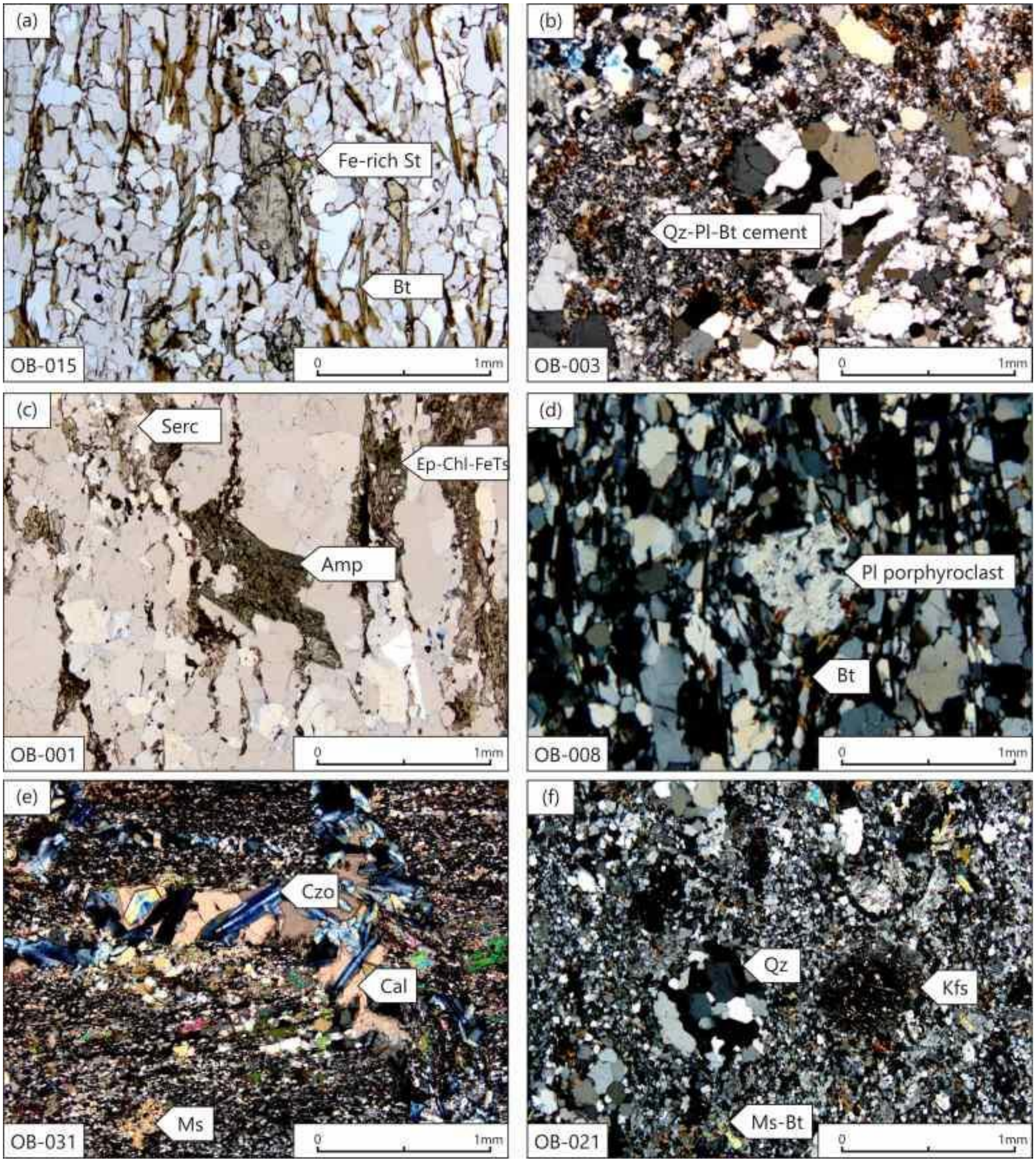

Figure 5: Photomicrographs in plane light and crossed polars. A) Fe-rich staurolite-biotite schist. Staurolite contains core foliation pitching to the left of image and a curved steep rim foliation. B) Conglomerate matrix showing aggregated quartz pebble in quartz-feldspar-biotite matrix. C) North-rim amphibolite with amphibole overprinting foliation defined by recrystallized quartz, chloritized amphibole minor epidote and illitized feldspar. Sample has been carbon coated. D) North-rim biotite garnet schist with plagioclase porphryoblast in quartz-plagioclase-biotite matrix. Note clockwise curving inclusion trains at both the top and bottom of plagioclase. Foliation in the matrix truncates foliation observed in the core of the porphyroclastt. E) Central-belt muscovite quartz schist containing calcite-clinozoisite vein and abundant muscovite overgrowing foliation. Note foliation in matrix curves both ways away from vertical at top and bottom end of Czo/Cal vein. F) Central-belt muscovite quartz schist displaying K feldspar porphryoblast and quartz aggregates in quartz-feldspar-muscovite matrix. Bt: biotite, Cal: calcite, Czo: clinozoisite, Ep: epidote, Amp: amphibole, Kfs: potassium feldspar, Ms: muscovite, Pl; plagioclase, Qz: quartz, St: staurolite.

Markop Lake conglomerates

A polymictic, matrix-supported conglomerate horizon is present from slightly west of the Pipestone River to Central Markop Lake, occurring on both the southern and Northern flanks of the horseshoe-shaped fold of the Zeemal Heaton Lake metasedimentary rocks and Opapimiskan metavolcanic rocks (**Figure 3**). Another occurrence of polymictic conglomerate (OB-036) was observed south of the Musselwhite Mine at Zeemal Lake and forms an unconformity with the Opapimiskan metavolcanic rocks. The occurrence of the conglomerate and unconformity is also reported by Oswald et al. (2015).

Samples OB-003 and 004 taken on the northern flank of the Zeemal Heaton Lake metasedimentary rocks occur in contact with a gabbro which intruded sedimentary rocks as a cooling contact is apparent (**Figure 4a**). The conglomerate appears white/pinkish and contains sub-angular to sub-rounded clasts ranging in size from 1-15 cm of felsic volcanic and intrusive material. The matrix consists of medium grained (~1 mm), rounded to sub-angular quartz aggregates and abundant plagioclase and rarer K feldspar with zones of finer grain (<0.1 mm), aggregated plagioclase + quartz + biotite cement **(Figure 5b).** Biotite forms fine-grained (<0.1 mm) blades or aggregated in the finer matrix with quartz and feldspar surrounding coarser quartz and feldspar grains. Minor to moderate white mica alteration of feldspars occurs throughout, but no chlorite retrogression is present. Peak metamorphic minerals include biotite, plagioclase and K feldspar, which defines the metamorphic conditions as biotite zone. Accessory minerals include apatite, monazite, and zircon (<20 μm) and sub-angular to sub-rounded intrusive felsic and volcanic clasts are present.

OB-111 was taken from between Pipestone River and Markop Lake (**Figure 3**). The angular clasts range in size and include oxide facies banded iron formations, ultramafic, mafic, felsic volcanic rocks and argillic fragments (2-10 cm clast size). The clast zone of the outcrop is bound by tension gashes and quartz fill. Trace monazite occurs as an accessory mineral. Zircon occurs as <15μm euhedral grains.

Samples OB-006 and 007 occur on the eastern limb of a fold in contact with deformed mafic Opapimiskan metavolcanic rocks. These conglomerates contain angular to subrounded clasts ranging in size from <1-20 cm, consisting of mafic volcanic rocks, and felsic volcanic and intrusive rocks. The matrix consists of finer grained primary polycrystalline recrystallized quartz (<10 μm, subhedral) with coarse metamorphic plagioclase grains and rare K feldspar and biotite parallel to foliation. Biotite has undergone partial retrogression to chlorite. Pyrite altered to Fe-oxides is elongate parallel to the foliation.

North-rim metasediments

Two amphibolite samples (OB-001, 104) taken ~5 km west of Heaton Lake along the North-rim have been classified as having a quartz-rich metawacke protolith based on the abundance of quartz with relic clastic material noted in thin section. Matrix consists predominantly of primary recrystallized quartz and minor completely sericitized feldspar, indicating a high level of maturity of the rock. Subhedral to euhedral almandine-rich garnets (0.1-1mm) occur throughout (garnet zone). Ilmenite, pyrrhotite and chalcopyrite inclusions were present in some of the garnet porphyroblasts. Amphibole lies both parallel to and crosscuts the matrix foliation (**Figure 5c**). Peak metamorphic conditions are indicated by amphibole and garnet (garnet-zone). All grains of biotite have been retrogressed to chlorite. Further hydrothermal alteration (alkali metasomatism) is indicated by minor clinozoisite, calcite, and quartz in veins and disseminated throughout. Accessory minerals include ilmenite, pyrite, pyrrhotite, chalcopyrite, zircon and apatite.

Nine biotite garnet schist samples were taken across the Zeemal Heaton Lake metasedimentary rocks and classified as having a sublithic-wacke protolith. Seven samples were collected on the banks of Heaton Lake and two from Obabigon Lake (**Figure 2**), which is the easternmost sampling site of the greenstone belt in this study. The matrix is comprised of fine (~50 µm) quartz + plagioclase with aggregated coarser boudinaged quartz veins (~200 µm width) and plagioclase feldspar grains (<500 µm). Rare K feldspar was identified with petrography and HF staining. Coarser feldspar grains appear to be altered along rims to white mica. Metamorphic biotite defines the foliation throughout the sample and forms fine (100 µm in length), elongated grains and aggregates (**Figure 5d**). Muscovite is very rare. Trace anhedral to subhedral spessartine-rich garnets (<100 µm) occur throughout these samples (**Figure 8d**). Peak metamorphic minerals include plagioclase, biotite, and garnet, and the mineral assemblage suggests that they have metamorphosed under garnet zone conditions. Minor chlorite retrogression of biotite occurs in some samples. Accessory minerals include foliated ilmenite (~5 vol.%), pyrite (<1 vol.%) rimmed by Fe-oxide, apatite, zircon and rare monazite.

Central-belt metasediments

Seven muscovite quartz schist and two mica schist samples were collected over ~12 km between the Heaton and Markop Lakes in the Zeemal Heaton Lake metasedimentary rocks and are classified as having arkosic sandstones protoliths, based on the feldspar mode. The samples from the southern portion of the Markop Lake were collected by Duff (2014). No original sedimentary textures remain (**Figure 5e-f**). The matrix is comprised of fine grain (<10 µm) polycrystalline primary recrystallized quartz with metamorphic K feldspar, trace plagioclase feldspar, very fine (<5 µm) trace metamorphic biotite and abundant medium to coarse grained metamorphic muscovite occurring parallel to or obliquely overprinting the foliation (**Figure 5f**). Coarse (1-2 mm) K feldspar porphyroblasts and porphyrobclasts are minor to moderately altered to white mica. These coarse feldspar porphyroblasts contain inclusions (<10-50 µm) of muscovite and calcite. Muscovite and calcite also form a foliation surrounding these coarse feldspars along with elongated quartz aggregates (0.5-2mm). The coarser grained quartz aggregates (20-200 µm) are interpreted to be boudinaged quartz veins. Peak metamorphic minerals include K feldspar and muscovite which defines the foliation. Muscovite also appears as coarse blocky porphyroblasts over printing foliation which appears to be a retrogression product. The samples also contain abundant hydrothermal (calcite and clinozoisite as it occurred in veins (10-20 mm in width) and disseminated throughout, indicating alkali metasomatism. The veins occur both parallel and oblique to the foliation (**Figure 5e**). Fine white mica and coarse muscovite have an affinity with veins but are not limited to them and are disseminated throughout. Accessory minerals include Fe-oxide replacing pyrite, apatite, monazite and zircon.

Analytical Methods

Whole Rock Geochemistry

Samples for whole rock geochemistry were prepared following standard methods for crushing and grounding using a grinding dish from ~40-100 cm^3 of rock. 27 samples collected during the summer of 2013 were analyzed for whole rock minor and trace elements by Actlabs, Inc. in Ancaster, Ontario. 30 grams of sample were then analyzed using the Instrumental Neutron Activation Analysis for Au, Ag, Ni, Zn, As, Ba, Br, Co, Cr, Cs, Fe, Hf, Na, Sb, Sc, Se, Ta, Te, U, W, and a 4-acid digestion ICP-MS for Cu, Cd, Mo, Mn, Pb, Be, Bi, Ga, Ge, In, Li, Mg, Nb, Rb, Re, Sn, Sr, Te, Tl, V, Y, Zr, La, K, Ce, Pr, Nd, Sm, Eu, Gd, Dy, Tb, Ho, Hg, Er, Tb, Yb, and Lu. Total digestion uses a 0.25 g sample is digested with 4-acids beginning with HF, HCl, followed by a mixture of HNO_3 and $HClO_4$, heated using precise programmer controlled heater in several ramping and holding cycles, which takes the samples through to being dry. Digested samples were diluted and analyzed by Perkin Elmer Sciex ELAN 6000, 6100 or 9000 ICP-MS at Actlabs, Inc. One blank was run every 40 samples at the laboratory. In-house control was run every 20 samples at the laboratory. Reference material with known compositions was digested every 80 samples. After every 15 samples, a digestion duplicate was analyzed. The instrument was recalibrated every 80 samples. 23 of these samples were later analyzed for all major oxide chemistry including Si by AcmeLabs Ltd in Vancouver, BC using $LiBO_2/Li_2B_4O_7$ fusion ICP-ES analysis. 11 samples collected in 2014 were analyzed for major, minor and trace elements by ActLabs Ltd in Lancaster, Ontario using Major Elements Fusion ICP(WRA)/Trace Elements Fusion ICP-MS(WRA4B2). Fused samples were diluted and analyzed by Perkin Elmer Sciex ELAN 6000, 6100 or 9000 ICP/MS. Three blanks and five controls (three before sample group and two after) were analyzed per group of samples. Duplicates were fused and analyzed every 15 samples. The instrument was recalibrated every 40 samples. Data for these analyses are presented and compared in **Appendix II-III.**

SEM-EDS Analysis

The chemical composition of clinozoisite/epidote was determined *in situ* on the JEOL 6610LV Scanning Electron Microscope (SEM) at the University of Ottawa. Minerals for analysis were chosen from polished thin sections during transmitted light microscopy. Polished thin sections were then cleaned, carbon coated, and placed in high vacuum mode using an accelerating voltage of 20 kV on the SEM. Multiple analysis spots were chosen per mineral and average elemental compositions obtained were used to identify the mineral name.

EMPA Analysis

The chemical compositions of garnet were determined *in situ* on the JEOL 8230 SuperProbe electron microprobe analyzer (EMPA) at the University of Ottawa. EMPA analysis locations were selected to avoid inclusions, at equal distance from rim to rim for garnet. This analysis was completed to determine the metamorphic conditions that have affected sedimentary lithologies across the eastern portion of the belt from both the Eyapamikama assemblage and Zeemal Heaton Lake metasedimentary rocks. P-T variation across these lithologies is important for interpreting separate depositional events and the overall tectonic history of the belt. Data for these analyses are presented in **Appendix I**.

Elements and X-ray lines used for all analysis are K (Kα), Ca (Kα), Sr (Lα), F (Lα), Al (Kα), Zn (Lα), Zr (Lα) Cr (Kα), Fe (Lα), Mn (Lα), V (Lα), Zn (Kα), Cl (Kα), Ti (Kα), Na (Kα), Mg (Kα), and Si (Kα). Operating conditions included an accelerating voltage of 20kV, beam current of 20nA, and an electron beam diameter of ~1µm. The count time was set to 10 s. specimens used for calibration were $K(AlSi_3O_8)$ (for K, Al and Si), $MgCaSi_2O_6$ (for Ca and Mg), $SrSO_4$ (for Sr), CaF_2 (for F), ZnS (for Zn), $ZrSiO_2$ (for Zr), Fe_2O_3 (for Fe), Mn_2SiO_4 (for Mn), $Pb_5(VO_4)_3Cl$ (for V), $Na_4(AlBeSi_4O_{12})Cl$ (for Cl), $(Fe, Mg)Cr_2O_4$ (for Cr), TiO_2 (for Ti), and $NaAlSi_3O_8$ (for Na). Wavelength-dispersive spectrometry (WDS) X-ray maps were collected using an accelerating voltage of 20kV, beam current of 50nA and a counting time of 30ms/step for select garnet grains. The WDS scans were performed against synthetic and natural materials to avoid interference on the peak and background for (K, L)-lines during major and trace elements analyses. Each sample was transected at equal distances from rim to rim with between 5-15 analysis spots depending on grain size.

Geochronology

Zircon grains were liberated from approximately 2-6 kg of rock using a jaw crusher followed by a steel disc mill. Both machines were thoroughly cleaned with alcohol and pre-contaminated with a small amount of each sample. The disc mill plates were spaced apart far enough, so the majority of the material was between 100-250 µm. Although sampling bias may have been introduced during this stage, the physical handling of zircon <100 µm is very difficult and the ability to only ablate cores of zircon may have resulted in mixed core-rim ages. Crushed rock was sieved and a fraction between 63µ and 125µ was collected. Approximately 100 ml aliquots of this fraction were washed and decanted in a graduated beaker to remove silt and clay-size material and low specific gravity (SG) minerals. The aliquots were rinsed with alcohol and allowed to dry at ~ 40 °C overnight.

Heavy minerals were concentrated using methylene iodide (SG = 3.32 g/cm3) in a separator funnel apparatus. Grains were agitated in the funnel and allowed to settle for ~10 to 30 minutes or until enough concentrate sank. Heavy minerals were collected in filter paper and thoroughly washed with acetone. Zircon grains were picked dry, using a lightly oiled "dental pick" and then placed on a piece of double-sided tape affixed to a clean glass plate. Grains were oriented with their crystallographic c-axis horizontal on the tape. The grains were cast in a mount epoxy resin was allowed to cure for 24 hours.

Zircons were polished using coarse to fine polishing mediums. First, 400 grit paper and 800 grit papers used to level the mount and remove excess epoxy covering the grains. The mount was polished with a 1000 grit tungsten carbide powder-in-water on a glass plate to coarsely abrade the zircon. The mount was examined periodically during this polishing stage to determine whether any grains were being plucked from the epoxy. A few grains were lost during this stage. Fine polishing employed 5 and 1 µm alumina powder on a felt polishing mat. Lastly, a 0.5 µm diamond powder mixed with polishing oil on a glass plate was used to polish the surface of epoxy mount flat. Before carbon coating, the mount was thoroughly cleaned with acetone to remove oil and polishing compound. Grain numbers analyzed per sample are described in *Geochronology*.

Cathodoluminescence imaging of each grain was carried out at the University of Ottawa using a Gatan MNIN-CI detector attached to a JEOL 6610V scanning electron microscope operating at 15 V accelerating voltage. Uranium-Pb isotopic analysis employed LA-ICP-MS methods carried out at the University of New Brunswick using a Resonetics M-50-LR 193 nm Excimer laser coupled to Agilent 7700x quadrupole ICP-MS. Analysis spots were pre-determined on a motorized stage attached to a Zeiss Axiomager microscope and spots were entered into the sequence imaging program AxioVision. Automated analysis runs used a 20 µm static mode spot size at a repetition rate of 4 Hz and energy attenuation of $3J/cm^2$. The ablation cell was continuously flushed with He (750 mL/min), Ar (630 mL/min) and N_2 (2.8 mL/min) gasses. Isotopes collected included Pb^{204}, Pb^{206}, Pb^{207}, Pb^{208}, Th^{232}, U^{238}, Hg^{202}, and Hg^{204}. Ablation occurred from approximately 7-30 seconds per grain. Analyses of the unknowns were bracketed by analysis of FC-1, 91500, KVT, and NIST 610 synthetic glass. These standard reference materials were mounted on a separate epoxy mount, and their locations were programmed into the automated analysis runs.

Isotopic abundances of the unknown analyses were normalized to those of FC-1 (Paces and Miller, 1993) and integrated using Iolite (Hellstrom et al., 2008). Vizual Age (Petrus and Kamber, 2012) was used to aid selecting the optimal time-integrated signal to reduce the discordance of each analysis. In order to detect the maximum number of age populations in each sample and limit sampling bias, zircons were randomly selected to include different shapes, colours and sizes**.**

Only analyses with > 98% of total Pb being radiogenic Pb were considered. No common Pb correction was used. Total Pb was calculated from the final fraction of common Pb which was determined in the original analysis. Selecting analyses with a <15 % $^{207}Pb/^{206}Pb$ discordance were further discarded. This cut-off is routinely used for Archean studies and is conservative (Gehrels, 2012). Relative age probability plots were generated using Isoplot/Ex 3.00 (Ludwig, 2003) using the final $^{207}Pb/^{206}Pb$ ages and their associated internal standard error (2σ). Cumulative probability plots were generated using the same data as the relative age plots using CUMULATIVE PROB PLOT Excel macro program of Gehrels (2012). Full analytical results and images are presented in **Appendix IV.**

Trace Element Geochemistry of Zircon

Most grains used had been previously ablated 1-2 times for U-Pb dating. Grains were cleaned and re-polished before trace element analysis. Zircon analyses were performed at the Geological Survey of Canada with a Photon Machines Analyte G2 excimer laser ablation system attached to an Agilent 7700x

ICP-MS with a second interface pump that approximately doubles instrument sensitivity. A spot size between 20-40 µm was used depending on grain size and previous ablation spots, and a 10 Hz laser repetition rate was employed. Calibration was achieved using standard procedures (Longerich et al., 1996) that included the use of a NIST 612 glass reference material for external standardization and the stoichiometric zircon SiO_2 content for internal standardization. Data were processed using GLITTER (Griffin et al., 2008) and GeoREM 236 "preferred" concentration values (http://georem.mpch-mainz.gwdg.de) for NIST612. Six to ten representative zircon grains were selected from each of the five sedimentary samples of this study (3 from the North-rim and 2 from the Central-belt). 36 masses were analyzed including ^{27}Al, ^{29}Si, ^{31}P, ^{42}Ca, ^{45}Sc, ^{49}Ti, ^{51}V, ^{57}Fe, ^{88}Sr, ^{89}Y, ^{93}Nb, ^{96}Zr, ^{118}Sn, ^{137}Ba, ^{177}Hf, ^{201}Hg, ^{204}Pb, ^{206}Pb, ^{207}Pb, ^{208}Pb , ^{232}Th, ^{238}U and ^{139}La, ^{140}Ce, ^{141}Pr, ^{146}Nd, ^{147}Sm, ^{151}Eu, ^{157}Gd, ^{159}Tb, ^{163}Dy, ^{165}Ho, ^{167}Er, ^{169}Tm, and ^{173}Yb. Since sector-zoned zircon grains commonly show highly heterogeneous distributions of elements (Jackson et al., 2013), cathodoluminescence images of grains were carefully examined, and zircon grains with no apparent sector zoning were selected for analyses. Areas without mineral inclusions and cracks were analyzed. Full analytical results are displayed in **Appendix V**.

Nd Isotope compositions

Nd isotope analysis was completed to aid in the interpretation of provenance of the Zeemal Heaton Lake metasedimentary rocks. The age used for calculation was the maximum age of detrital zircon. Samples were trimmed to remove weathered surfaces prior to crushing in a steel jaw crusher. Rock chips were then homogenized to a powder consistency in a ceramic pulveriser. Both steel plates and ceramic pulveriser assemblage were pre-contaminated with a small portion of each sample and then cleaned with alcohol between samples to minimize cross contamination. Silicate rock powders were spiked with a mixed ^{148}Nd-^{149}Sm spike solution before being dissolved in the mixed acid of ~29 M HF and ~16M HNO_3; the samples were dried down on the hotplate before being re-dissolved with 8M HNO_3 and 6M HCl sequentially. The dried residue of each sample was dissolved in 2.5 M HCl and loaded into 14-ml Bio-Rad borosilicate glass chromatography columns containing 3.0 ml of Dowex AG50W-X8 cation resin. The columns were then washed with 23 ml of 2.5 M HCl before the rare earth elements were eluted using 9 ml of 6M HCl. Light REE fractions were dissolved in 0.26M HCl and loaded onto Eichrom Ln Resin containing Teflon powder coated with HDEHP [di(2-ethylhexyl) orthophosphoric acid (Richard et al., 1976). The isotope ratios were measured using a ThermoFinnigan's Trion TIMS. The samples were loaded with H_3PO_4 in a double rhenium filament assembly. The isotope ratios were measured at temperatures of 1600-1800 °C. Isotope ratios were normalized to ^{146}Nd/^{144}Nd = 0.7219. An IGGRC's in-house Nd standard were routinely measured with $^{143}Nd/^{144}Nd$ = 0.511826 ± 0.000007 (1σ) over a period of three years; this value is very similar to $^{143}Nd/^{144}Nd$ = 0.511855 for the La Jolla Nd standard; Sm and Nd concentrations were measured precisely within 1%. Analyses of the USGS standard BCR-1 yield Nd = 29.02 ppm (recommended value 28 ± 2 μg/g), Sm = 6.68 ppm (recommended value 6.7 ± 0.3 μg/g), and $^{143}Nd/^{144}Nd$ = 0.512668 ± 0.00002 (n=4). Total procedural blanks for Nd were less than 50 picograms.

Nitrogen Isotope Analysis of Biotite

A total of nine samples from across the Zeemal Heaton Lake metasedimentary rocks were analyzed for N isotope composition at the University of Ottawa GG Hatch Stable Isotope Lab. Samples were crushed from whole rocks using the jaw crusher and then sieved to a 63-250 µm grain fractionation at the University of Ottawa by the author. Biotite grains were separated under a microscope by hand and cleaned in acetone. Once the biotite was separated, it was crushed by hand using a mortar and pestle. In order to eliminate contamination between samples, all tools used were cleaned first with water, then with acetone to remove residue before each sample was crushed and sieved. The N concentration of each sample was determined prior to $\delta^{15}N$ isotope analysis. Samples and standards were weighed into tin capsules and loaded into an elemental analyzer interfaced to an isotope ratio mass spectrometer. Sample/Std is flash combusted at about 1800C (Dumas combustion) and the resultant gas products carried by He gas through columns of oxidizing/reducing chemicals optimized for CO_2 and N_2. The gasses are separated by a '*purge and trap*' adsorption column and sent to an IRMS interface and then to IRMS. Internal standards used are ($\delta^{15}N$, $\delta^{13}C$ in ‰): C-51 Nicotinamide (0.07,-22.95), C-52 mix of ammonium sulphate + sucrose (16.58,-11.94), C-54 caffeine (-16.61,-34.46), blind std C-55: glutamic acid (-3.98, -28.53). Analysis of K_2O in the samples was not completed. Therefore results represent a minimum concentration of N as the biotite separates contain minor quartz and plagioclase.

Results

Whole Rock Geochemistry

Rock types were determined primarily using petrography and mineral mode as the sedimentary rocks show a large compositional variation even a single outcrop. Metamorphism and hydrothermal alteration (silicification, saussuritization, and illitization) have likely affected major element chemistry, so this major element plots have not been used to evaluate the protolith. However, whole rock geochemistry, combined with U-Pb dating of detrital zircon and Nd isotopic signatures, provided useful information in determining the provenance of the sedimentary rocks.

Table 3: Select whole rock geochemistry of metasedimentary rocks in the Zeemal Heaton Lake assemblage

Unit	#	SiO_2 %	Al_2O_3	FeO (t)	MgO	CaO	K_2O	Ni ppm	Cr ppm	Total REE ppm	La/Sm *	Ce/Yb *	Eu/Eu *
Near-mine metasediments	2	58.0-80.6	9.59-17.5	4.45-8.98	1.26-3.52	0.80-4.86	1.11-4.40	30-106	130-192	35-129	5.12-7.81	17.6-32.8	0.89-0.95
Conglomerate matrix	4	57.7-80.9	7.71-17.3	1.56-10.67	0.79-5.72	0.31-3.59	0.96-1.94	<20-106	39-335	37-115	6.20-9.24	21.7-134	0.61-0.91
Central-belt metasediments	5	68.1-72.5	13.4-15.33	1.97-4.63	0.78-1.36	2.50-4.18	1.51-3.61	12.7-25	9-56	104-166	8.60-15.7	47.0-81.4	0.64-1.15
North-rim metasediments	6	68.4-84.6	6.65-16.9	2.82-4.82	1.22-2.15	0.95-1.53	0.68-2.93	29-102	113-144	44-88	6.53-9.00	29.3-71.5	0.87-0.99

Fe total is expressed as FeO.
*Weight ratio.
$Eu/Eu_N=Eu_N/((Sm_N+Gd_N)/2)$.
The composition of each sample is listed in Appendix II-III.

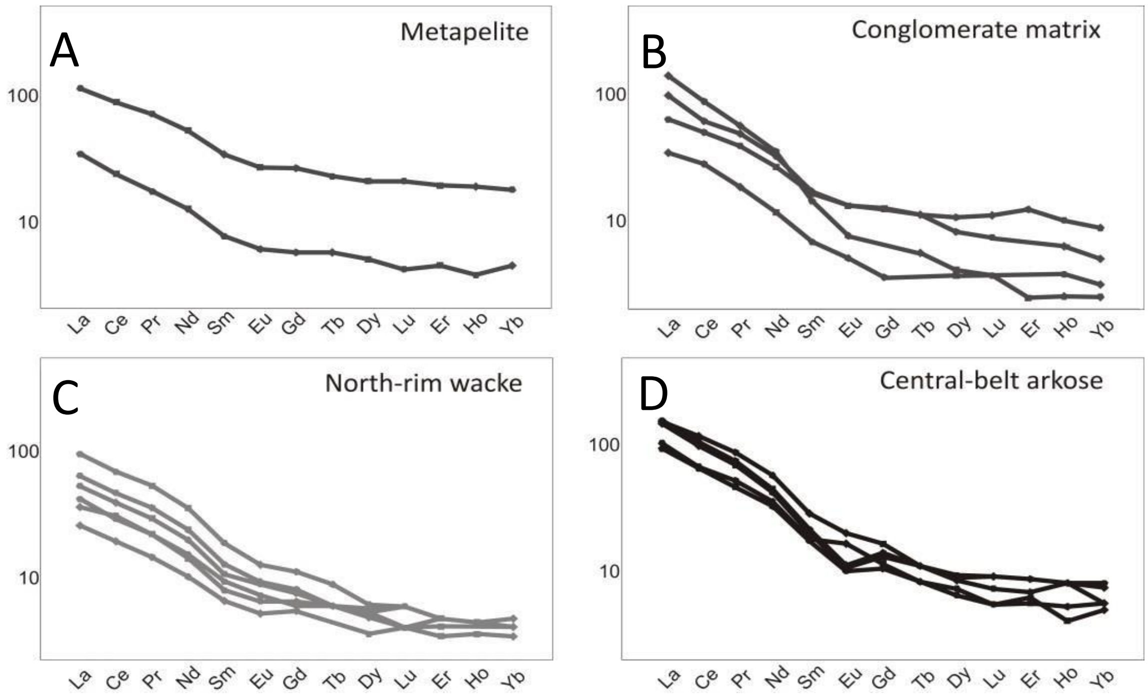

Figure 6: Whole rock rare earth element plot chondrite-normalized to Sun and McDonough (1995) of metasedimentary rocks from the Zeemal-Heaton Lake assemblage. A) Metapeltie, B) Conglomerate matrix, C) North-rim metasediments, D) Central-belt metasediments.

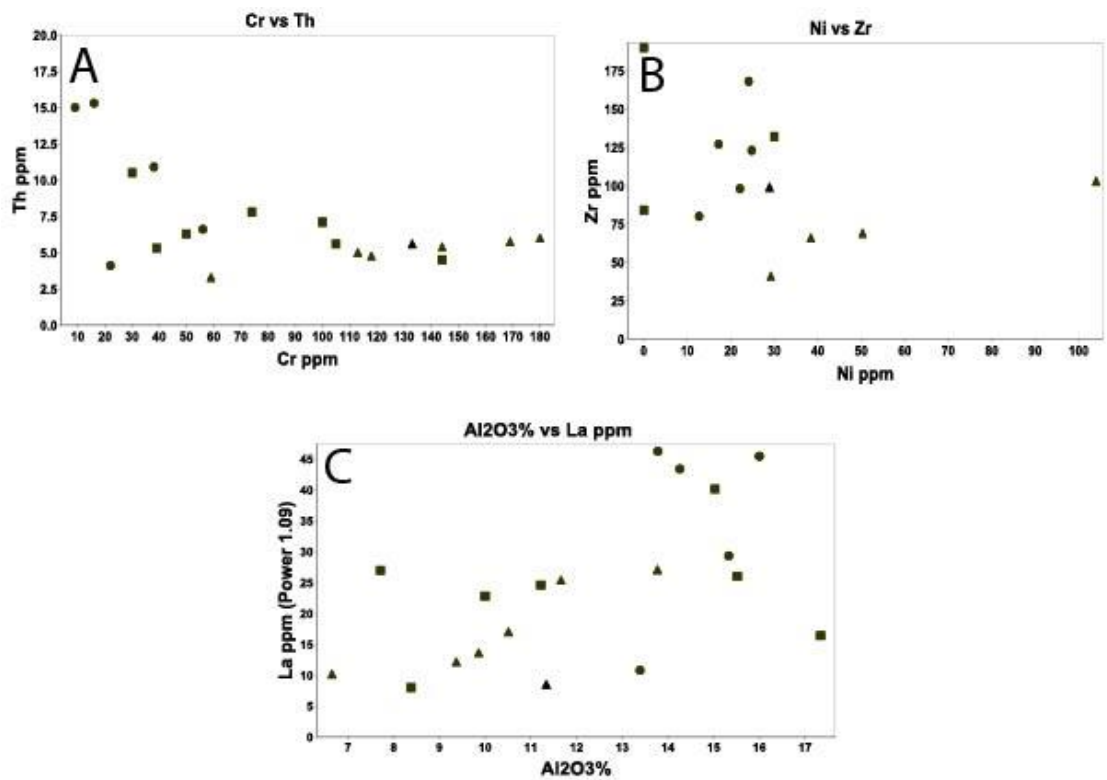

Figure 7: Whole rock major and trace element chemistry of metasedimentary rocks from the Zeemal-Heaton Lake assemblage. A) Cr vs. Th, B. Ni vs Zr, C Al_2O_2% vs La. Circles: Central-belt metasediments, Squares: Conglomerate matrix, Triangles: North-rim metasediments.

Near-mine metasediments

Garnet biotite schist samples (OB-034, 035) display typical LREE enrichment in chondrite-normalized plots but show a less steep REE slope than seen in the North-rim and Central-belt metasediments (**Figure 6a-d**), which is indicative of a mafic contribution of detritus. The metapelites also contain high concentrations of mafic detritus related elements, such as Ni, Cr, Sc, V and low felsic detritus related elements (Th, Zr) about the metasedimentary rocks to the east **(Table 4, Figure 7a-c**). When plotted compared to MORB, andesite, upper continent crust and sedimentary recycling (**Figure 23b**) the metapelites show an affinity toward a mafic source, while the sedimentary rocks to the east show a more upper continental crust contribution. Tb and Ho anomalies shown in **Figure 6** are not naturally occurring and therefore may be related to analytical errors.

Markop Lake conglomerate matrix

Conglomerate clasts were avoided and matrices were chosen for analysis as they should contain a more homogeneous geochemical signature. Overall, the conglomerate matrices show extremely variable major and trace element values with little to no correlation between samples. Even samples collected from a single outcrop show extreme variability in elements. For example, OB-003 and OB-004 taken 20 m apart show ~20 % variation in SiO_2 content and ~10% Al_2O_3 (**Table 4**). This is expected, as the nature of the environment for deposition of the conglomerate can be high energy and rapid resulting in a heterogeneous rock. The conglomerate matrix geochemistry does however reflect the clast population. Samples OB-006 and 007 which are in direct contact with the Opapimiskan metavolcanic rocks contain abundant mafic, with minor felsic volcanic clasts, within a finer grain matrix. The rocks display a flatter pattern on chondrite normalized REE plots (**Figure 6b**), as well as the presence of abundant elements commonly high in mafic rocks (Cr, Ni etc.; **Figures 7a-b**). Samples OB-004 and OB-111 contain abundant granitic and felsic volcanic clasts and consequently more steeply dipping LREE/HREE slope on the chondrite-normalized plot than OB-003 and OB-004 (**Figure 6b**). Low Zr and small zircon grains (>20 µm) within all conglomerate matrix samples is unusual as there is a high abundance of granitoid clasts within the matrix and the high energy environment in which conglomerates are deposited is ideal for heavy mineral accumulation. Zr concentration in whole rock ranges from 25-190 ppm, however even in samples with >100 ppm Zr, no zircon grains were recovered during heavy mineral separation. Examination of thin sections with SEM, small zircon grains (<20 μm) were apparent in fabric forming minerals such as biotite. However, these grains are too small to be recovered by the zircon separation methods used in this study.

Central- vs. North-rim metasediments

North-rim biotite garnet schists display higher SiO_2 concentration than the Central-belt. The North-rim range between 70 to 84% SiO_2 in the amphibolites of Heaton and Obabigon Lake. This is likely a product of the significant quartz clast contribution and quartz veining, noted in thin section and outcrop. The SiO_2 contents in the Central-belt metasediments range between 68.05-72.45% SiO_2, and the values are positively correlated with abundances of Al_2O_3 (**Table 4**). The biotite garnet schists in North-rim however, contain higher abundances of MgO ranging between 1.22 and 2.15% and metasandstones in the Central-belt display <1% MgO (**Table 4**). The metasediments of the Central-belt display higher abundances of K_2O and CaO (**Table 3**) due to the presence of muscovite, K feldspar, calcite and clinozoisite, all of which rarely seen in North-rim samples.

Chondrite-normalized spider plots show very similar patterns between lithologies **(Figures 6c-d).** However, there is a higher abundance of REE in the Central-belt metasediments display a more pronounced negative Eu anomaly (<0.9). North-rim metasediments display a higher abundance of compatible elements including Cr, Ni, Sc, V and Co with lower Al_2O_3, La, Zr, and Ce/Yb (**Table 4, Figure 7a-c**) indicating a high mafic detritus contribution. Cr vs Th and Ni vs Zr was plotted to display the variation in typical compatible mafic elements vs more incompatible felsic elements (**Figure 7a-b**) between the lithologeis. The Central-belt metasediments display a high LREE abundance, high La, Zr and Sm indicating heavy mineral rich sedimentary rocks and a granitic contribution.

Garnet Morphology and Major Element Chemistry

Rocks observed with garnet include; (i) a biotite garnet schist (OB-035) collected on the shore of Zeemal Lake in close proximity (~2 km) to the Musselwhite mine, (ii) a biotite garnet schist (JD-033) from the Central-belt on the southern bank of Markop Lake within the Markop Lake deformation zone and (iii) biotite garnet schist (010, 023, JD-100) and (iv) amphibolite (OB-001) spanning ~20 km E-W from across the North-rim. Select grains of garnet were analyzed for Ca, Cr, Na, Al, Fe, Mn, Ti, Zr, Mg, and Si. Thin sections of garnet porphyroblasts were cut perpendicular to foliation which occurs sub-vertically in all samples.

Three garnet porphyroblasts ranging in size between 600 and 1500 µm (Figure. 10a) were analyzed from the near-mine biotite garnet schist (OB-035). Garnet grain size ranges from 500 µm in thin section to 3 cm, as seen in outcrop. Biotite with minor chlorite occurs retrogressing along garnet fractures. The garnet porphyroblasts from this sample were taken the farthest to west in this study and display the highest almandine component with X_{alm} 71.8-75.2. The concentrations of FeO(t) show discontinuous zoning with decreasing FeO(t) correlated minor increases in MnO (X_{sps} 2.8-3.8) with no direct correlation in a variation of CaO (X_{grs} 7.9-10.3) (**Figure 9a, Appendix I**). The strong variation in the grossular component across the porphyroblast compared to other major elements is likely due to interaction with Ca-rich fluids or a Ca-rich protolith. The MgO component remains stable across the grain (X_{pyr} 14.0-14.8).

Three garnet porphyroblasts were analyzed from the amphibolite (OB-001) taken from the North-rim (**Figure 8f**). Anhedral to euhedral garnets range in size from ~100-300 µm (**Figure 8f**) and occur in contact with chloritized biotite and amphibole, which defines the foliation. Subhedral garnets contain minor inclusions. Inclusions include matrix quartz as well as minor ilmenite, pyrite, pyrrhotite, chalcopyrite, chloritized biotite and amphibole. Euhedral grained garnet contain no inclusions. The garnet porphyroblasts show a distinctly different zoning pattern than other North-rim samples to the east. These porphyroblasts show a more continuous zonation than seen in the eastern North-rim, with decreases in MnO (X_{sps} 33.5-25.6) from core to rim with correlated increases FeO(t) (X_{alm} 47.1-53.6). This indicates typical prograde metamorphism to upper greenschist, lower amphibolite facies. CaO is relatively homogenous across the grains but shows higher values (X_{grs} 14.4-16.9) than seen in the other North-rim samples indicating higher pressure conditions (**Figures 9c, 10b and Appendix I**).

One to three garnet porphyroblasts were analyzed from each biotite garnet schist from the North-rim. These samples contain anhedral to subhedral garnets ranging in size from ~100-400 µm (Figures 10c-e). Lithologies occur along a ~12km E-W strike along the Northern margin of the sedimentary package within the belt. OB-010 only contained one partial garnet (garnet has been dissolved during retrogression or cut during thin section preparation; Figure 9d). OB-023 and JD-100 both contain multiple sub to anhedral garnets. Porphyroblasts contain a minor inclusions, and their mineralogy is identical to that in the matrix including quartz, plagioclase, and biotite. All garnets from this area of the North-rim show a distinctly high spessartine composition ranging from; OB-010: (X_{sps} 37.4-39.2), JD-100: (X_{sps} 59.7-69.1) and OB-023: (X_{sps} 46.3-51.6). All porphyroblasts display a concentration of FeO(t), ranging from 15.11 to 28.49 wt%, in all grains with an inverse correlation with of MnO (36.36-53.07 wt%). Both the CaO (<3.3 wt%) and MgO (<1.6 wt%) components are low (**Figure 9d-f**).

There is a difference of Mn content in garnet from the North-rim biotite garnet schist, the Central-belt, and the samples in the vicinity of Musselwhite Mine. Major element compositions of garnets, as well as by Kalbfleisch (2012) and Gagnon (2015), regardless of setting, are dominantly almandine (X_{alm} 59-81) while North-rim metasediments samples display consistently high Mn values ($_{Xsps}$ 36-62) (**Figure 10a**). The high MnO contents of the garnet do not correlate with the MnO contents of the bulk rock in the North-rim which are low (0.05-0.11 ppm), however this may be due to alteration and silicification. Near-mine biotite garnet schist (OB-035) display similarly low MnO contents (0.11-0.13), however contain zoned, primarily almandine garnets (**Figure 9**). The flat major element geochemical patterns of the garnets and the distinctly high Mn content of garnets from the North-rim indicate possible resetting due to contact metamorphism.

Three porphyroblasts were selected for analysis based on size and lack of inclusions from the garnet-biotite schist (JD-033) of the Central-belt. The size of garnet is similar (~500 µm) amongst other garnet grains throughout the sample. Fractures occur parallel across the grain, but perpendicular to foliation and contain biotite with minor chloritization. The garnet is primarily almandine (X_{alm} 59.9-67.1) but shows slightly lower FeO(t) concentrations (6.70-12.79 wt% less) than those in the metapelite (OB-035) sample taken in the vicinity of Musselwhite Mine (**Figure 9a**). FeO(t) concentrations show a gradual increase from core to mid-grain (X_{alm} 59.9-67.0) and then a drop again in concentration (X_{alm} 67.0-62.9) toward the rim (**Figure 9b**). MnO component follows a similar trend from core to rim with spessartine component showing a typical decrease in concentration from core to rim (X_{sps} 15.8-12.8) and an increase at the rim (X_{sps} 12.8-17.1). The CaO component also displays a decrease from core to mid-grain (X_{grs} 16.9-13.2) followed by a slight increase at the rim (X_{grs} 13.2-15.3). MgO displays a gradual increase in concentration to mid-grain (X_{pyr} 4.4-5.7) and sharp decrease at the rim (X_{pyr} 5.7-4.4) (**Figures 9b, 10b and Appendix I**). MgO patterns indicate typical prograde metamorphism, while increased CaO concentration occurred during plagioclase breakdown (or in the presence of Ca-rich fluids) when compared to the metapelitic sample to the east, the garnets display less interaction with multiple Ca-rich fluid events or due to Ca-rich protolith.

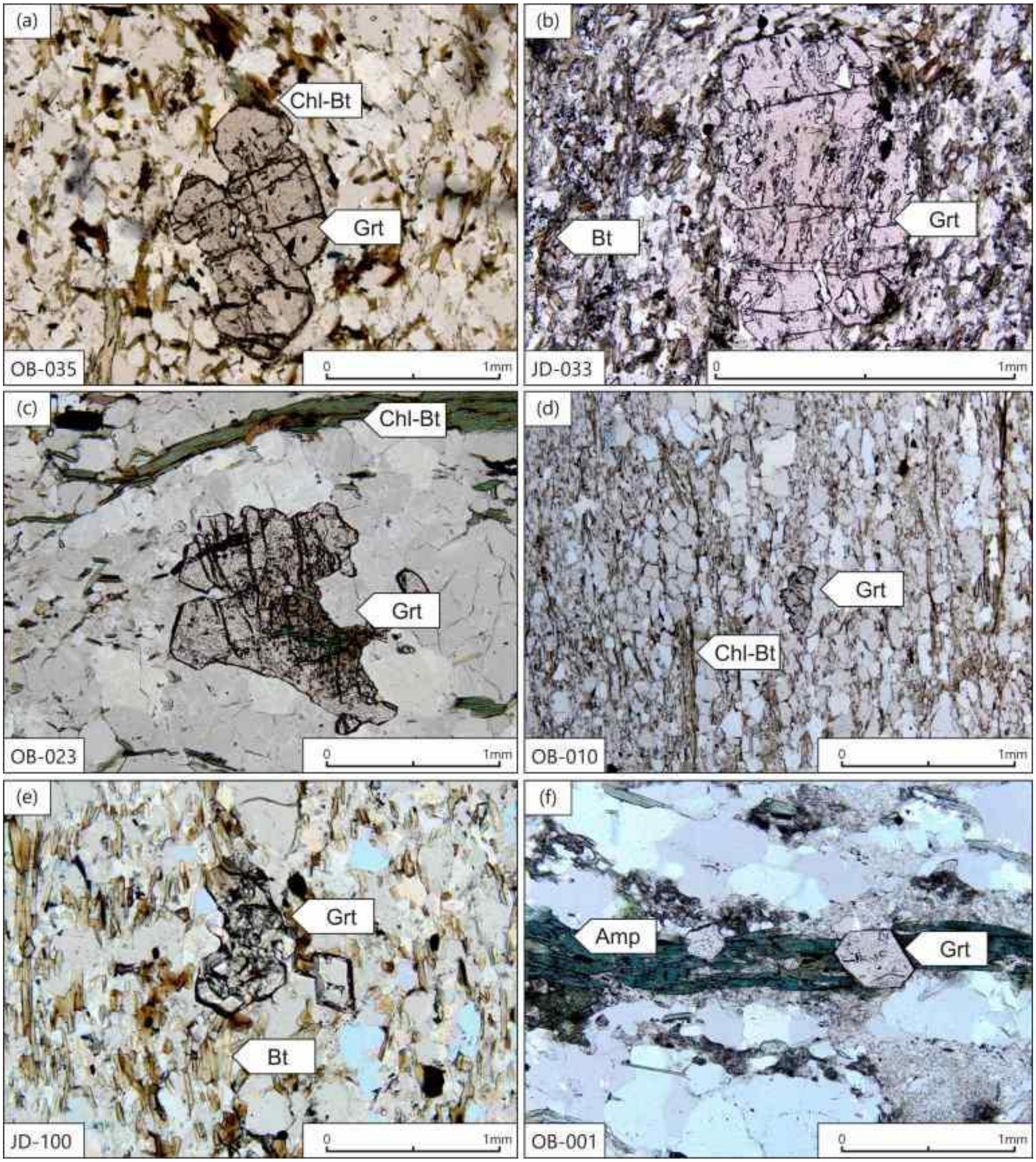

Figure 8: *Garnet porphyroblast photomicrographs in plane light. A) Metapelite taken from the shore of Zeemal Lake (Sample OB-035) Note matrix foliation present in garnet and strain shadow pitching to the left of the image. B) Biotite garnet schist sampled from Markop Lake shear zone (Sample JD-033). Note truncated sub horizontal foliation preserved in strain shadow which is truncated by the matrix foliation. C-E) North-rim biotite garnet schist (Samples OB-023, OB-010, JD-100). F) North-rim amphibolite euhedral garnets within foliated amphibole and chloritized biotite (Sample OB-001). Note sample has been carbon coated. Chl: chlorite, Bt: biotite, Grt: garnet, Amp: amphibole.*

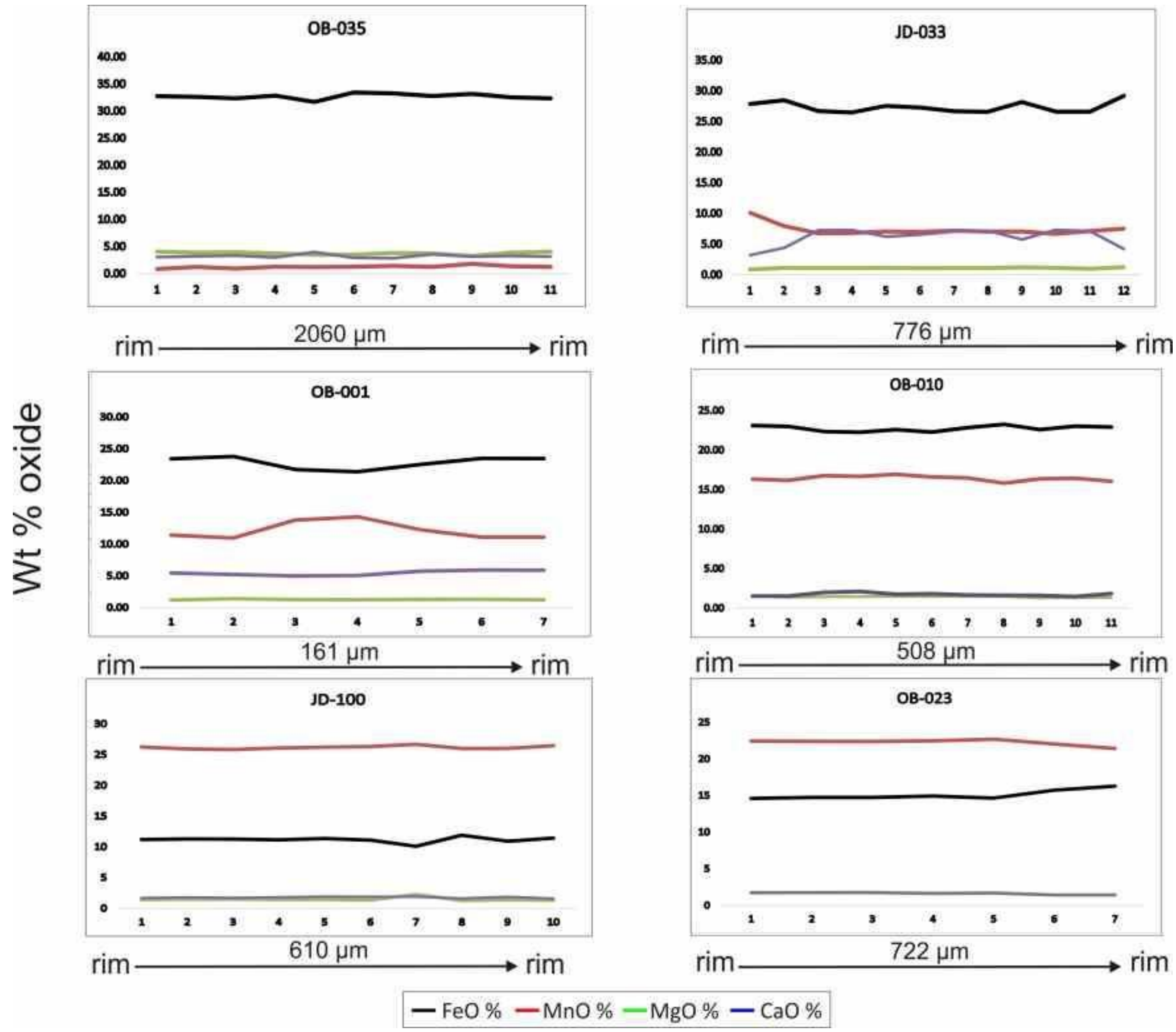

Figure 9: Major element weight oxide % of garnet porphyroblasts. The grains are shown in Figure 10. Analysis of completed from rim to rim. Distance from rim to rim indicated on Y-axis. Gray points on X-axis indicate each analysis per grain. B): JD-033 and C) OB-001 grain analysis traverse are displayed in Figure 12.

Table 4: EMPA garnet major element transects from rim to rim of biotite garnet schists from across the Zeemal Heaton Lake assemblage.

Sample	FeO	MnO	MgO	CaO
OB-035-01	32.75	0.85	4.06	3.05
OB-035-02	32.65	1.27	3.91	3.23
OB-035-03	32.36	0.94	3.97	3.34
OB-035-04	32.85	1.30	3.71	2.99
OB-035-05	31.68	1.24	3.52	3.99
OB-035-06	33.45	1.29	3.50	2.95
OB-035-07	33.30	1.45	3.81	2.84
OB-035-08	32.78	1.25	3.74	3.60
OB-035-09	33.19	1.81	3.28	3.16
OB-035-10	32.56	1.38	3.87	3.28
OB-035-11	32.36	1.26	4.07	3.17
JD-033-01	27.89	10.12	0.87	3.19
JD-033-02	28.47	7.95	1.14	4.39
JD-033-03	26.73	6.77	1.10	7.26
JD-033-04	26.48	6.82	1.11	7.30
JD-033-05	27.55	7.07	1.13	6.20
JD-033-06	27.29	7.02	1.08	6.56
JD-033-07	26.69	7.19	1.10	7.06
JD-033-08	26.59	7.06	1.10	7.19
JD-033-09	28.18	7.07	1.21	5.76
JD-033-10	26.62	6.67	1.13	7.33
JD-033-11	26.63	7.15	0.99	7.14
JD-033-12	29.20	7.53	1.23	4.21
OB-001-01	22.14	13.69	1.31	4.88
OB-001-02	24.70	10.88	1.34	4.90
OB-001-03	24.53	10.90	1.42	5.16
OB-001-04	20.18	15.65	1.44	4.97
OB-001-05	22.32	12.89	1.26	5.56
OB-001-06	20.85	14.97	1.27	5.26
OB-001-07	17.44	17.96	1.24	5.67
OB-001-08	16.99	18.34	1.25	5.51
OB-001-09	17.71	17.25	1.32	5.92
OB-001-10	17.83	17.15	1.30	5.66
OB-010-01	23.11	16.34	1.56	1.54

OB-010-02	23.01	16.18	1.38	1.54
OB-010-03	22.34	16.78	1.45	2.00
OB-010-04	22.27	16.69	1.46	2.11
OB-010-05	22.59	16.96	1.49	1.78
OB-010-06	22.30	16.60	1.49	1.84
OB-010-07	22.86	16.49	1.49	1.67
OB-010-08	23.27	15.81	1.49	1.64
OB-010-09	22.59	16.38	1.30	1.62
OB-010-10	23.03	16.45	1.33	1.49
OB-10-11	22.91	16.07	1.33	1.85
JD-100-01	11.2	26.26	1.44	1.7
JD-100-02	11.31	25.94	1.50	1.79
JD-100-03	11.28	25.84	1.52	1.71
JD-100-04	11.17	26.09	1.44	1.8
JD-100-05	11.37	26.24	1.47	1.93
JD-100-06	11.11	26.32	1.37	1.9
JD-100-07	10.09	26.71	2.26	1.91
JD-100-08	11.9	26	1.29	1.62
JD-100-09	10.93	26.03	1.41	1.89
JD-100-10	11.45	26.47	1.34	1.61
OB-023-01	14.62	22.44	1.71	1.79
OB-023-02	14.76	22.43	1.75	1.8
OB-023-03	14.75	22.4	1.76	1.76
OB-023-04	14.94	22.48	1.66	1.66
OB-023-05	14.66	22.72	1.72	1.7
OB-023-06	15.74	22.06	1.43	1.41
OB-023-07	16.3	21.44	1.44	1.41

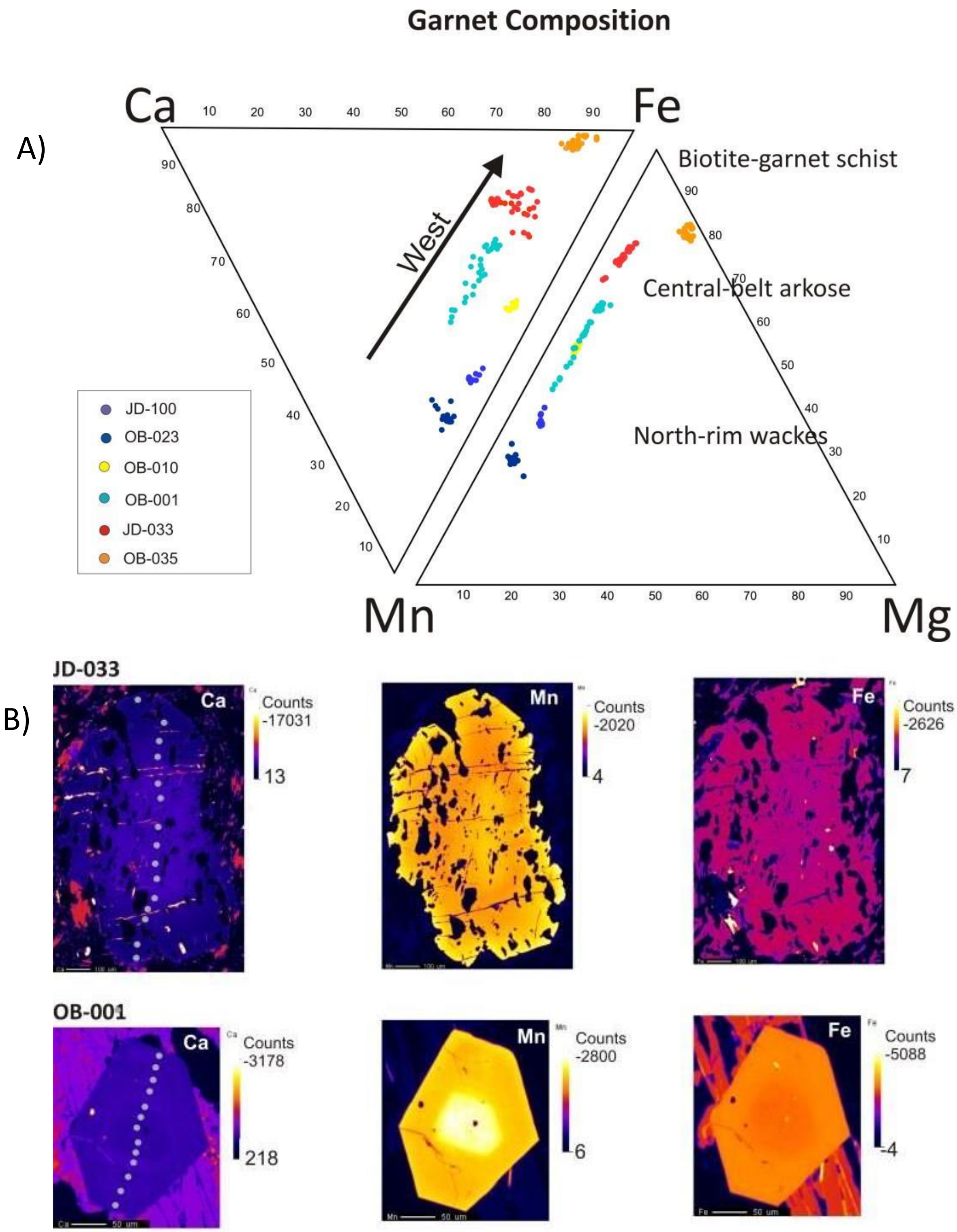

Figure 10 A: Ternary plots of major element molar compositions of garnet porphyroblasts from the Zeemal Heaton Lake assemblage. A trend of increasingly Fe-rich garnet occurs towards the western portion of the belt. B: Chemical maps of garnets

displaying Ca (Kα), Mn (Lα) and Fe (Lα) from JD-033 (Central-belt biotite garnet schist) and OB-001 (North-rim amphibolite). Analysis traverse is indicated by gray dots displayed on garnet porphyroblast Ca maps.

Structure and Deformation

Near-mine metasediments

Biotite garnet schists (OB-034, 035) in the vicinity (<2km) of the Musselwhite mine display a strong foliation with the intensity becoming less penetrative to the south, no original bedding was identified. The foliation strikes WNW and dips sub-vertical. As the foliation intensity decreases, 1 mm to 3 cm garnet porphyroblasts become visible. A pegmatite intruded post-deformation along strike, and the matrix foliation locally intensifies against it.

Garnets display sigmoidal inclusion trails displayed in Figure **8a**. These inclusions include quartz, feldspar, ilmenite, and biotite. The inclusions trails show crenulations perpendicular to the dominant sub-vertical matrix foliation. These oblique inclusion trail geometries are still visible in the matrix but rotated by a younger steep foliation producing event (**Figure 8a**). Therefore the garnets have undergone deformation before the main penetrative foliation defined by D_2.

Markop Lake conglomerates

OB-003 and OB-004 have no foliation apparent, but recrystallization of quartz and metamorphic biotite and muscovite crystallized likely due to contact metamorphism caused by the gabbroic intrusion. Biotite and muscovite form euhedral laths and do not appear detrital. The lack of deformation is possibly due to strain in the partitioning belt.

OB-111 deformation in most of the outcrop and appears more mineralogically mature consisting of a quartz arenite matrix with aggregated biotite. Crossbedding is apparent with tops to the south away from the clast zone. Again, strain partitioning in the belt likely played a role in the lack of deformation present.

OB-005 and OB-006 contain deformed and elongated clasts at the contact with the Opapimiskan metavolcanic rocks (**Figure 4b**). Clast elongation and abundance decrease away from the contact into a clast-free, undeformed zone. Quartz veins obliquely crosscut foliation throughout and appear to have resulted from dextral shearing along the latter.

North-rim metasediments

The amphibolite (OB-001) taken ~5 km west of Heaton Lake along the North-rim is intensely deformed (strike EW and sub-vertical dip) and highly siliceous consisting of abundant primary quartz and also secondary quartz veining.

The biotite garnet schists near Heaton Lake have a strong foliation defined by biotite striking WSW-EW with sub-vertical dip as is common across the belt. The foliation intensity varies from moderate to strong over a 250 x 50 m sample area regarding the spacing between foliation and the amount of quartz veining (**Figure 4c-d**). Plagioclase porphyroclasts display clockwise curving in thin sections (in the photomicrograph, **Figure 5d**) indicated by inclusion trains at both the top and bottom. Foliation (D_2) defined by biotite in the matrix truncates foliation observed in the core of the porphyroblast (**Figure 5d**). Later-stage unfoliated biotite overprints foliated biotite and is interpreted to have formed after deformation. As the thin section was cut perpendicular to the dominant sub-vertical matrix foliation, inclusion trails in garnet porphyroblasts from OB-023 (**Figure 8c**) indicate the garnet grew in an earlier foliation event as it preserves an originally gently dipping foliation in its core. Garnet then grew again over the later foliation in its top rim in a deformation event producing gently dipping crenulations (**Figure 8c**). OB-010 garnet contains tiny (less than 0.5 mm) inclusions that are vertical (parallel to those in the matrix), and define a foliation that likely predates that in the matrix. To form these inclusion trails in the garnet porphyroblasts, they had to grow during a deformation event defined by a gentle axial plane crenulation and then a later deformation even oblique to this foliation (**Figure 8d**).

Central-belt metasediments

Central-belt metasediments display increasing deformation and quartz veining occurs with proximity to the Totogan shear zone on the Northern margin with anastomosing foliation planes (**Figure 4d**). Foliation strike range through WSW-EW-WNW with a sub-vertical dip as seen across the North Caribou greenstone belt.

Garnet porphyroblasts in the most western Central-belt biotite garnet schists show sigmoidal inclusions trails of matrix material including quartz, plagioclase, and biotite with minor ilmenite and magnetite. Inclusions indicate these garnets also grew in an oblique crenulation event that is well preserved in the trails (**Figure 10b**). It is also possible a subsequent oblique truncational foliation is preserved the strain shadow and then in turn truncated by the matrix foliation (D_2) defined by biotite (Figure 10b).

Overall, all metasediments studied within the Zeemal Heaton Lake assemblage display WSW-EW-WNW foliation with a sub vertical dip which defines D_2, thus the sediments have undergone a minimum D_2

deformation. The porphyroblast inclusions trails indicated a deformation event before D_2, however, do not display isoclinal folding which delineates D_1.

Geochronology

24 samples were chosen for U-Pb detrital zircon dating across the belt. However only four samples yielded zircons >30 µm for analysis. The remaining samples contained high Zr (>100ppm) and grains <20 µm were visible in thin section, but zircon grains were not able to be recovered during heavy mineral separation due to the sieve size >63µm selected for this study. The analyzed samples include two samples from the North-rim metasediments and two samples from the Central-belt metasediments. Sample locations are displayed in **Figure 2** and **Table 2**. The grain morphology is described below associated with age population. Full analytical results and grain images are displayed in **Appendix IV and Table 5.**

North-rim amphibolite

Sample OB-001 yielded 41 zircon grains that range between 40 and 120 µm in size. They occur throughout the matrix, mostly oblique to foliation along matrix quartz and feldspar grain boundaries. The grains occur in contact with most matrix minerals, usually quartz and chloritized biotite. All zircon grains contain inclusions of phosphate minerals, primarily monazite with minor apatite. Zircon grains with abundant inclusions were discarded. Two grains were discarded for discordance >15%. Discordance was calculated using 1-$^{206}Pb/^{238}U$ age/$^{207}Pb/^{206}Pb$. Most grains are fractured but still maintain fine oscillatory zoning in back scattered electron and cathodoluminescence images (**Figures 12a-h)**. Four main concordant age populations spanning ~360 Ma from 2698 ± 20 to 3060 ± 30 Ma were dated from the remaining 34 grains (**Figure 11b**). The first major peak occurs between 2698 ± 20 to 2762 ± 20 Ma (n=12). The majority of grains from this population (n=8) are small (≤50 µm), equant, and subrounded with a ≤2:1 length to width ratio (**Figures 12a-d**). They display fine zoning and little fracturing. Three elongate grains (~200 µm) with a columnar habit and 3:1 length to width ratios also display oscillatory zoning. One of the elongate grains (75 x 150 µm) displays at xenocrystic core with no zoning and a mottled appearance. The rim (15-25 µm) shows fine zoning. The core (60-75 µm) was not analyzed, but the rim yielded an age of 2707 ± 21 Ma. This was the only xenocrystic core observed in this population. The second peak occurs between 2844 ± 19 to 2903 ± 27 Ma (n=14). The majority of grains from this population (n=10) are elongate (3:1) and columnar (100-150 µm). Three grains have a 2:1 ratio (50-75 µm). They are euhedral and display a rectangular and pointed crystal habit on opposing points of the c- axis. Four grains have a 2:1 (50-75 µm) habit and appear sub rounded due to ablation during sedimentation. All grains display moderate to intense fracturing and zoning is not as pronounced or bright as in the >2698 population. The third peak occurs between 2922 ± 20 to 2984 ± 17 Ma (n=6). All but one grain displays an equant, rectangular crystal habit (50-85 μm) with primarily parallel zoning. One acicular grain (40 x 150 μm) with bright, fine zoning gives an age of 2983 ± 19 (**Figure 12e-f**). The final age population contains only two grains dated at 3048 ± 17 and 3060 ± 30 Ma. The grain dated 3048 ± 17 is a fractured partial grain (50 x 150 μm) with parallel zoning (**Figures 12g-h**). The 3060 ± 30 Ma grain is euhedral and displays columnar crystal habit with a 3:1 ratio (50 x 150 μm) and fine zoning from centre to rim. All zircon grains display Th/U > 0.28 (mean 0.57)

Table 5: LA-ICPMS U-Pb results of the youngest detrital zircons from the North-rim and Central belt of the Zeemal Heaton Lake assemblage

Sample	**Location**	**$^{207}Pb/^{206}Pb$**				**$^{207}Pb/^{235}U$**				**$^{206}Pb/^{238}U$**					
		Ratio	2δ	Age	2δ	Ratio	2δ	Age	2δ	Ratio	2δ	Age	2δ	Th/U	Discordance*
OB-001-31	NR	0.1842	0.0037	2698	20	12.59	0.27	2648	21	0.4951	0.0068	2592	30	0.50	3.1
OB-001-45	NR	0.1860	0.0036	2706	22	13.90	0.28	2744	20	0.5422	0.0056	2792	24	0.69	0.8
OB-012-34	NR	0.1852	0.0039	2696	39	11.95	0.49	2603	50	0.4766	0.0150	2518	70	0.58	6.6
OB-012-14	NR	0.1879	0.0034	2716	15	13.73	0.30	2730	21	0.5286	0.0089	2735	37	0.75	0.06
OB-031-10	CB	0.1967	0.0022	2799	18	12.61	0.39	2650	35	0.4663	0.0094	2467	43	0.77	11.9
OB-031-37	CB	0.1965	0.0012	2800	6.7	13.75	0.31	2733	22	0.5067	0.0062	2641	27	0.60	5.7
JD-101-43	CB	0.2002	0.0034	2831	19	14.99	0.32	2815	20	0.5409	0.0088	2787	35	0.34	1.6
JD-101-22	CB	0.2011	0.0035	2833	16	14.68	0.46	2796	35	0.5430	0.0160	2795	41	0.30	1.3

*Discordance = (1-$^{206}Pb/^{238}Pb$ age/$^{207}Pb/^{206}Pb$ age)

NR: North-rim, CB: Central belt.

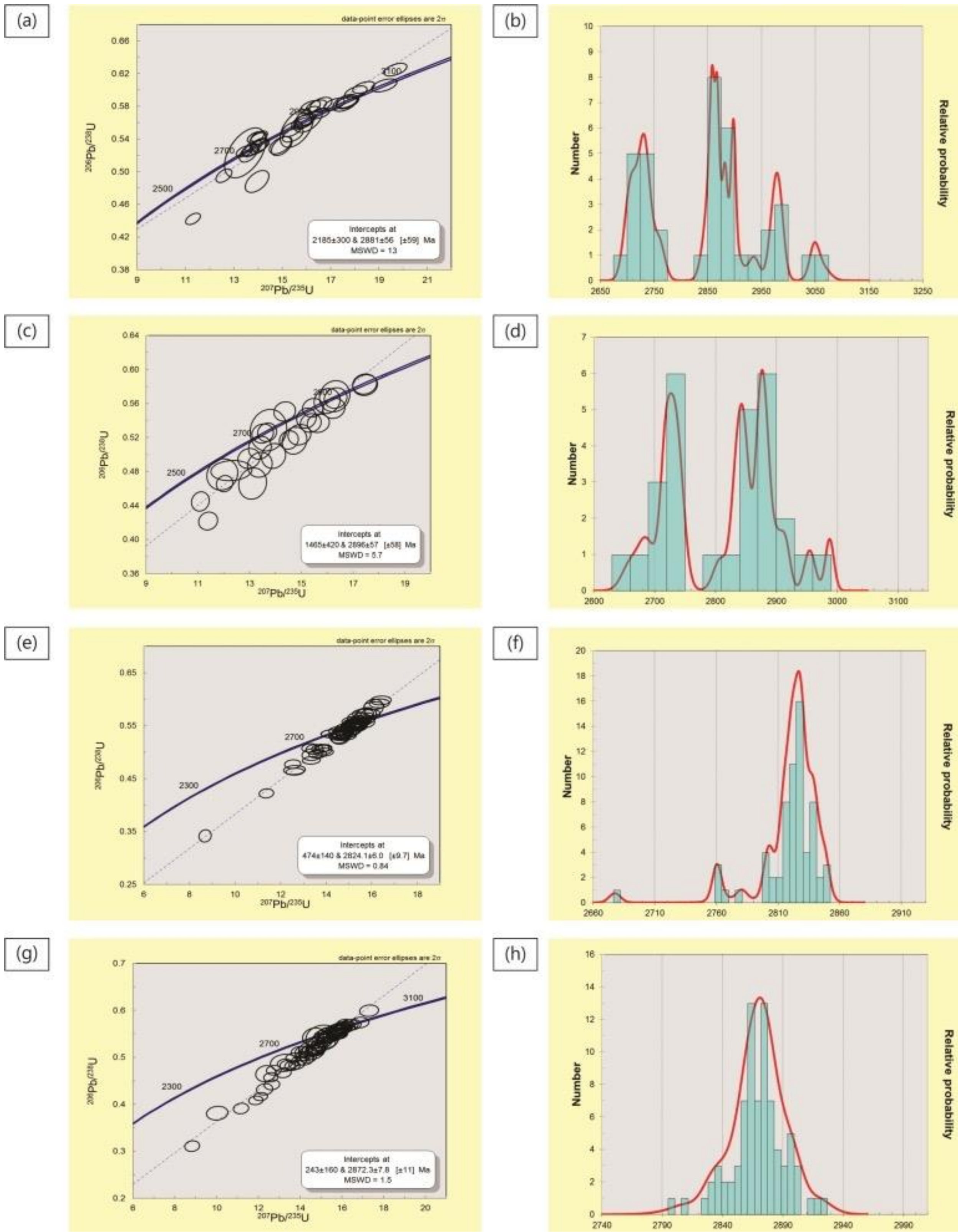

Figure 11: U-Pb Zircon Concordia plot and age frequency histogram. a) North-rim OB-001 Concordia. b) North-rim OB-001 age frequency. c) North-rim OB-012 Concordia. d) North-rim OB-012 age frequency. e) Central-belt OB-031 Concordia. f) OB-031 age frequency. g) Central-belt JD-101 Concordia. H) Central-belt JD-101 age frequency. All Concordia plots with 2δ error.

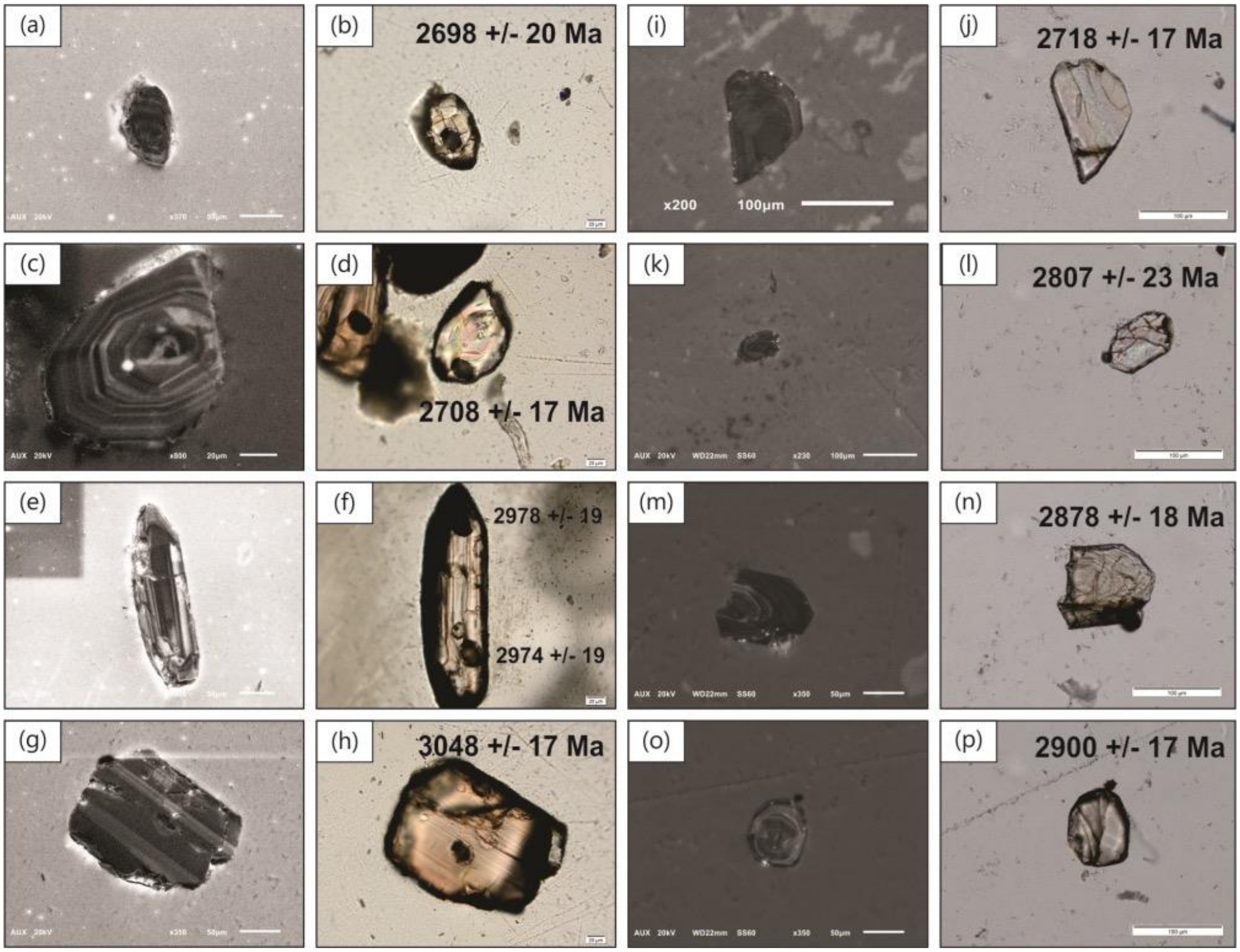

Figure 12: Cathodeluminescence (CL) and plane light (PL) images of selected zircon grains from each age population in the North-rim. a-b) CL and PL OB-001-31 dated 2698±20 Ma. c-d) CL and PL OB-001-38 dated 2708±17 Ma. e-f) CL and PL OB-001-15 dated 2978 and 2974±19 Ma. g-h) CL and PL OB-001-23 dated 3048±17 Ma. i-j) CL and PL OB-012-14 dated 2718±17 Ma. k-l) CL and PL OB-012-11 dated 2807±23 Ma. m-n) CL and PL OB-012-22 dated 2878±18 Ma. o-p) CL and PL OB-012-01 dated 2900±17 Ma.

North-rim biotite garnet schist

Sample OB-012 was collected ~200 m from the sample JD-100 of Duff (2014), near the bank of Heaton Lake. Sample OB-012 consists primarily of quartz and plagioclase feldspar with biotite defining the foliation. No muscovite is present in this sample. Zircon grains occur between grain boundaries and within foliated biotite. The sample yielded 31 grains of zircon. Grains are small, typically ≤50 µm, which includes both euhedral and partial grains (most likely broken during sample preparation). No inclusions were noted or analyzed. Most grains were completely ablated during analysis. Three grains were discarded for discordance >15%. The sample contains two main age populations which define a discordant line; however discordance does not reach >15%. 15 grains show <5% discordance with multiple grains occurring in each age population (**Figures 11c-d**). The first population occurs between 2684 ± 23 to 2742 ± 19 Ma (n=9) with seven concordant (<5%) grains. This population includes eight partial (fractured) grains and one euhedral grain. All zircons display fine continuous oscillatory zoning although crystal habit was difficult to determine for partial grains (~50 µm; **Figures 12i-j**). The euhedral grain is ~100µm, elongated (3:1), columnar and rounded. The second age population occurs between 2808 ± 11 to 2885 ± 17 Ma (n=13) with eight concordant grains. This population shows a similar trend with only partial grains (<50 µm) and one euhedral (2:1) grain (~100 µm). All zircon grains in this population also show fine continuous zoning with rounded to angular crystal habit (**Figures 12k-n**). The final population occurs between 2900 ± 17 and 2987 ± 14 Ma (n=4). This includes two partial and two euhedral grains. The euhedral grains are equant (~50 µm), subrounded with continuous zoning (**Figures 12o-p**). This sample has very similar age populations to the North-rim amphibolite to the west (OB-001), but it is hard to compare crystal habit as most grains are fractured and broken during the sample preparation. All grains have a Th/U >0.21 with a mean of 0.87.

Central-belt metasediments

A total of 57 zircon grains were recovered from the muscovite quartz schist OB-031. OB-031 occurs to the east and outside of Markop Lake deformation zone and contains metamorphic K feldspar, rare plagioclase feldspar, and quartz with the foliation defined by muscovite and trace biotite. Central-belt metasediments show abundant evidence for hydrothermal alteration consisting of veined and disseminated clinozoisite and calcite. Zircon grains occur throughout the matrix but are primarily associated with fabric forming muscovite and rare biotite. Six analysis were discarded for discordance >15%. Four grains were not selected for dating due to lack zoning. These grains appear mottled, are highly fractured, and contain abundant inclusions of phosphate minerals, apatite and monazite are common and abundant (**Figures**

16a-h). Zircon grains from OB-031 show a darker brown shade in transmitted light microscope than seen in JD-101 to the east or any of the North-rim lithologies. Grains plot with a lower intercept of 474 ± 140 Ma and an upper intercept at 2824 ± 6 Ma. All the discarded grains (due to discordance or texture) display ages between 2222 ± 19 Ma to 2616 ± 12 Ma. One main continuous age population plotting on or very close to Concordia, occurring between 2799 ± 19 to 2849 ± 8 Ma (**Figures 11e-f**). There is little variation in crystal habit of grains with the majority being euhedral, elongate (3:1) and 150-250 µm with sub-rounded edges (**Figures 13a-h**). Several grains were analyzed at the core and rim and show very similar ages, however, three grains occur with younger cores than rims, and two grains display older cores than rims. Grains with younger cores display mottling of the core but finely zoned rims. The cores are dated between 2678 ± 9.4 to 2761 ± 6 Ma while the rims are dated between 2815 ± 7 to 2826 ± 7 Ma. The two grains which display younger rims returned ages of 2735 ± 7 Ma and 2786 ± 8 Ma with 2823 ± 6 and 2828 ± 7 Ma cores. These grains have dark overgrowths in CL without zoning and apparent oscillatory zoned igneous cores. All grains show minor differences in Th/U between core and rim, showing higher Th/U in rims or cores, depending on the sample. All grains have a Th/U > 0.23 the mean value is 0.44, which is lower than observed in the North-rim. Zircons which appear mottled or lack zoning have not been included in the presented data. All U-Pb ages of zircon included in the study are interpreted to be igneous.

JD-101 was collected by Duff (2014) in the summer of 2011, ~6 km to the east of OB-031 and shows very similar mineralogy to the previous sample, OB-031. The abundant veined and disseminated hydrothermal calcite and clinozoisite with coarse muscovite overgrowing the foliation, however, does not occur in this sample location. Zircon grains occur throughout the matrix and but are associated primarily with fabric forming micas. At total of 66 grains were recovered from the sample. Most grains were analyzed on core and rim, with both giving similar ages, less than 20 Ma difference. All grains contain oscillatory zoning, are euhedral and range in size 100-250 µm. They vary between 2:1 and 3:1 length to width ratios, but there does not appear to be any correlation between these ratios and age (**Figures 13i-p**). Fractures and inclusions are common. A minor population of grains (n=6) is without zoning which may be a result or alteration or total homogenization of zoning these grains or spots were not analyzed because they would likely not return igneous dates. There were no xenocrystic cores. Nine analysis were discarded for high common ^{204}Pb >2%. Ten grains were discarded for high discordance >15%. The zircon grains which were not discarded plot on or near Concordia, with an age population between 2831 ± 18 to 2927 ± 21 Ma and lower and upper intercept age of 243 ± 60 and 2872 ± 8 Ma (**Figure 11g**). All grains analyzed without inclusions or loss of zoning have a Th/U >0.23 with a mean value of 0.54.

Kalbfleisch (2012) dated zircon grains in a sample in proximity to JD-101 *in-situ* and determined an upper intercept age of 2858 ± 8 Ma with the six younger ages (1694-2782 Ma) and three older ages (2904-2916 Ma) which failed to define a significant discord of their own. She interpreted that these zircon ages had no significance. The main cluster of ages at ~2826-2926 Ma (n=78) from this study overlaps with Kalbfleisch (2012), giving a very robust population of ages.

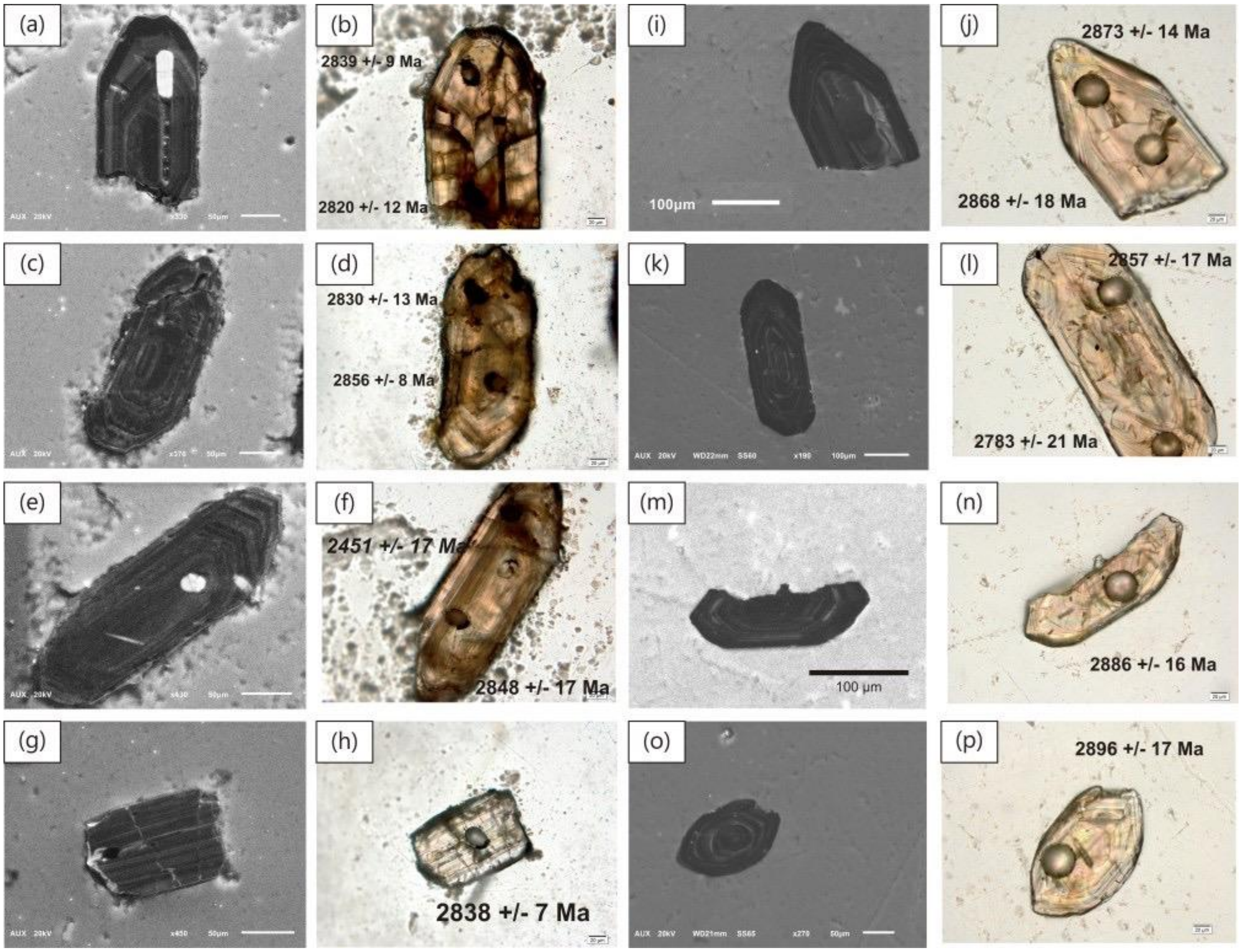

*Figure 13: Cathodoluminescence (CL) and plane light (PL) images of select zircon grains from each age population in the Central-belt. a-b)*1 CL and PL OB-031-48 dated 2839±9 and 2820±12 Ma. c-d) CL and PL OB-031-16 dated 2830±13 and 2856±8 Ma. e-f) CL and PL OB-031-05 dated 2451±17*2 and 2848±17 Ma. g-h) CL and PL OB-031-81 dated 2838±7 Ma. i-j) CL and PL JD-101-06 dated 2873±14 and 2868±18 Ma. k-l) CL and PL JD-101-73 dated 2857±17 and 2783±21 Ma. m-n) CL and PL JD-101-37 dated 2886±16 Ma. o-p) CL and PL JD-101-28 dated 2896±17 Ma. Circles indicate laser ablation locations.*

**1Note the mottled dark brown appearance in zircons from OB-031 (b,d and f).*

Detrital Zircon Trace Element Geochemistry and Alteration

Trace element analysis of zircon was also completed on grains used for U-Pb dating. Trace element analysis of the dated zircons was used to try and delineate between igneous, metamorphic and hydrothermally alerted grains. It was also used for comparison of compositions in the surrounding intrusive complexes zircon grains reported by Van Lankvelt (2013), to determine provenance. Three samples previously dated from the North-rim, including OB-001, and JD-100 and JD-071 (dated by Duff, 2014) and two samples from the Central-belt (OB-031 and JD-101) were also analyzed. REE patterns for zircons in this study and zircons analyzed Van Lankvelt (2013) are displayed in **Figure 14**.

Ablation locations were chosen from U-Pb dated and non-dated grains based on euhedral crystal structure, oscillatory zoning and lack of visible inclusions. Although inclusions were not visible on the surface of the selected grains, many mineral inclusions were detected during the ablation. They include monazite and apatite and Fe/Ti-rich minerals.

Raw data was first reduced using GLITTER. The geochemical data was further reduced in Excel to areas with no inclusions; the reduction resulted in a maximum of 10-35s of clean ablation times for most grains. In some grains, multiple, non-consecutive ablation times were used to avoid multiple small inclusions. Even with the reduced clean data, the abundance of inclusions may have an impact on the REE plots and the subsequent interpretations. Ti concentration is extremely variable due to small inclusions, even in reduced ablation times and therefore Ti-in-zircon thermometry could not be accurately completed. Possible alteration and inclusion effects have been considered. Full analytical results displayed in **Appendix IV and V.** Select geochemistry is displayed for all grains in **Table 6**.

North-rim metasediments

One amphibolite (OB-001) was analyzed from the North-rim. A total of 10 spots were analyzed on 10 grains. All zircon grains contain inclusions of apatite and minor monazite as determined by the LA-ICP-MS. Fe and Ti-spikes are also common, which may or may not be associated with REE spikes. Three grains were discarded due to abundant inclusions, even after reduction. This included grains with Ca values > 3258 ppm, Fe >770 ppm, and/or P >509 ppm. The inclusion-free zircons contain four main zircon populations, which fall between 2698 ± 20 to 2762 ± 20 Ma (n=5), 2844 ± 19 to 2903 ± 27 Ma (n=1), 2922 ± 20 to 2984 ± 17 Ma (n=0) and 3048 ± 17 and 3060 ± 30 Ma (n=1). Detailed zircon age populations and morphologies are described previously. Two samples from 2844 ± 9 to 2903 ± 27 Ma age population and one sample from the 3048-3060 Ma age population had to be discarded due to inclusions, leaving only two reliable grain outside the ~2698-2762 Ma age population. All samples analyzed for trace element concentrations fall on or near Concordia and have a Th/U ratio between 0.55-1.28. They show typical HREE enrichment over LREE but with a wide variation in slope (Figure 17). All zircons have variable LREE abundances with sums between 40-494 ppm and a moderate variation in HREE abundance, with sums between 268-891 ppm (**Figure 14a**). Eu anomalies are weakly negative between 0.45-0.69. When compared with geochemical signatures of zircon grains from the surrounding batholiths (Van Lankvelt, 2013), the steep average Lu/Nd (2.0) of detrital zircon grains shows the main correlation with values of the Schade Lake complex. The sum of the REE abundances of zircon grains recovered from OB-001 plot consistently lower than the North Caribou batholith (**Figure 14a**). Overall, the values plot with median to low LREE abundances when compared to the zircons recovered directly from the batholiths (**Figure 14a**).

Two biotite garnet schist detrital zircon samples (JD-100 and JD-071) collected and dated by Duff (2014) were also used for trace element analysis in this study. A total of 9 spots from 9 grains were analyzed from JD-100. Three grains were discarded due to abundant apatite inclusions with Ca >161 ppm and P >458 ppm. The mineralogy of inclusions appears similar to those seen in JD-071 and includes apatite and monazite and Fe±Ti oxides. Grains show a wider range (than JD-071) of LREE slopes with the sum of HREE abundances between 509-1112 ppm and the sum of LREE abundances between 94-583 ppm. Grain JD-100-10 shows relatively elevated LREE compared to other grains and thus a flatter REE slope (**Figure 14b**). Th/U ratios fall between 0.24-0.81. REE abundances again plot overlapping with the Southern Batholith and Schade Lake complex but below values found in the North Caribou batholith (**Figure 14b**).

Table 6: Select trace elemental concentrations from all zircon grains analyzed from the both the North-rim (NR) and Central belt (CB).

Zircon	Age	Location	P	Ti	Ca	Fe	^{238}U	Nb	^{204}Pb	^{206}Pb	^{207}Pb	^{208}Pb
OB-001-45	2706	NR	406	13.8	139	95	152	3.62	2.19	315	64	33
OB-001-38	2708	NR	521	11.7	620	95	227	1.43	1.20	485	98	82
OB-001-08	2724	NR	111	6.8	<79	36	617	3.46	1.48	1314	270	101
OB-001-19	2734	NR	204	5.1	116	66	221	0.78	1.08	514	106	34
OB-001-54	2759	NR	263	10.6	<54	78	207	1.24	2.37	454	103	50
OB-001-11	2865	NR	260	10.1	<64	88	200	1.11	1.17	456	91	74
OB-001-12	3048	NR	354	3.1	<86	75	148	0.72	1.30	389	97	32
JD-100-01	NA	NR	267	7.6	95	202	294	1.53	1.75	624	137	26
JD-100-02	NA	NR	211	8.7	<58	65	202	1.34	1.02	472	107	21
JD-100-03	NA	NR	495	34.8	56	173	429	3.92	0.96	874	198	26
JD-100-04	NA	NR	202	6.6	<59	94	175	0.81	1.22	351	74	36
JD-100-05	NA	NR	110	5.9	<53	241	241	1.18	1.24	498	111	15
JD-100-06	NA	NR	310	3.6	<41	115	146	0.75	2.06	315	71	16
JD-100-09	NA	NR	316	69.4	130	373	303	2.57	1.83	644	144	46
JD-071-01	NA	NR	328	10.7	190	96	500	3.26	2.86	1240	298	61
JD-071-03	NA	NR	452	6.9	157	62	362	2.09	2.35	882	213	44
JD-071-04	NA	NR	415	3.5	238	16	434	2.08	4.29	982	242	52
JD-071-05	NA	NR	231	6.1	153	120	179	1.04	2.90	446	107	16
JD-071-09	NA	NR	494	177	177	87	386	2.76	6.55	973	218	43
JD-101-10	NA	CB	484	33.8	561	302	397	2.57	3.66	874	196	67
JD-101-12A	NA	CB	225	66.2	<71	691	221	1.42	4.66	391	89	19
JD-101-12B	NA	CB	408	74.1	<69	411	564	4.98	2.10	1134	260	110
JD-101-20	2903	CB	262	7.7	<32	27	266	1.40	1.46	592	138	31
JD-101-31A	2800	CB	194	25.1	<81	328	500	2.66	2.21	1137	257	24
JD-101-31B	2800	CB	358	6.5	150	577	232	0.94	2.96	525	121	36
OB-031-77	2830	CB	400	46.7	136	139	526	2.78	1.90	1271	282	58
OB-031-38	2827	CB	238	5.9	254	902	513	1.09	5.10	536	122	39
OB-031-37B	2817	CB	231	12.9	222	1091	157	1.51	2.30	397	88	25
OB-031-29	2827	CB	384	40.1	598	736	912	7.15	1.20	2350	519	116
OB-031-05	2848	CB	108	9.6	469	213	791	5.03	1.04	1979	443	141

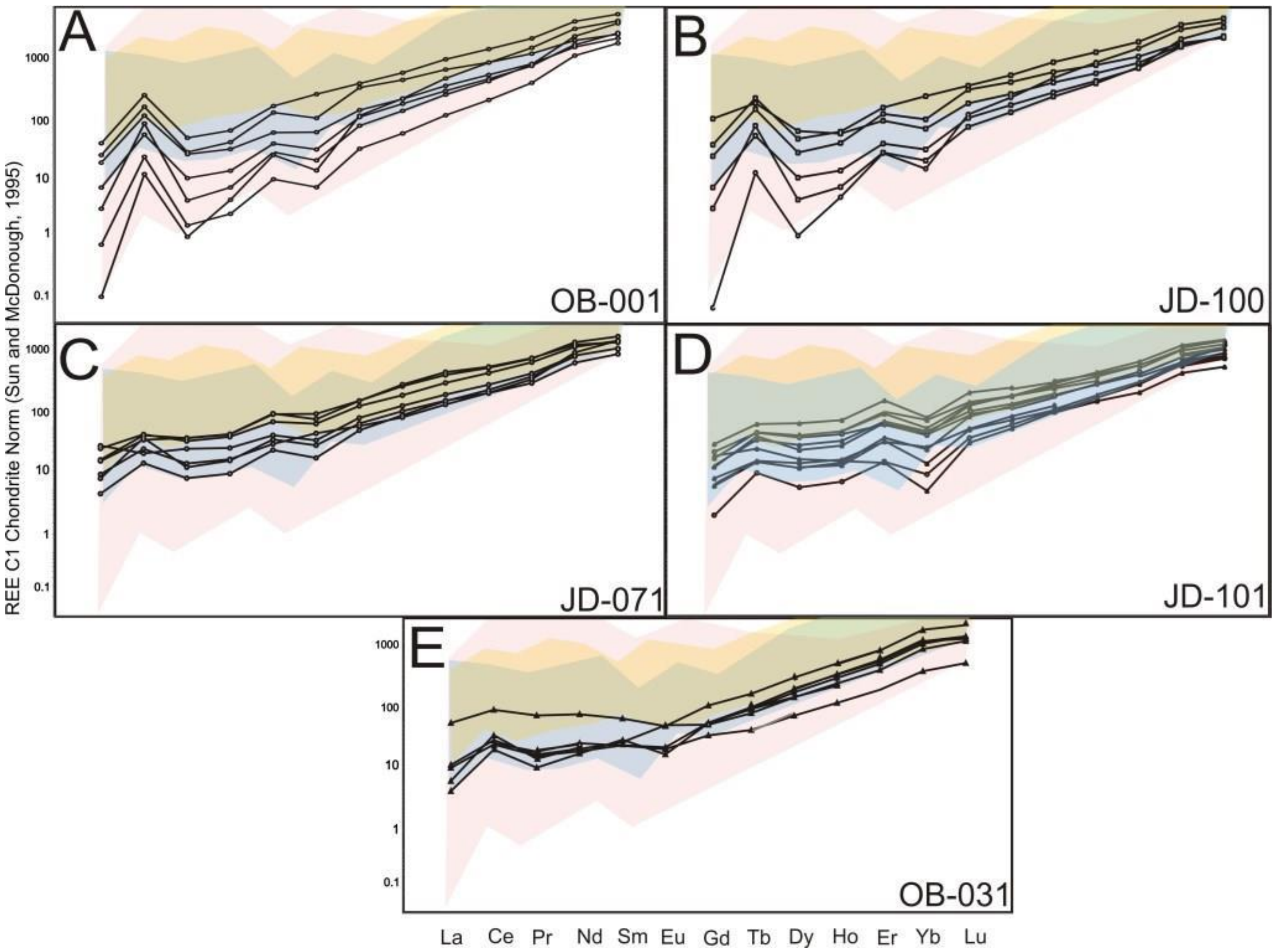

Figure 14: Rare earth element plots of zircon grains normalized to chondrite values of Sun and McDonough (1995). REE element concentrations of zircon from Van Lankvelt (2013) from the Southern Batholith are indicated by the pink polygon (n= 10). The North Caribou batholith is indicated by the yellow polygon (n= 11). The Schade Lake complex is indicated by the blue polygon (n= 14). North-rim amphibolite and biotite garnet schist: A) OB-001. B) JD-100. C) JD-071. Central-belt meta-muscovite quartz schist: D) JD-101. E) OB-031.

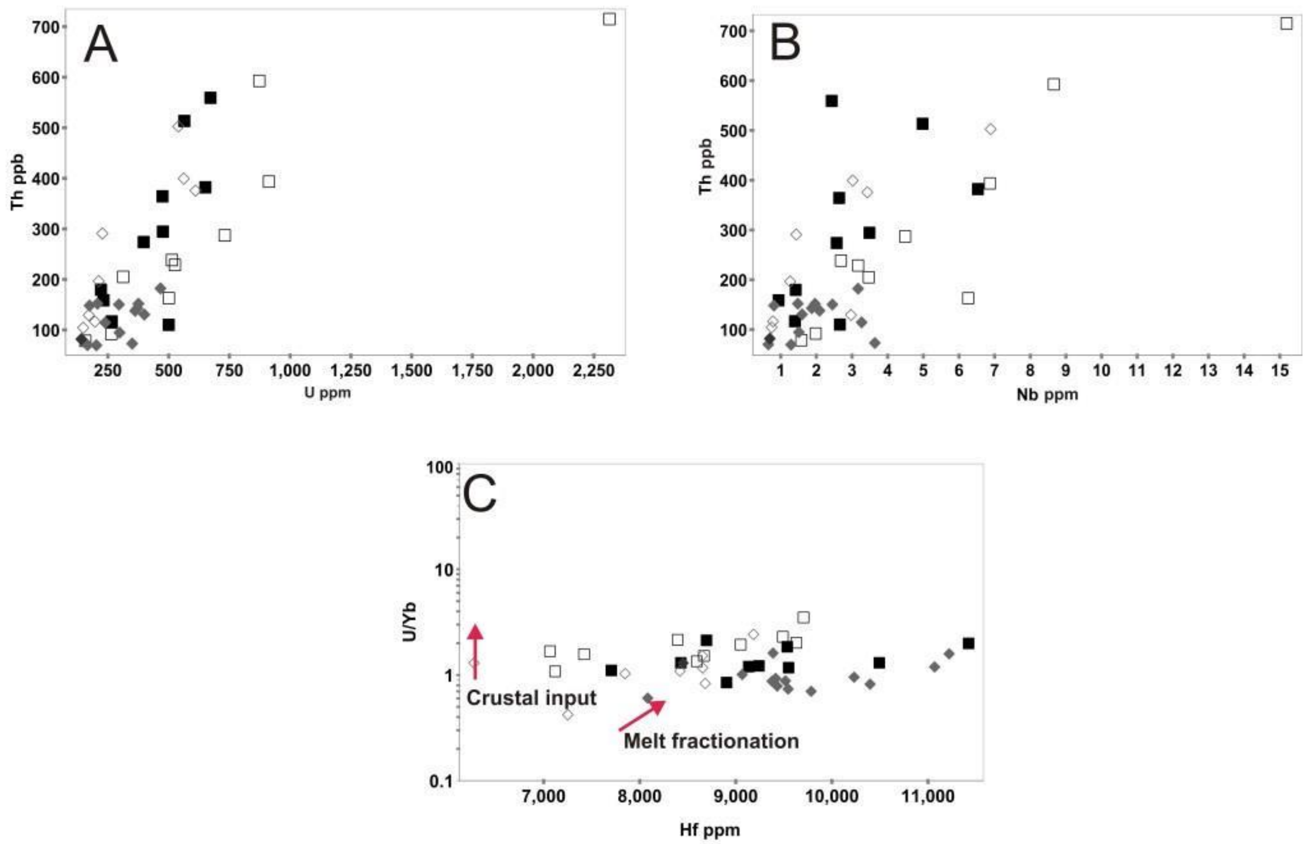

Figure 15: X-Y plots of trace element abundances in zircon grains from metasedimentary rocks of the Zeemal Heaton Lake assemblage. A) U vs Th. B) Nb vs Th. C) Hf vs U/Yb indicating continent vs island arc sources inferred from Grimes et al., 2015. Diamonds: North-rim amphibolite and biotite garnet schist (OB-001, JD-100 and JD-071). Squares: Central-belt muscovite quartz schist (JD-101, OB-031). Solid symbols represent zircons from lithologies without clinozoisite/calcite observed in thin section (JD-101. JD-100, JD-071). Open symbols represent zircons from lithologies with clinozoisite/calcite observed in thin section (OB-031, OB-001). Arrows represent increasing crustal input and melt fractionation, respectively. Hydrothermal alteration is inferred by the presence disseminated clinozoisite, calcite and Fe-oxide that replaces sulphides.

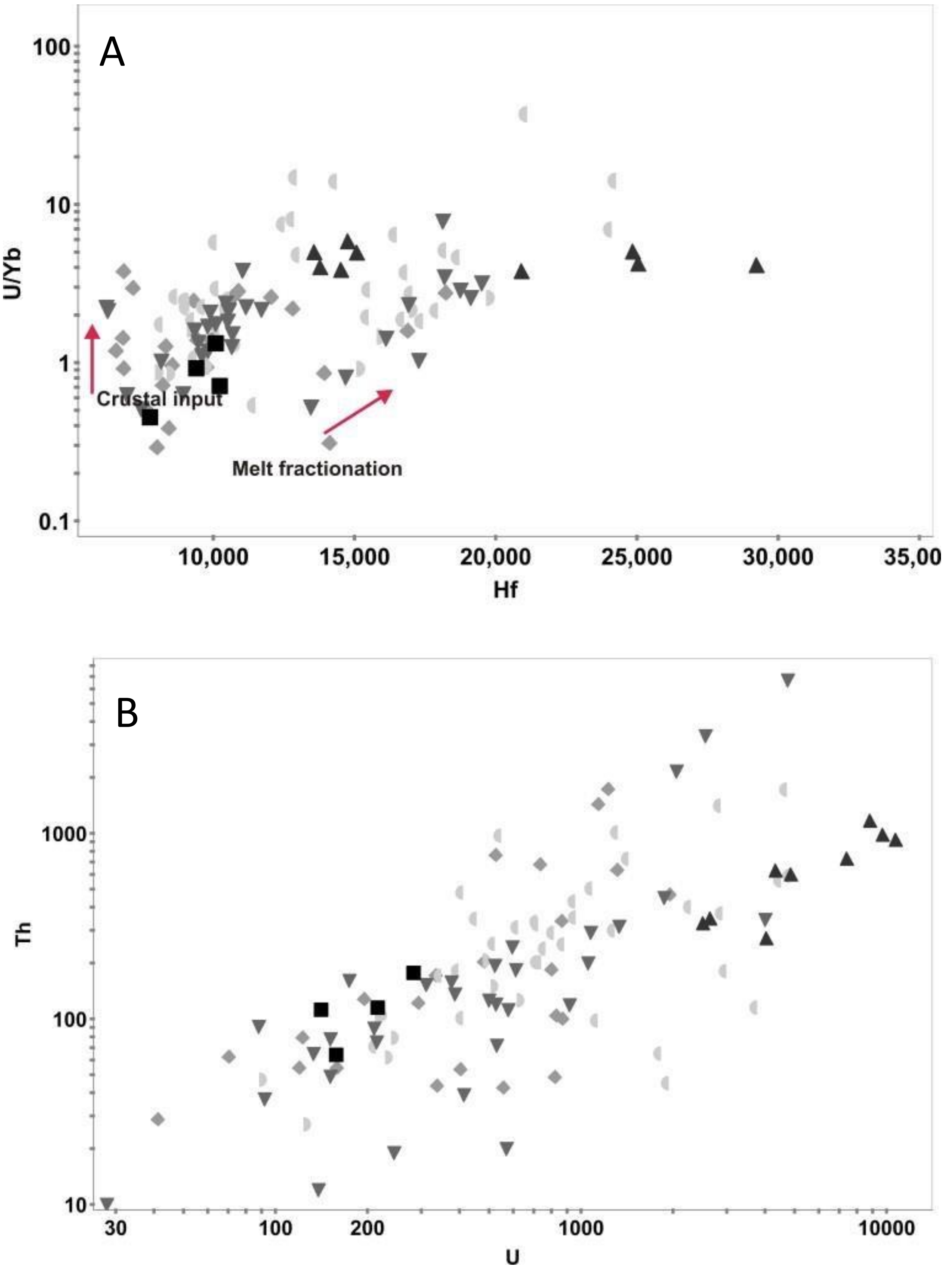

Figure 16: *X-Y plots of trace element abundance in zircons from intrusions surrounding the North Caribou greenstone belt (data from Van Lankvelt, 2013). A: U/Yb vs Hf. Diagram labels determined from Grimes et al. 2015. B: U vs. Th. Triangles: pegmatites. Squares: Libert Lake pluton. Diamonds: Southern batholith. Half-crescent right: Schade Lake complex. Half-crescent left: Skinner Lake complex. Reverse-triangle: North Caribou Lake batholith.*

A total of 9 spots from 9 grains were analyzed from JD-071. Three grains were discarded due to abundant inclusions (**Appendix V**). All grains analyzed have a narrow range of Th/U ratios between 0.33-0.45. Grains show similar REE patterns (**Figure 14c)** with the sums of HREE between 251-889 ppm and those of LREE between 51-199 ppm. Negative Eu anomalies between 0.34-0.47. REE abundances again plot overlapping with the Southern batholith and Schade Lake complex. REE concentrations of all grains in JD-071 are consistently lower than seen in the North Caribou batholith, and LREE remains relatively low overall (**Figure 14c**).

Trace element plots from JD-071 and JD-100 in the North-rim display overlapping provenances having undergone variable degrees of fractionation as indicated by Hf concentrations (8376-11181 ppm) (**Figure 15c**) (Grimes et al., 2015). Both samples are relatively low in U (138-500 ppm), Th (55-182 ppm) and Nb (0.75-3.26 ppm). Values in the Central-belt show some overlap but are typically higher in U (252-678 ppm), Th (110-565 ppm) and Nb (1.04-4.98 ppm). This may indicate a provenance for the North-rim sedimentary rocks is less enriched in incompatible elements, therefore likely not sourced from the younger pegmatites (**Figures 16a-b**). The Libert Lake granitic pluton displays similar Hf values (<10,410 ppm) (**Figure 16a**) and similarly low U, Th and Nb values in zircon (**Figure 16b**). The Libert Lake pluton displays an age population dated 2675-2742 Ma (Van Lankvelt, 2013) and correlates with the younger zircon age population from the North-rim. Zircons from the Schade Lake complex display overlapping Hf values (8050-12810 ppm) with those recovered from the North-rim, but the complex also contains a significant population Hf >12,000 ppm, which is not seen in the North-rim. The Schade Lake complex contains typically older zircon grains (>2822 Ma), and may have sourced the older age populations from the North-rim meta biotite garnet schists (JD-071 and JD-100). OB-001 displays lower Hf values (<9184 ppm), and higher Th (<502 ppm), relative to the other North-rim lithologies. These values are similar to that of the Southern batholith granodiorite (**Figure 16**).

Central-belt metasediments

Two meta-arkosic samples (OB-031, JD-101) were analyzed from the Central-belt. The samples both contain zircon age populations >2800 Ma; however, OB-031 displays a much narrower age range between 2799 ± 19 to 2849 ± 8 Ma. The sample displays abundant clinozoisite and calcite disseminated throughout indicating hydrothermal alteration. Zircon grains recovered from OB-031 display typical igneous morphology described earlier in *Geochronology*, however they also exhibit a dark brown color under the microscope (**Figures 13a-h,**) not observed in any other samples from across the belt in this study. A total of 12 spots from 10 zircon grains were analyzed. All grains (including those which appear altered) fall on Concordia or within <15% discordance, except the rim of grain OB-031-32 that falls far below Concordia curve with an upper intercept age of 2222 ± 19 Ma. The core of this grain returned a date of 2816 ± 8 Ma. Both core and rim returned nearly identical Th/U values of 0.33 and 0.31 and displayed nearly identical REE patterns. High Fe (>800 ppm) and Ca (>513 ppm) which does not correlate with REE spikes, appear to have affected seven analyses. This likely indicates a hydrothermal modification, rather than inclusions. Because of this, the seven analyses were discarded. All zircon grains analyzed from the sample display Th/U values between 0.31-0.68. Grain display a similar REE slope (**Figure 14e**) with positive Ce anomalies between 1.78-3.98. Slight elevation in LREE is likely due to hydrothermal alteration of the zircon grain.

JD-101 occurs ~6 km to the east of OB-031 displays a broader age range with zircons falling within one age populations between 2831 ± 19 to 2927 ± 21 Ma. The mineralogy of the rock displays no obvious hydrothermal alteration/alkali metasomatism (as indicated by calcite and clinozoisite). 11 analysis spots were chosen from eight grains. Inclusions in BSE are more common than seen in OB-031 and consist of primarily apatite and monazite. Three analyses were discarded for abundant inclusions. Although the sample contains abundant inclusions, the zircon grains have little fracturing and show oscillatory zoning throughout all grains. Most grains are light pink in color. The Th/U values from the grains analyzed are consistently higher than those seen in OB-031 (0.31-0.68) to the east with values ranging between 0.54-0.91. The REE slope is steep and similar to that seen in OB-031 with relatively low LREE abundances (<248 ppm) (**Figure 14d**). All grains show a typical, slightly positive Ce anomaly and show a narrow range of consistently negative Eu anomalies between 0.24-0.64. Ca and Fe values overall are typically lower than seen in OB-03. Elevated Ca, and Fe appears associated with other spikes such as P and REE and therefore does not appear related to hydrothermal alteration. When JD-101 REE patterns are compared to signatures from the batholiths an overlap with the Southern batholith, Schade Lake complex and the North Caribou batholith is observed (**Figure 17**).

Overall, when the Central-belt metasediment samples (~2850 Ma detrital ages) are plotted against the North rim metasediments (>2698 Ma detrital ages), there is a trend towards increasing U-Th-Nb in the older Central-belt metasediments, while all North-rim metasediments, regardless of age, remain low (**Figures 15a-b**). These high U, Nb, and Th values are also displayed in the Southern batholith and Schade Lake complex zircon but not the North Caribou batholith zircon (**Figure 16**)**,** therefore making it an unlikely provenance for both the Central-belt and North-rim sedimentary rocks. Hf values vary from low to high in both the Central-belt and North-rim rocks and indicate overlapping variably differentiated sources for both sample areas.

Whole Rock Nd Isotope Analysis

Nd isotopic compositions of sedimentary rocks are commonly used to evaluate the source of the detritus (Goldstein et al., 1984). Depleted mantle model (T_{DM}) ages provide quantitative insight into the crustal residence time of the detritus and therefore can be useful for determining provenance. Nd analysis of whole rock samples has been previously completed on surrounding batholiths and South Rim volcanic rocks (Wyman et al., 2011), as well as on two biotite garnet schist samples from the North-rim (Duff, 2014). All values from this study and Wyman et al. (2011) are displayed in **Table 7** for comparison. Wyman et al. (2011) determined εNd^{2860Ma} values between -1.6 to 1.4 for intrusions with assumed ages of 2860 Ma and more evolved εNd^{2730Ma} values between -6.8 to -0.6 for intrusions dated 2680-2730 Ma. The South Rim mafic volcanic rocks show near-CHUR values and εNd at 2980 Ma between -0.1 to 0.2 (Wyman et al., 2011). Metasedimentary rocks analyzed by Duff (2014) showed relatively restricted εNd^{2850Ma} range from 0.9 to -1.71. Based on the maturity of the North-rim metasediments and their proximity to mafic volcanic rocks Duff (2014) separated the rocks into two groups; those with εNd^{t} less than 0 and those with εNd^{t} greater than 0. The first group with εNd^{t} less than 0 consists of the mature samples that were sampled within the Central-belt of the Zeemal Heaton Lake metasedimentary rocks and distal from a mafic volcanic rock. The values of sediments in Duff's (2014) study overlap with that of the surrounding granitoids and both studies found an indication of these rocks (2730 to 2980 Ma) had εNd^{t} values showing both juvenile and evolved signatures.

A total of 13 samples has been analyzed in this study across the eastern portion of the North Caribou greenstone belt. This includes three samples from the North-rim, eight samples from the Central-belt, one conglomerate matrix sample near the Markop Lake and one metapelite from the North-rim of the Zeemal Heaton Lake assemblage. Metasedimentary rocks from the North-rim have been calculated as evolving from 2680 Ma (**Figure 17, Table 6)** as this represent the maximum age of deposition based on the youngest detrital zircon age. Central-belt lithologies have been calculated evolving from 2800 Ma as this represents the youngest detrital zircons returned from these populations. Lithologies which have not been dated have been calculated evolving from 2800 Ma. The North-rim metasediment samples (OB-001, 009, 023) show slightly negative values of εNd^{2680Ma} -0.9 to -1.2. The biotite garnet schist (OB-034) displays a juvenile signature between εNd^{2800} at -0.5. Central-belt metasediments (OB-021, 031, 04, 06, 07,) and conglomerates north of Markop Lake (OB-110, 111) show a similar evolution with εNd^{2800Ma} values plotting between -1.6 to 0.1. While the two sediment packages display significant overlap, the evolving εNd values overtime indicate detritus from the Central-belt was likely sourced from the older (~2850 Ma) surrounding intrusions (Schade Lake complex and Southern batholith), without significant input from mafic volcanics or younger felsic volcanics.

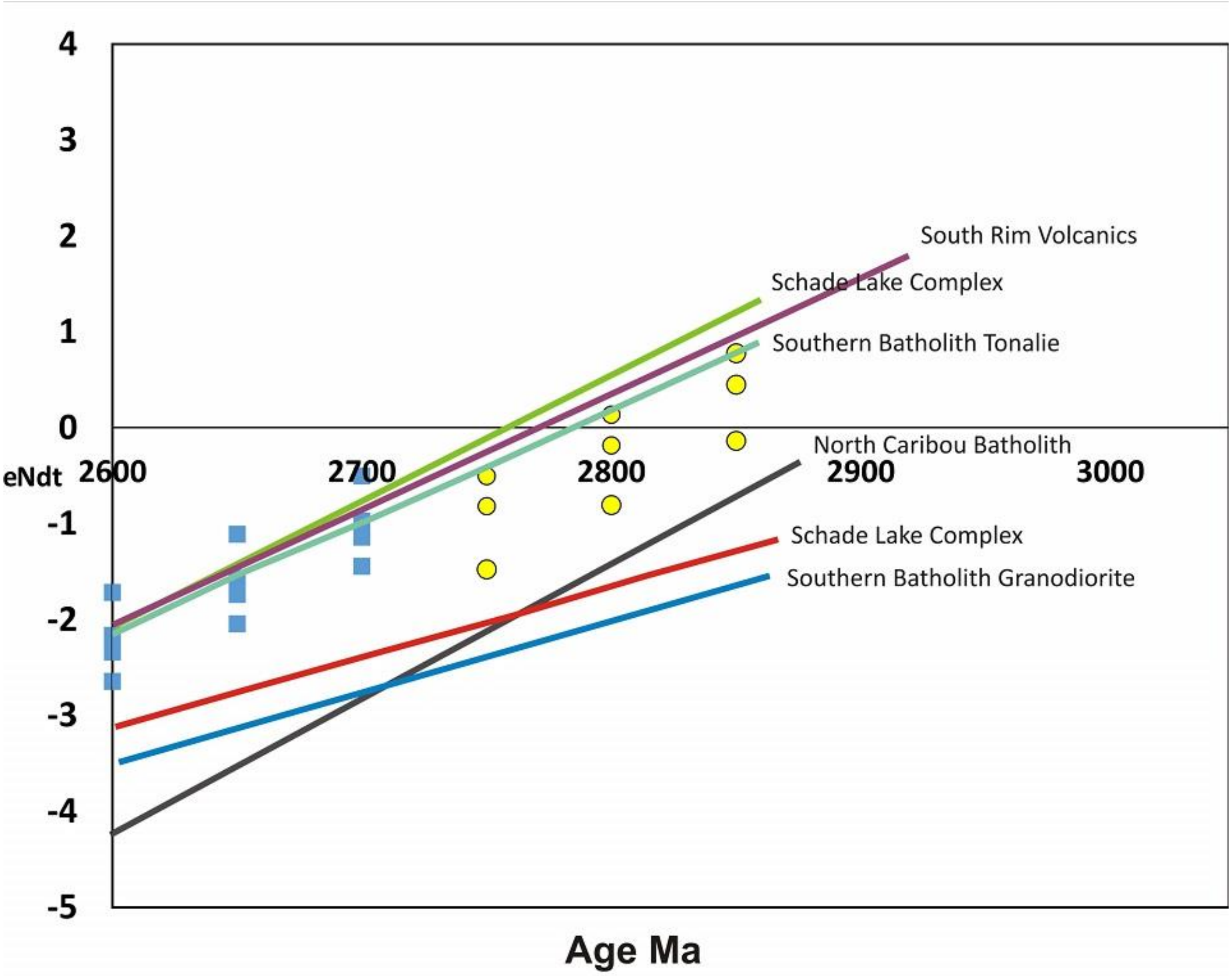

Figure 17: εNd[t] values at various ages. Nd isotopic evolution of the North-rim metasediments from 2680 Ma and the Central-belt metasediments from 2850 Ma. These values are compared to the isotopic evolution of surrounding batholiths (Wyman et al., 2011). SLC: Skinner Lake complex. SRV: South rim volcanics. SBT: Southern batholith tonalite. NCB: North Caribou batholith. SBG: Southern batholith granodiorite.

Table 7: Sm-Nd data including metasedimentary units from this study and surrounding intrusive complexes from Wyman et al., 2011.

Sample	Lithology	Age (Ma)	$^{147}Sm/^{144}Nd$	$^{143}Nd/^{144}Nd$ current	$^{143}Nd/^{144}Nd(t)$	εNd(t)
OB-034	Near-mine	<2800	0.1297	0.511425	0.509029	-0.5
OB-009	NR	<2680	0.1053	0.510959	0.509098	-1.2
OB-023	NR	<2680	0.1037	0.510956	0.509122	-0.9
OB-001	NR	<2680	0.1072	0.511022	0.509127	-0.6
OB-021	CB	<2800	0.0999	0.510841	0.508993	-0.2
OB-026	CB	<2800	0.0943	0.510703	0.508962	-0.8
OB-031	CB	<2800	0.0987	0.510834	0.509089	0.1
OB-106	CB	<2800	0.0988	0.510749	0.508923	-1.6
OB-104	CB	<2800	0.1196	0.511124	0.508913	-1.8
OB-110	CB	<2800	0.1042	0.510887	0.508962	-0.8
OB-111	Conglomerate	<2800	0.0836	0.510551	0.509006	0
Southern batholith*	Tonalite	2730	0.1046	0.510946	0.508971	0.9
Southern batholith*	Granodiorite	2730	0.1053	0.510938	0.509041	-2.6
Schade Lake complex*	Tonalite	2860/ 2730	0.1062	0.510954	0.508949/ 0.509041	3.3/ 1.9
Skinner Lake complex*	Tonalite	2860	0.0943	0.510774	0.508994	1.4
Skinner Lake complex*	Tonalite	2860	0.0865	0.510542	0.508909	-0.3
North Caribou batholith*	Tonalite	2860	0.0963	0.510659	0.508841	-1.6
Libert Lake pluton*	Granodiorite	2690	0.2362	0.512997	0.508805	-6.8
Pegmatites*	Kfs bearing	2690	0.2483	0.513391	0.508984	-3.5
South Rim volcanic rocks*	Mafic metavolcanic rocks	2980	0.1091	0.510902	0.508775	0.2

Sediment ages are maximum age of deposition

¶ εNdt values calculated with present day CHUR $^{143}Nd/^{144}Nd$ of 0.512638 and $^{147}Sm/^{144}Nd$ of 0.1967 from Wasserburg et al. (1981)

*Data calculated from Wyman et al. (2001).

Nitrogen Isotope Composition of Biotite

N isotopes are used to investigate the origin of fluids that form mineral deposits, including Archean orogenic gold deposits (Jia, 2001; Jia & Kerrich, 2001). Nitrogen as NH_4^+ commonly substitutes K in K feldspar, biotite, and muscovite. It can also be absorbed into clay minerals and found in organic material in sedimentary rocks and soils (Sharp, 2007). As sedimentary rocks undergo diagenesis, metamorphism and/or interactions with hydrothermal fluids N isotope compositions can be affected (Haendel et al., 1986, Jia & Kerrich 2001, Jerrich et al., 2005). Therefore, N concentration and stable isotope can be used as a potentially powerful tracer of crustal processes.

A total of nine metamorphic biotite samples were analyzed for N concentration and $\delta^{15}N$ from across the eastern North Caribou greenstone belt. This included four samples from the North-rim metasedimentary samples (OB-001, JD-071, OB-009, OB-012), two samples from the Central-belt two mica schist (JD-031, JD-101), two conglomerate matrix samples (OB-006, OB-111) and biotite garnet schist (JD-094) taken ~2 km south of the Musselwhite Mine. The locations are shown in **Figure 2**. The results are displayed in **Figure 18.**

All samples, regardless of rock type, plot within or near the sedimentary field between the greenschist and amphibolite-greenschist transition as defined by Jia & Kerrich (2000) (**Figure 18**). Metasedimentary samples from the North-rim and Central-belt, which have under gone amphibolite facies metamorphism and greenschist retrogression (indicated by chlorite alteration of biotite), plot within the greenschist facies domain (**Figure 18).** Two of these lithologies (OB-001 and JD-094) have also experienced hydrothermal alteration indicated by disseminated and veined clinozoisite and calcite. Metasediments without extensive greenschist retrogression (or hydrothermal alteration) plot within the greenschist-amphibolite transition zone (**Figure 18**). The $\delta^{15}N$ values of biotite for all samples fall between 0.35-6.50 ‰, and minimum N concentration ranges between 120-620 ppm. Both the isotopic and N concentrations fall within typical sedimentary and metamorphic rock boundaries. Metasedimentary lithologies, which have undergone amphibolite facies metamorphism with greenschist retrogression indicated by chloritization of biotite, and have also undergone hydrothermal alteration indicated by disseminated clinozoisite ± calcite display higher N concentrations and lower $\delta^{15}N$ than those without hydrothermal alteration or greenschist retrogression. Nitrogen values in biotite from these hydrothermally altered and retrogressed rocks show a minimum concentration of 530ppm and $\delta^{15}N$ values between 1.4 to 2.5 ‰. These samples include the near-mine and Central-belt metasediments (JD-094, JD-101 dated 2799 ± 2 Ma), as well as the

North-rim amphibolite (OB-001 dated 2698 ± 20 Ma). North-rim metasediments exhibiting no clinozoisite or calcite alteration all show similar N concentrations in biotite with a minimum concentration between 130 and 290 ppm, and $\delta^{15}N$ between 5.4 and 6.5 ‰. The conglomerate matrix samples (OB-006, OB-111) and two mica schist (JD-031) sample from south Markop Lake all display low values of N concentrations in biotite with a minimum of 120 ppm and median values for $\delta^{15}N$ occur between 2.0 and 4.8 ‰. These samples lack precise metamorphic grade mineral indicators and do not appear hydrothermally altered.

Concentrations of N (10-150 ppm) in biotite taken from the mineralized zone of the Musselwhite Mine by Isaacs (2008) typically show much lower concentration values (130-620 ppm) than those in any unmineralized sedimentary rocks from across the North Caribou belt (**Figure 18**). $\delta^{15}N$ values of biotite from the mineralized samples occur between -1.3 and +11.1 ‰, which falls within both the metamorphic and magmatic fields defined by Jia & Kerrich (2000). These values also fall within the field for granites and the upper amphibolite metasedimentary domain using the discrimination diagram of Jia and Kerrich (2000). A sample analyzed regionally from Issacs' (2008) study show elevated N values similar to this study (<553 ppm) in a single granitoid sample which occurs on the border between the North Caribou terrane and the adjacent Island Lake domain. All other regional samples from her study remain <36 ppm. The elevated N concentration within the granite is similar to that of the metasedimentary samples OB-001 and JD-101 which occur adjacent to the Totogan shear zone and JD-094 which occurs ~5 km south of the Musselwhite Mine (**Figure 2**).

Overall, unmineralized (non Au-bearing) regional lithologies display overlapping $\delta^{15}N$ values with that of mineralized mine units but display higher N content in biotite. It is important to note that the concentrations of N in the samples from this study is only a minimum (due to impurities such as quartz and may represent 10-30% of sample size) and the real values are likely higher. The regional metasedimentary lithologies have undergone upper greenschist to lower amphibolite conditions while the auriferous mine samples sit at upper amphibolite facies, as P-T conditions increase to the west of the belt. The biotite present in the Musselwhite mineralized zone is likely formed from the ore-forming fluids (magmatic + metamorphic fluids) and contain significantly less N. A negative trend occurs within the regional unmineralized metamorphosed sediments (**Figure 18**) which are common in typical prograde metamorphism (Haendel et al. 1986). The mineralized mine units, however, show a positive trend. A positive trend in nitrogen concentration vs. $\delta^{15}N$ has been documented where magmatically derived fluids have interacted with metamorphic rocks (Bebout et al., 1999; Issacs, 2008). Issacs (2008) noted that biotite-garnet schists corresponding with the stratigraphic top of the deposit, along with metavolcanics in the vicinity of the mine plot between the granite and greenschist field. Both a conglomerate matrix sample within the vicinity of the mine (<1km) and North-rim metasedimentary rocks also plot between the granite-greenschist zones. These unmineralized which occur near the Totogon and Markop Lake shear zones or within the vicinity of the mine (**Figure 2**) appear to represent samples which have had interaction with metamorphic fluids and also minor interaction with magmatic fluids.

Table 8: Minimum nitrogen concentration (ppm) and δ15N values of biotite from metasedimentary lithologies in this study and mine units from Issacs (2008).

Sample	Lithology	Location	N concentration (ppm)	$\delta^{15}N$ (o/oo)	Chloritization of biotite	Data source
JD-071	Biotite garnet schist	ZHL	220	+6.5	X	This study
JD-094	Two mica schist	ZHL	530	+2.5	X	This study
JD-101	Two mica schist	ZHL	530	+1.4	X	This study
OB-001	Amphibolite	ZHL	620	+1.5	X	This study
OB-006	Conglomerate matrix	ZHL	120	+2.0		This study
OB-009	Biotite garnet schist	ZHL	290	+5.4		This study
OB-012	Biotite garnet schist	ZHL	130	+6.2		This study
OB-111	Conglomerate matrix	ZHL	210	+4.7		This study
E354010	Oxide facies BIF	Mine	6.57	-0.3		Issacs, 2008
E354013	Silicate facies BIF	Mine	8.41	+5.4	X	Issacs, 2008
E354016	Oxide facies BIF	Mine	22.51	+5.1	X	Issacs, 2008
E354018	Oxide facies BIF	Mine	27.16	+2.1	X	Issacs, 2008
E354020	Oxide facies BIF	Mine	38.06	+3.3	X	Issacs, 2008
E354026	Silicate facies BIF	Mine	26.27	+6.5		Issacs, 2008
E354029	Biotite-garnet schist	Mine	33.64	+8.0		Issacs, 2008
E354032	Biotite-garnet schist	Mine	61.02	+8.3		Issacs, 2008
E354039	Silicate facies BIF	Mine	34.98	+6.3		Issacs, 2008
E254040	Oxide facies BIF	Mine	22.04	+6.2		Issacs, 2008
E254041	Mafic metavolcanic	Mine	176.38	+2.4	X	Issacs, 2008
E254043	Biotite-garnet schist	Mine	127.54	+5.3		Issacs, 2008
E254045	Meta-sedimentary	Mine	115.83	+2.1		Issacs, 2008
E354050	Oxide facies BIF	Mine	22.52	+11.5		Issacs, 2008
E358105	Biotite-garnet schist	Mine	38.13	+8.7	X	Issacs, 2008
E358108	Mafic metavolcanic	Mine	44.47	+6.0	X	Issacs, 2008
E358109	Mafic metavolcanic	Mine	20.64	+5.1	X	Issacs, 2008
E358110	Mafic metavolcanic	Mine	8.44	-1.7		Issacs, 2008

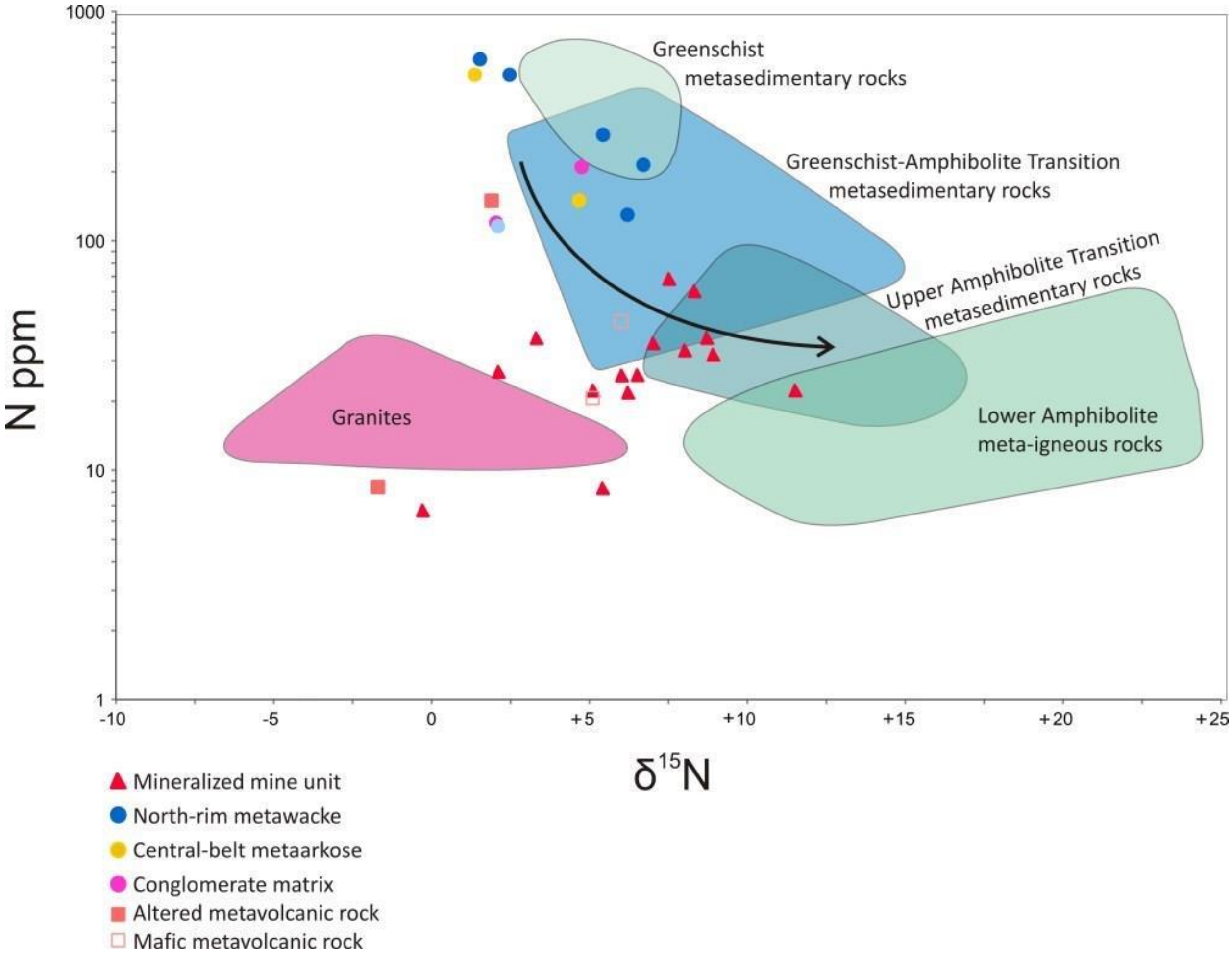

Figure 18: Nitrogen content versus δ15N of biotite from igneous and sedimentary lithologies in the eastern limb of the North Caribou greenstone belt and within the Musselwhite Mine. Metasedimentary fields after Haendel et al., (1986); meta-igneous fields after Jia & Kerrich (2000). Sedimentary lithologies data from this study. Mineralized mine and mafic volcanic unit data from Issacs (2008). Black arrow represents typical prograde metamorphism. It is important to note that N values determined in this study are the minimum values because of impurities such as quartz.

Discussion

Provenance

Lithology and Geochemical Characteristics

Geochemical and isotopic compositions of the varying lithologies indicate variable, yet overlapping sources for all sedimentary rocks in the Zeemal Heaton Lake metasedimentary rocks.

Near-mine metasediments in the west, including two garnet-biotite schists and one staurolite biotite schist, indicate significant contribution of mafic detritus which is indicated by relatively high concentrations of compatible elements; Ni (>69ppm), Cu (>93 ppm), Co (>27ppm), Sc (> 17 ppm), and low Th (<4ppm) and Y (<18 ppm) (**Figures 19 a-b, Table 4**). Based on the significant mafic-related detritus present it is likely the metapelite formed partially from the erosion of older mafic volcanic material that may include the North Rim volcanic rocks, South Rim volcanic rocks or the Opapimiskan metavolcanic rocks. The metapelites may represent the top of a graded turbidite sequence or slump. Most original sedimentary textures have been lost in this portion of the greenstone belt, and this interpretation is based on the occurrence of pelite in contact with crossbedded meta-arkose which grades into conglomerate, typical of turbidite sequences (Bouma, 1962).

When comparing the matrix mineralogy of the Central-belt to the North-rim metasediments to the east, both lithologies display angularity of matrix minerals and poor sorting of framework grains, which supports the rapid deposition of an immature sediment. The largest variation in lithologies is indicated by the presence of abundant K feldspar in the Central-belt vs. plagioclase in the North-rim. In the Central portion of the Zeemal Heaton Lake metasedimentary rocks, K feldspar forms coarse (~1 mm) porphyroclasts (**Figure 5f**) as well as finer grain matrix components, while no/trace K feldspar porphyroclasts were noted in the North-rim lithologies. Variation in mica is noted between the lithologies, with the Central-belt foliation defined by muscovite and the North-rim defined by biotite. The abundance of foliated biotite, and plagioclase porphyroclasts in North-rim vs. muscovite and K-feldspar in the Central-belt likely indicates mafic vs. felsic detritus sources.

The metasediments of the Central-belt contain abundant accessory monazite and zircon, as well as elevated Zr, Th, and Al_2O_3/TiO_2 (**Figure 19**) which is also indicative of a primarily granitic/crustal provenance. The North-rim sediments display high concentrations of compatible elements (MgO, Cr, Sc etc.; **Table 4**) which further indicates a more significant contribution of mafic detritus. Variable proximal provenances is further supported when lithologies are plotted displaying Zr/Sc vs Th/Sc which shows a more upper crustal contribution in the Central-belt. As well, when plotted on the Sc-Th-Zr/10 tectonic environment discrimination diagram by Bhatia and Crook (1986) (**Figure 20**) the North-rim metasediments plot in the continental arc setting, while the Central-belt metasediments plot between the active to passive margin settings (**Figure 20**).

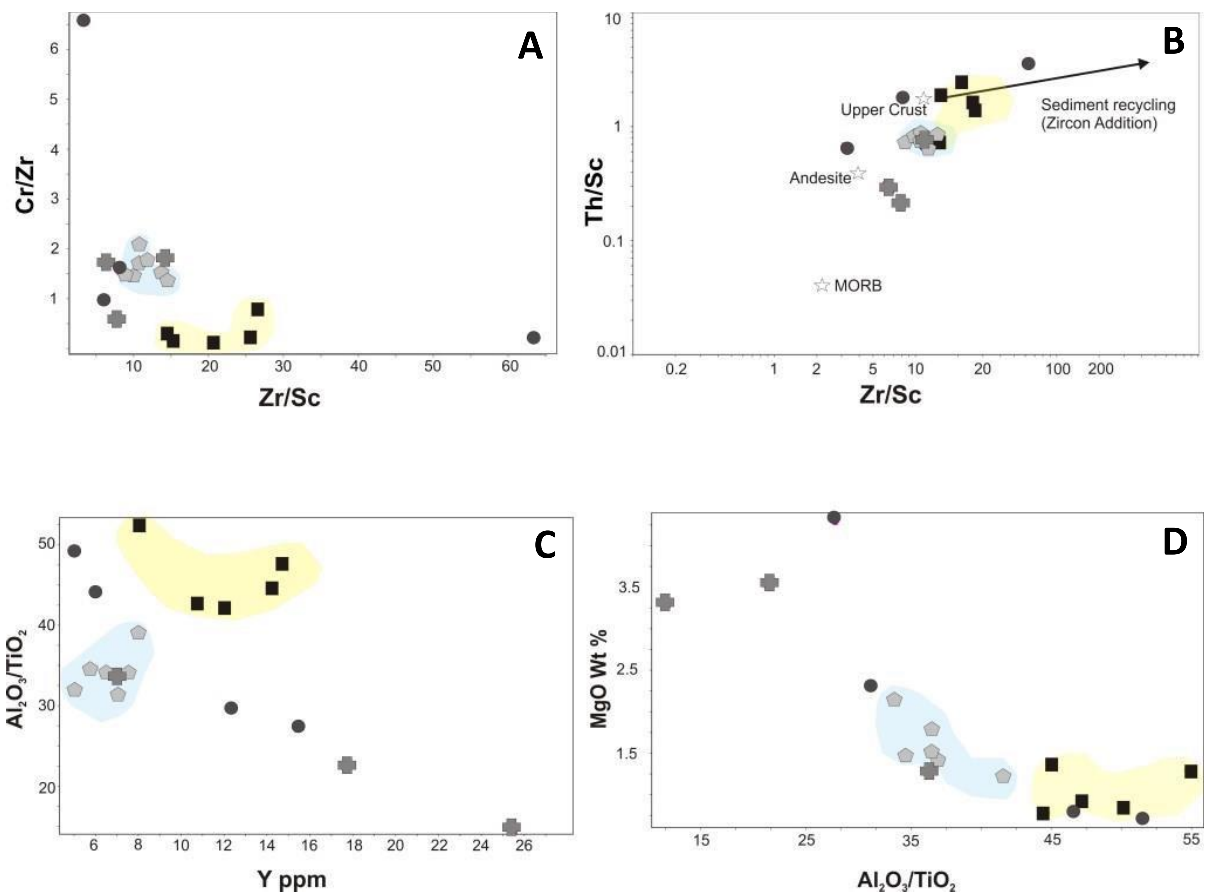

Figure 19: Whole rock geochemistry discrimination diagrams of metasedimentary rocks of the Zeemal-Heaton Lake assemblage. A) Cr/Zr vs. Zr/Sc. B) Th/Sc vs Zr/Sc. Labels defined by McLennan et al. (1993). C) Al2O3/TiO2 vs Y. D) MgO wt% vs Al2O3/TiO2. Cross: metapelites near-mine, circle: conglomerate matrix, in Central belt, square: Central-belt metasediments, pentagon: North-rim biotite garnet schist. Yellow polygon: Central-belt. Blue polygon: North-rim. Stars: provenance source.

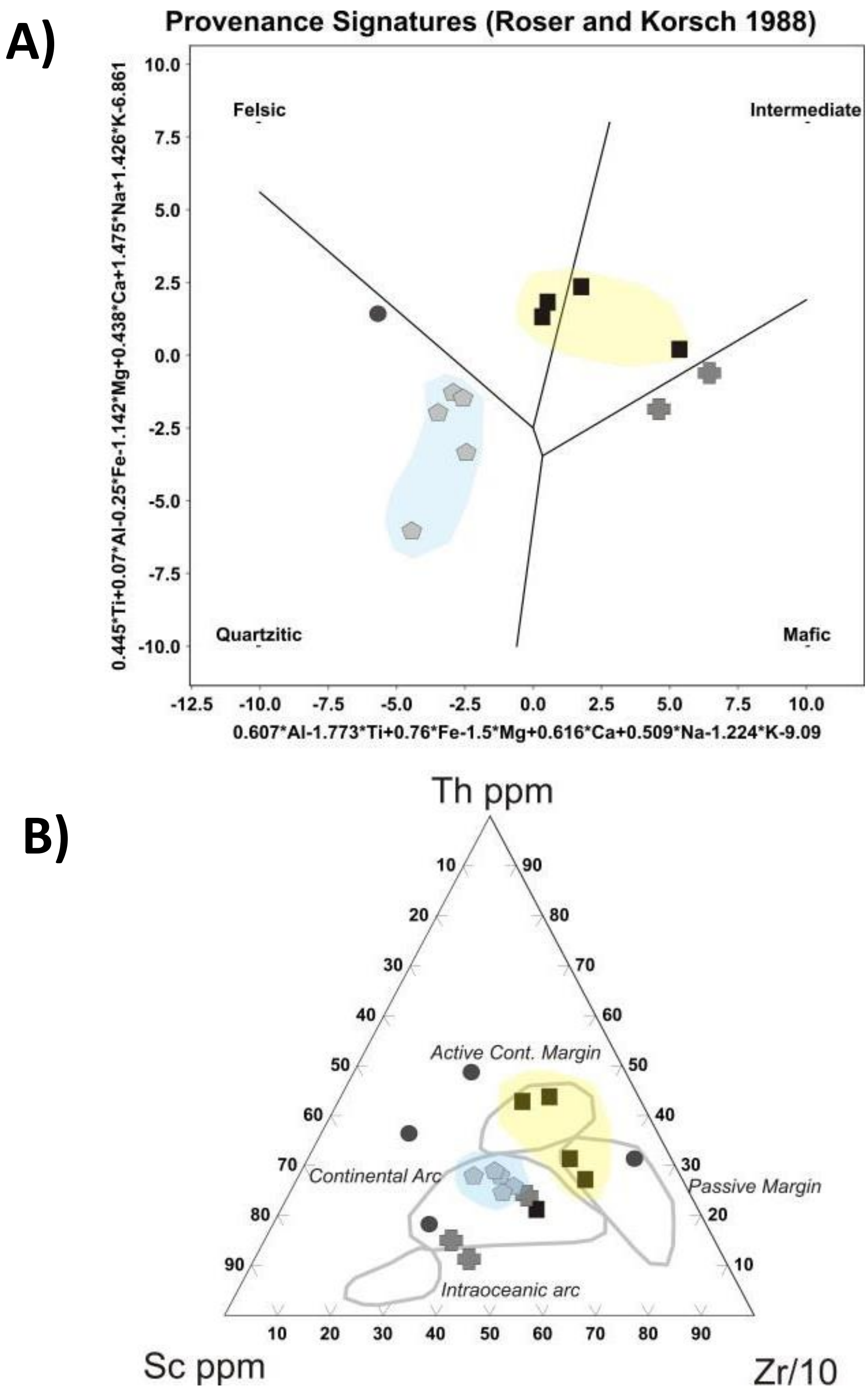

Figure 20: Whole rock geochemistry discrimination diagrams of metasedimentary rocks of the Zeemal Heaton Lake assemblage A) Provenance signatures modelled after Roser and Korsch (1988). B) Tectonic discrimination diagram with boundaries defined by Bhatia and Crook (1986). Cross: Near- mine metapelites circle: conglomerate matrix in Central-belt, square: Central-belt metasediments, pentagon: North-rim metasediments.

The geochemical signature of the conglomerate matrices correlates to the proximal sources and can be extremely variable across even a single outcrop. Lack of exposure and the extent of deformation make it difficult to resolve the transition from conglomerate to wacke, arkose, and pelite. The conglomerate units contain clasts or boulders from all surrounding lithologies including TTG's, mafic and felsic volcanic rocks, banded iron formations and sedimentary rocks, thus interpreted to have been deposited in a rapid erosional setting.

Neodymium Isotopic Signatures

Nd isotopic signatures of sedimentary lithologies also indicate that the North-rim rocks are likely sourced, in part, from a mafic provenance combined with younger evolved granitic rocks. The rocks display a somewhat evolved isotopic signature εNd (2680 Ma) from -1.2 to -0.9. These values overlap with several surrounding lithologies indicating the South Rim volcanic rocks, Southern batholith tonalite and the Schade Lake complex as provenances (**Figure 17, Table 5**). The Central-belt metasediments and Markop Lake conglomerates display similar values (εNd (2800 Ma) =-1.8 to 0.1), which overlap, but displays a slightly more negative value at a given time than those for the Southern batholith tonalite and Schade Lake complex reported by Wyman et al. (2011) (**Figure 17**). This indicates a mixed provenance with eroded upper crustal intrusions or other more distal sources.

Overall, these values indicate detritus for the Central-belt was likely sourced from the older (~2850 Ma), less differentiated (tonalite-granodiorite) surrounding intrusions (Schade Lake complex and Southern batholith). The younger (~2700 Ma) granitic intrusions (Libert Lake pluton) and rhyolites display a more evolved Nd isotope signature and therefore likely represent a source (in-part) for the North-rim sediments, along with some contributions from surrounding mafic volcanics.

Geochronology and Zircon Geochemistry

Metapelites and Conglomerates

Metapelite lithologies from across the Zeemal Heaton Lake metasedimentary rocks were unable to be dated due to the fine grain size of the mudstone. Conglomerate matrix samples also could not be dated due to small zircon grain size (< 20 μm). A quartz arenite clast in a conglomerate has been previously dated by Davis and Stott (2001) at 2856.0 ± 1.8 Ma, which is similar to age of the surrounding TTG intrusions (Van Lankvelt, 2013) and detrital zircon age populations determined in metasediments to the east.

Central-belt metasediments

Two muscovite quartz schist samples dated from the Central-belt returned similar concordant ages with one age population and the youngest detrital zircons dated >2831 ± 19 (JD-101) and 2798 ± 29 Ma (OB-031). These dates provide the maximum age of possible deposition. Sample JD-101 was taken from near the Northern contact of the Zeemal Heaton Lake metasedimentary rocks with the Schade Lake complex (**Figure 2**) in the vicinity of the Totogan shear zone. This sample returned a single abundant age population with zircon ages increasing steadily by ~1-3 My, with the highest population of grains occurring between 2831 ± 19 to 2904 ± 13 Ma and three outlying grains dated 2914 ± 18 to 2927 ± 29 Ma. The upper intercept occurs at 2872 ± 8 Ma. The zircons analyzed are interpreted to be igneous. These grains are unlike hydrothermal zircons which typically have sponge-like textures and lack zoning. While metamorphic vs igneous textures can be ambiguous, mottled zoning or migmatic textures are commonly apparent in metamorphic zircons. Th/U ratios remain high in all grains (>0.3) with a mean of 0.54 which is well above determined igneous values (<0.1 in metamorphic and hydrothermal zircon and >0.5 in igneous zircon; Rubatto, 2002; Hoskin and Schaltegger, 2003).

Central-belt samples from both OB-031 and JD-101 show higher U, Th and Nb than seen in the North-rim, which is may simply be a result of a signature inherited from the igneous provenance. REE abundances in the analyzed zircons correlate with numerous batholith samples (Van Lankvelt, 2013), primarily from the Schade Lake complex, which lies in contact with the Opapimiskan metavolcanic rocks, <1km North of the sample location and the North Caribou Lake batholith. Zircon grains from the Schade Lake complex have been dated between 2828 to 2976 Ma, which parallels the main population of ages returned from sample JD-101. The Southern batholith zircons also show trace elemental similarities in zircon returned overlapping ages between 2823-2853 Ma. Previous interpretations of the zircon population did not include the possibility of zircon sourced from batholiths lying to the North of the North Caribou greenstone belt, as docking with the Island Lake Domain was considered not to have occurred until 2860 Ma (Van Lankvelt, 2013). According to that interpretation, sedimentary rocks dated at <2860 Ma would not have been in contact with the Northern batholiths and complexes. A new interpretation for sedimentation that will be discussed below allows for provenance sourcing from all surrounding batholiths.

Kalbfleisch (2012) performed *in-situ* U-Pb dating of zircon on NCTK10-75, which was sampled from the same outcrop as JD-101, near the North contact of the Zeemal Heaton Lake metasediment package. She also dated another meta-arkosic sample NCTK10-08 of similar mineralogy sourced adjacent to Markop Lake where the outcrops lie within the projected termination of the Markop Lake deformation zone. Kalbfleisch (2012) attributed the robust age cluster around 2858 ± 8 Ma in both samples to metamorphic subsolidus recrystallization of zircon grains which can occur during amphibolite facies metamorphism of hydrous sedimentary rocks (Corfu et al., 2000). This interpretation varies from that presented in this study. Sub-solidus recrystallization may be possible at the amphibolite temperatures that this rock has experienced. Studies have shown that temperatures between 550 and 650 °C (at these upper amphibolite conditions), even in the presence of fluids, will not significantly impact Pb concentration in zircon (Carson et al., 2002) and therefore caution should be taken when attributing zircons with fluid interaction with a metamorphic age. The continuous age population spanning ~100 Ma, morphology (3:1 ratio), size (>100µm), oscillatory zonation, trace element patterns nearly identical to that of surrounding batholiths presented in this study, and low LREE abundances support an igneous origin.

North-rim metasediments

One amphibolite (OB-001) and one biotite garnet schist (OB-012) dated from the North-rim returned four main age populations with the maximum age of deposition at 2696 ± 39 Ma, coinciding with the youngest detrital age dated by Duff (2014) at 2674 ± 29 Ma. The four age populations defined from each North-rim sample in this study show concordant age populations between 2684 ± 23 to 2762 ± 20, 2807.9 ± 11.4 to 2884.7 ± 17 Ma, 2922 ± 20 to 2984 ± 17 and 3048 ± 17 and 3060 ± 30 Ma. All age populations have been interpreted as igneous as the zircons from these samples display oscillatory zoning and Th/U ratios >0.1, with a higher mean value than seen in the Central-belt samples (0.5-0.8), relatively low LREE abundances and REE signatures similar to that of signatures from igneous zircons retrieved from surrounding batholiths.

In the North-rim, zircons from each age population have likely been sourced in an active tectonic setting from a large, variable source area as indicated by the proximal conglomerates, higher abundances of framework quartz and abundant mafic detritus contribution. The age population 2696-2762 Ma which was not observed in the Central-belt samples has likely been sourced from a partially eroded rhyolitic unit dated ~2723 ± 2 Ma (McNicoll and Oswald, unpublished data, personal communication in January, 2015) which occurs in contact with the North-rim biotite garnet schists (samples OB-009 to 012) and in other small packages of felsic igneous rocks along the Northern portion of the belt. Several dates including 2702 ± 57 to 2715 ± 18 (Schade Lake complex), 2727 ± 12 (Southern batholith) and 2690 ± 8 to 2730 ± 8 Ma (Libert Lake pluton) and 2619 ± 14 Ma (pegmatite) have been dated from the surrounding batholiths and pegmatites. These intrusions, related volcanic eruptions provide an abundant source for the younger zircon population. Zircons dated at 2808 ± 11 to 2885 ± 17 Ma overlap with the significant age population recovered from the Central-belt metasediments and most surrounding batholiths. Zircons dated in this population show an age population increasing by 1-3 Ma indicating a (multiple) batholith sources with long lived emplacement spanning ~80-100 Ma. Zircons dated 2922 ± 20 to 2984 ± 17 Ma and 3048 ± 17 and 3060 ± 30 Ma can be attributed to the oldest period of magmatic activity preserved in the North Caribou Lake batholith and inherited cores of zircons in the Southern Batholith. Rocks of this age likely represent the original continental crust in the North Caribou terrane. U–Pb age dates of detrital zircon grains in the study are comparable to those reported by Stevenson et al. (2009) from the adjacent Berens River subprovince to the south which also displays a gap in magmatism after ~2760 Ma.

Igneous zircons dated ~2700-2730 ± 8 Ma from the surrounding batholiths have been interpreted by Van Lankvelt (2013) to represent possible partial melting of older 2830-2880 Ma TTG's. These dates may also represent their own period of continental arc-related magmatism. Based on the abundance in populations of zircons seen consecutively dated 2698-2762 ± 20 and 2800-2926 ± 29 Ma with ~1-3 My intervals, it is possible that longer lived episodes of TTG magmatism and volcanism occurred before ~2926 Ma. This period of magmatism was associated with a major period of crustal growth between 2800-2926 ± 29 Ma followed by subduction, subsequent arc plutonism, and volcanism, and finally sedimentation pre- to syn-orogenesis within the North Caribou terrane related to the southward propagating orogeny in the Western Superior Province between 2762-2698 ± 20 Ma.

It is important to note that sedimentary rocks were most likely sourced from multiple intrusions where rivers cross-cut the intrusive bodies. Intrusions and volcanic rocks occur between 2726-2697 Ma from across the North Caribou superterrane (Corfu and Stone, 1998). The sedimentary rocks were most certainly sourced from all surrounding intrusions, and likely include detritus from an area significantly larger than the current North Caribou greenstone belt.

Hydrothermal Alteration of Zircon in the Central-belt

Alteration of zircon grains has been suggested by Van Lankvelt (2013) for zircon grains recovered from the Schade Lake, North Caribou and Southern batholiths. These grains show elevated LREE (**Figure 14e**). Van Lankvelt (2013) observed mottled textures and disruption of zoning in the grains but did not observe spongy textures typically seen in hydrothermally precipitated zircons. Many grains which were interpreted by her to be hydrothermally altered are texturally ambiguous and maintain original igneous zoning. Th/U ratios were lower in the rim than the core, but still much higher (>0.7) than seen in typically altered zircons. No Discordia were observed in the interpreted hydrothermally altered grains from her study. Ages were interpreted by Van Lankvelt (2013) to be reset by alteration, which implies that nearly all of their radiogenic Pb was lost.

Sample OB-031 was collected from the Central belt of the Zeemal Heaton Lake metasedimentary unit (**Figure 2**) east of the Markop Lake. While the matrix mineralogy of both Central-belt metasediments is similar, including recrystallized quartz, K feldspar porphyroblasts, rare plagioclase and a foliation defined by muscovite with rare biotite, OB-031 shows significant hydrothermal veins. This is indicated by the occurrence of clinozoisite and calcite in veins and disseminated throughout matrix with coarse muscovite over growing the foliation (**Figures 5e-f**). The age population returned from the altered arkosic sample displays a tight age range spanning ~50 Ma between 2799 ± 19 to 2849 ± 8 Ma with an upper intercept value of 2824 ± 6 Ma. The main age population is ~20-50 Ma younger than JD-101 and arkosic NCTK10-75 dated by Kalbfleisch (2012). Zircon grains from sample OB-031 show typical igneous zoning in CL images (**Figures 12 a-h**) however they exhibit a brown hue, abundant fractures with abundant coarse (up to 20μm) inclusions of apatite and monazite. REE elements in the zircons show the typical igneous HREE enrichment over LREE which is unlike zircon grains interpreted by Van Lankvelt (2013) to be hydrothermally altered. The grains do show a higher LREE abundance (<197 ppm) compared to the North-rim, however, they do not show the level of elevation noted in hydrothermal rims by Van Lankvelt (2013).

Due to i) the high population of concordant grains with discordance in an acceptable range (<15%) spanning ~50 Ma. ii) overlaps with dates of numerous surrounding intrusive complex samples and unaltered sedimentary rocks detrital ages, iii) the unlikelihood of fluids having significant impact on U-Pb in zircon at these temperatures <550 C° (Carson et al., 2002), iii) typical igneous zircon LREE values; the zircons likely retain an original igneous U-Pb age.

Metamorphism and Deformation in the Eastern North Caribou greenstone belt

Prograde Metamorphism

Regional metamorphic conditions in the Northern and Central North Caribou greenstone belt have been studied by Breaks et al. (2001) and Gagnon et al. (2015). Gagnon et al. (2015) determined that the metamorphic grade of the greenstone belt rocks ranges from lower greenschist facies up to middle amphibolite facies conditions with two metamorphic zones. The first zone displays an increase of metamorphic grade to the assemblage garnet + staurolite + grunerite ± sillimanite in the northwestern portion of the belt that extends between Musselwhite Mine to the northern extent of the N-W striking limb (**Figure 2**). Sediments in the eastern portion of the belt display upper greenschist to amphibolite conditions as the peak metamorphism as indicated by the presence of biotite, garnet, andalusite and staurolite. This suggests hotter conditions or the structural uplift of deeper rocks to the NW of the gold deposit than in the eastern portion of the belt. In the eastern portion of the belt metamorphic grade is more difficult to determine. Gagnon et al. (2015) noted andalusite, garnet, and staurolite are only present in a few locations that tend to lie proximal to major shear zones such as the Totogan shear zone and the Markop Lake deformation zone.

The presence of muscovite grains cros in the Central-belt is an indication of higher metamorphic temperature (>550°C) than seen in the North-rim. Muscovite grains crosscutting foliation may be an indication of upper amphibolite facies retrogression. This amphibolite facies metamorphism within the Central-belt indicates deep burial across the entire eastern limb of the North Caribou greenstone belt, and intermediate P-T metamorphism is not just associated with shear zones.

The amphibolite sample (OB-001) displays garnet porphyroblasts with typical prograde zoning, with decreasing Mn and increasing Fe towards the rim. This indicates amphibolite facies-garnet zone metamorphism. Abundant chloritized biotite suggests significant greenschist retrogression.. Due to the high Mn content in North-rim garnets it is interpreted that the garnet may have been reset by a thermal aureole metamorphism likely facilitated by nearby intrusions or volcanics. The Central-belt garnet represents more regional metamorphic conditions.

Deformation

Near-mine metasediments

Based on the metamorphic mineral assemblages and deformation events interpreted from inclusion trails, a deformation history has also been evaluated. As stated previously, thin sections were cut perpendicular to foliation which is subvertical, therefore interpretations of the orientation of inclusion trails can be made. Near-mine metapelite samples (OB-035, 034, 015 and 102) have reached amphibolite facies-garnet zone, based on the assemblage of almandine-rich garnet, biotite, staurolite, and andalusite. These samples occur south of the Musselwhite Mine and along the northern-rim of the Zeemal Heaton Lake metasedimentary rocks near where the Totogan shear zone and Markop Lake deformation zone meet (**Figure 2**). Staurolite (OB-015) contains core foliation pitching to the left of photomicrograph (**Figure 5a**). The staurolite core has been interpreted to have grown in an earlier deformation event while the matrix foliation was likely defined later. That late foliation defines an ~EW strike and is interpreted to postdate the core foliation. OB-035, which has an NW strike and a subvertical foliation sampled south of the mine contains abundant almandine-rich garnet porphyroblasts. The porphyroblasts also contain matrix foliation that has been interpreted to have grown in earlier crenulations that are still visible in the matrix but rotated by a younger deformation event, similar to that seen in the biotite-staurolite schist. The main penetrative foliation (NW and sub/vertical) is defined by $D_{2.}$ Therefore, the porphyroblasts have been interpreted to have grown in a deformation prior to D_2, which may represent a deformation event post-$D_{1,}$ as isoclinal folding is not noted in the studied metasediments (McNicoll et al. 2015).

Central-belt metasediments

The Central-belt metasediments show the pervasive WNW-EW strike with subvertical foliation seen across the eastern portion of the belt which indicates a minimum D_2 deformation. Inclusions within garnets in the Markop Lake deformation zone also appear to have grown in an oblique crenulation to current foliation event that is well preserved in the trails (**Figure 8b**). This indicates deformation prior to $D_{2,}$ however, similar to the near-mine metasediments, the lack of isoclinal folding does indicate the previously described D_1 deformation.

North-rim metasediments

The amphibolite (OB-001) occurs close to the contact with the Schade Lake complex and in the vicinity of Totogan shear zone. It displays the typical E-W strike in foliation and subvertical dip seen across the eastern limb of the belt. North-rim biotite-garnet schists (samples OB-009, OB-023, and JD-100) also occur near the Totogan shear zone and vary between a WSW to WNW strike with subvertical foliation. Garnets display deformation history defined by a gently crenulated foliation present in inclusion trails (**Figure 8c-d**). The North-rim metasediments indicate similar deformation histories to the Central-belt and near-mine metasediments.

Overall, garnet porphyroblasts occurring from across the eastern limb of the North Caribou greenstone belt display similar deformation histories defined by growth in early crenulations cleavages and followed by a second stage of growth during a younger event. Therefore, all metasediments studied in the eastern portion of the North Caribou greenstone belt indicated a minimum D_2 deformation as defined by McNicoll et al. (2015) but have experienced a previous deformation event that does not appear to be currently defined.

Orogenesis appears to be protracted. Prograde metamorphism causing the crystallization of garnet, staurolite and andalusite accompanied regional deformation and metamorphism. This took place during a deformation that postdates the first foliation producing event based on the work and approaches to porphyroblast interpretation described in Bell et al. (2013). Due to the complex nature of the tectonic inclusion trails in the garnet, it appears the complicated tectonic history of the belt may extend beyond four main tectonic events. For the purpose of this study and time constraints, this will not be further examined.

Timiskaming-type Sediments

Timiskaming-type assemblages have been defined previously as fluvial to alluvial conglomerates through to slates with lateral facies variation, and associated calc-alkaline to alkaline volcanics. They represent the youngest supracrustal assemblage in a greenstone belt and form unconformities overlying older volcanics and sediments. They are associated with transpressional deformation and crustal-scale shear zones and have been determined to be deposited rapidly in either pull-apart basins (Thurston et al. 1991; Leclair et al., 1993), or during diapirism and sagduction during uplift and erosion of batholiths (Lin et al. 2013). In the Abitibi, the typical age of deposition is between 2685 to 2700 Ma (Legault, 1993).

Metasedimentary rocks from the North-rim of the Zeemal Heaton Lake assemblage are spatially associated with the major crustal scale Totogon and Markop Lake shear zones. Detrital zircon grains from this study returned a maximum age of deposition of 2696 ± 39 Ma. This coincides with the youngest detrital age dated by Duff (2014) at 2674 ± 29 Ma. The North-rim metasediments are ~100 Ma younger than the Central-belt metasediments which are dated 2798 ± 29 Ma (this study), and ~170 Ma older than the South Rim volcanic unit in the belt. Therefore, based on the maximum age of deposition and the apparent unconformity with underlying sediments and volcanics, the North-rim metasediments of the Zeemal Heaton Lake assemblage have been determined to represent a Timiskaming-type event within the North Caribou greenstone belt. The Timiskaming-type basin environment in the eastern limb of the belt is further delineated by an unconformity/thrust boundary and a polymictic conglomerate in the upper stratigraphic sequence at the Musselwhite mine which has been interpreted to indicate the presence of a major structure (McNicoll et al. 2015).

One or Two Sedimentary Basins?

The Zeemal Heaton Lake assemblage displays varying detrital zircon age populations but similar deformation history across the eastern limb of the belt. Garnet porphyroblasts in biotite garnet schists from within the vicinity (<2km) of the Musselwhite mine, the western Central-belt, and North-rim all display inclusion trails with foliation oblique to that of the matrix foliation. The main penetrative EW foliation has been defined as forming during D_2 (McNicoll et al. 2015), therefore all metasediments have undergone deformation prior this event, but do not display evidence for D_1, which is indicated by tight isoclinal folding.

Variation in detrital zircon age populations between samples across the Zeemal Heaton Lake metasedimentary rocks could be explained by diapirism and sagduction (dome and keel) sedimentation (Lin et al. 2013) that has been interpreted to occur adjacent to the North Caribou greenstone belt in the Island Lake belt. Lin et al. (2013) noticed a nearly identical trend in the variable detrital zircon age populations across stratigraphy, which they attributed to detritus being derived from down-stratigraphy erosion of rising domes being deposited in sinking synclinal keels (**Figure 21**).

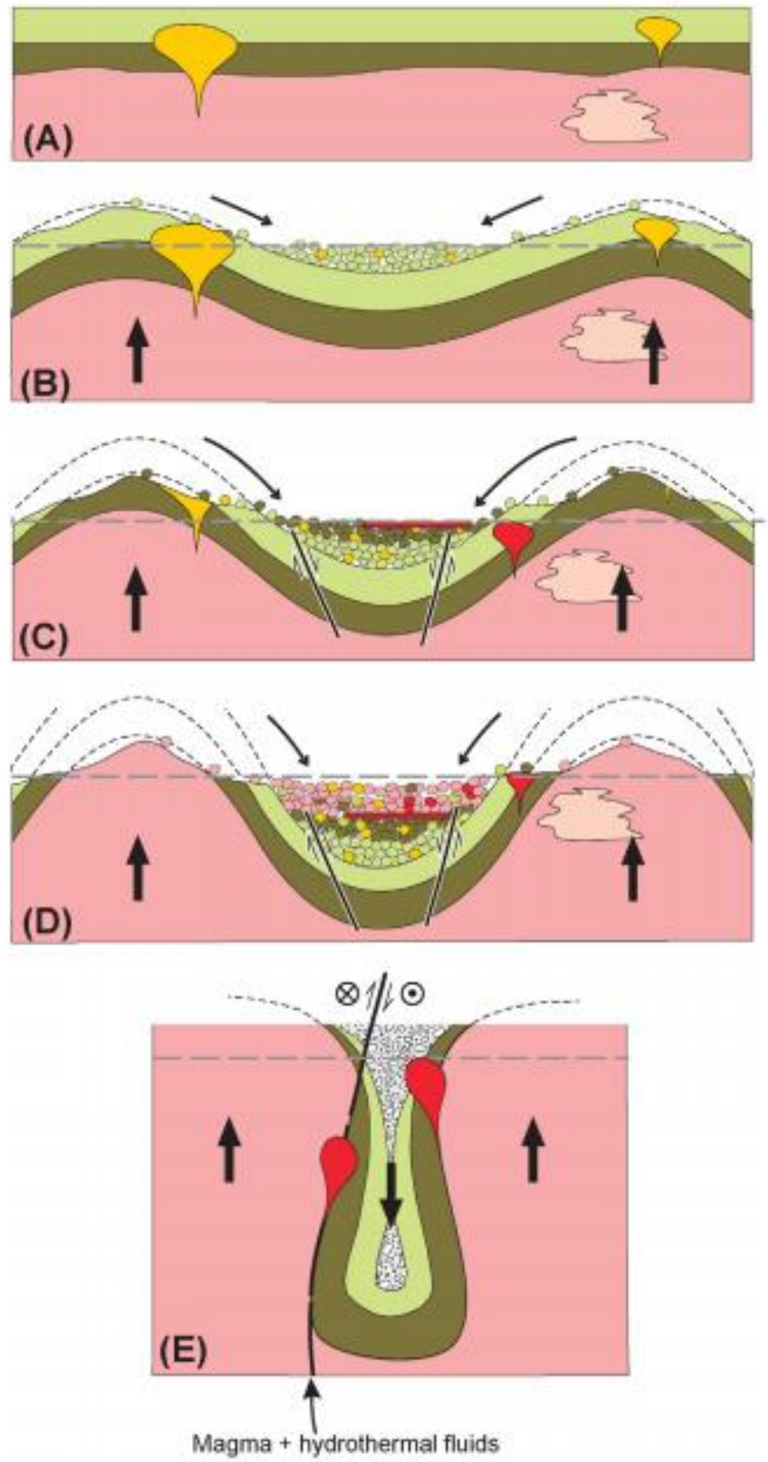

Figure 21: Lin et al. 2013 schematic model for Timiskaming-type sediments deposited during diaprism and sagduciton in the Northern Superior Province.

As erosion occurs downward through the supracrustal pile only the younger supracrustal rocks were exposed (~2700 Ma felsic volcanic rocks) above the granitoid domes to supply detritus into the sedimentary basin in the keel. As erosion continued, older supracrustal rocks became exposed and were the main or only source of detritus. Later ~2740 to 2690 Ma felsic intrusions (Libert Lake pluton and Southern Lake batholith granodiorite) in the domes were unroofed and became the main source of detritus to the basin. The theory readily accounts for variable age populations displayed across sedimentary lithologies with similar tectonic histories. While deep burial is not indicated by granulite facies metamorphism, upper amphibolite retrogression is noted in the Central-belt metasediments. This Timiskaming-model explains how a late extensional D4 event does not account for the multiple earlier deformation events and upper greenschist to amphibolite facies metamorphism in which all sedimentary rocks, regardless of age population, have experienced. It is well known that rocks in active margins are uplifted and eroded quickly, in <5 km/million years (Fukahata and Matsu'ura, 2000), which supports the theory of rapid erosion and sedimentation in the basin. The overall orientation of foliation in the southern North Caribou greenstone belt is sub-vertical to vertical and striking ~EW. This can be induced in an active convergent margin dominated by horizontal tectonics similar to present day convergent margins, which implies horizontal and vertical tectonics occurred synchronously during orogenesis.

It is important to note that no structural or metamorphic indicators were observed in the field to support the diapirism and sagduction model. Therefore, the variation in detrital zircon ages may represent two separate basins. The Central-belt sediments dated at 2798 ± 29 Ma also form an unconformity with the underlying volcanics, however, may have been deposited prior to the Timiskaming-event and then subsequently deformed with the younger North-rim sediments. However, based on the apparent identical deformation histories across the eastern portion of the belt and the metasedimentary unconformity noted by McNicoll et al. 2015 at the Musselwhite mine, the author interprets the entire Zeemal Heaton Lake assemblage to represent a younger Timiskaming-type assemblage. While sedimentary rocks north of the Musselwhite Mine have not been examined in this study, they have been interpreted to represent an older, stable shelf assemblage (Breaks et al. 2001).

Geological Evolution of the North Caribou Greenstone Belt

Metasedimentary lithologies from the eastern limb of the North Caribou greenstone belt display a WSW-WNW strike with a subvertical foliation dip and contains minerals indicative of amphibolite facies metamorphic conditions. The main phase of penetrative ductile deformation in the North Caribou greenstone belt has been regionally recognized as D_2 but formed at least during a D_3 event as determined by the complex history preserved in porphyroblasts. The various deformation events have been recorded in all lithologies including sedimentary rocks and the mafic and felsic volcanic rocks on the southern flanks of the limb. This event was interpreted as being initiated by the collision of the Oxford-Stull domain with the North Caribou terrane and the subsequent southward propagating orogeny that took place between ~2720 to 2680 Ma when amalgamation of the Western Superior took place (Breaks et al., 2001, Percival et al., 2006a, Kalbfleisch, 2012, Oswald et al., 2015, McNicoll et al., 2015). The North Superior terrane and North Caribou terrane were interpreted to have collided 2720-2710 Ma initiating southward subduction below the North Caribou terrane (Lin et al., 2006). Arc-related volcanic rocks have been noted in the Island Lake Domain and the Oxford-Stull Domain (Parks et al., 2006) to the south of the North Caribou greenstone belt. Docking of these terranes was suggested by the appearance of ~3500 Ma zircons in young (<2711 Ma) synorogenic sedimentary rocks (Corkery et al., 2000) and volcanic rocks. Arc magmatism also occurred between 2748 to 2708 Ma, and syn-sedimentary volcanism in the English River terrane occurred during an Archean orogeny related to terrane amalgamation (Pervical et al., 2006). Similar aged plutonism and volcanism (Van Lankvelt, 2013; McNicoll, 2015) surrounding the North Caribou greenstone belt may be a result of this subduction-related magmatism from either the north or the south during orogenesis. This period of magmatism is supported by ~2700-2730 Ma igneous zircons in the Libert Lake pluton, Southern batholith, Schade Lake Complex and Heaton Lake rhyolitic unit (Van Lankvelt 2013; McNicoll and Oswald, 2015).

Detrital zircon dated from this study and from Duff (2014) have been plotted and compared with all igneous dates from surrounding intrusions determined by Van Lankvelt (2013) and all zircons which have been interpreted as metamorphic along with hydrothermal monazite (Kalbfleisch, 2012; Gagnon et al., 2015) to determine timing of metamorphic events (**Figures 22a-c**). Detrital zircons show two main peaks at 2680 and 2800 Ma, which correlate with the periods of major crustal growth during ~2700 and 2830 Ma. While both the detrital and igneous populations show peaks at these times, the zircon age populations also indicate continuous magmatism, which is common during long-lived subduction zones as documented in the Rocky Mountain area by Cao et al. (2012). Small peaks are also noted at >3000 Ma in the igneous population, which has been interpreted as older re-worked crustal material. Metamorphic ages (>3000, ~2700-2880 Ma) displayed in **Figure 22c** correlate with the timing of intrusions which can be expected due to high temperatures associated with the large magmatic bodies at ~3000 Ma (North Caribou batholith core), and the docking of the Island Lake Domain and North Caribou terrane between

2870-2830 Ma. The spike of metamorphic ages between 2550-2650 Ma has been interpreted to represent fluids associated retrogression following an orogenic event (Gagnon et al., 2015).

Late Archean orogenesis affecting the North Caribou greenstone belt occurred between 2720-2680 Ma. Therefore these fluids could just as likely represent prograde metamorphism associated with deep burial across the region. The occurrence of S-type pegmatite dykes (Breaks et al., 2001) may indicate melting of deeply buried rocks during this time, a further indication of abundant fluid during high-temperature prograde metamorphism.

The metamorphic ages between 2500 and 2300 Ma have been interpreted by Gagnon et al. (2015) to represent another metamorphic event. This event is interpreted to have occurred during reactivation of crustal-scale shear focused in the southern arm of the belt as ages are broadly coeval with the ~2490 Ma $^{40}Ar/^{39}Ar$ age of biotite in an unmineralized garnet-biotite schist unit at Musselwhite mine (Biczok et al., 2012).

Breaks et al. (1985) and Breaks et al. (2001) have interpreted that gold mineralization in the Opapimiskan Lake area of the North Caribou greenstone belt is syn-D_2 and syn-peak metamorphism. The youngest age of gold mineralization has been constrained to 2666 Ma, determined by monazite dating (Oswald et al., 2015) in garnet interpreted to be coeval with gold mineralization. Based on the timing of late Archean orogenesis (Percival et al., 2006a) and syn-sedimentation and magmatism occurring at ~2720 to 2680 Ma, gold mineralization would have had to happen post-2680 Ma, and as young as 2666 Ma based on U-Pb monazite ages (Oswald et al., 2015). Metamorphic and magmatic signatures indicated by N isotopes in the mineralized zones of the Musselwhite Mine (Issacs, 2008) can be explained by multiple metamorphic fluid events post 2680 Ma (Gagnon, 2015) and abundant fluid derived from magmatic activity during this time (Henry et al., 2000, Percival et al., 2006a; Van Lankvelt, 2013).

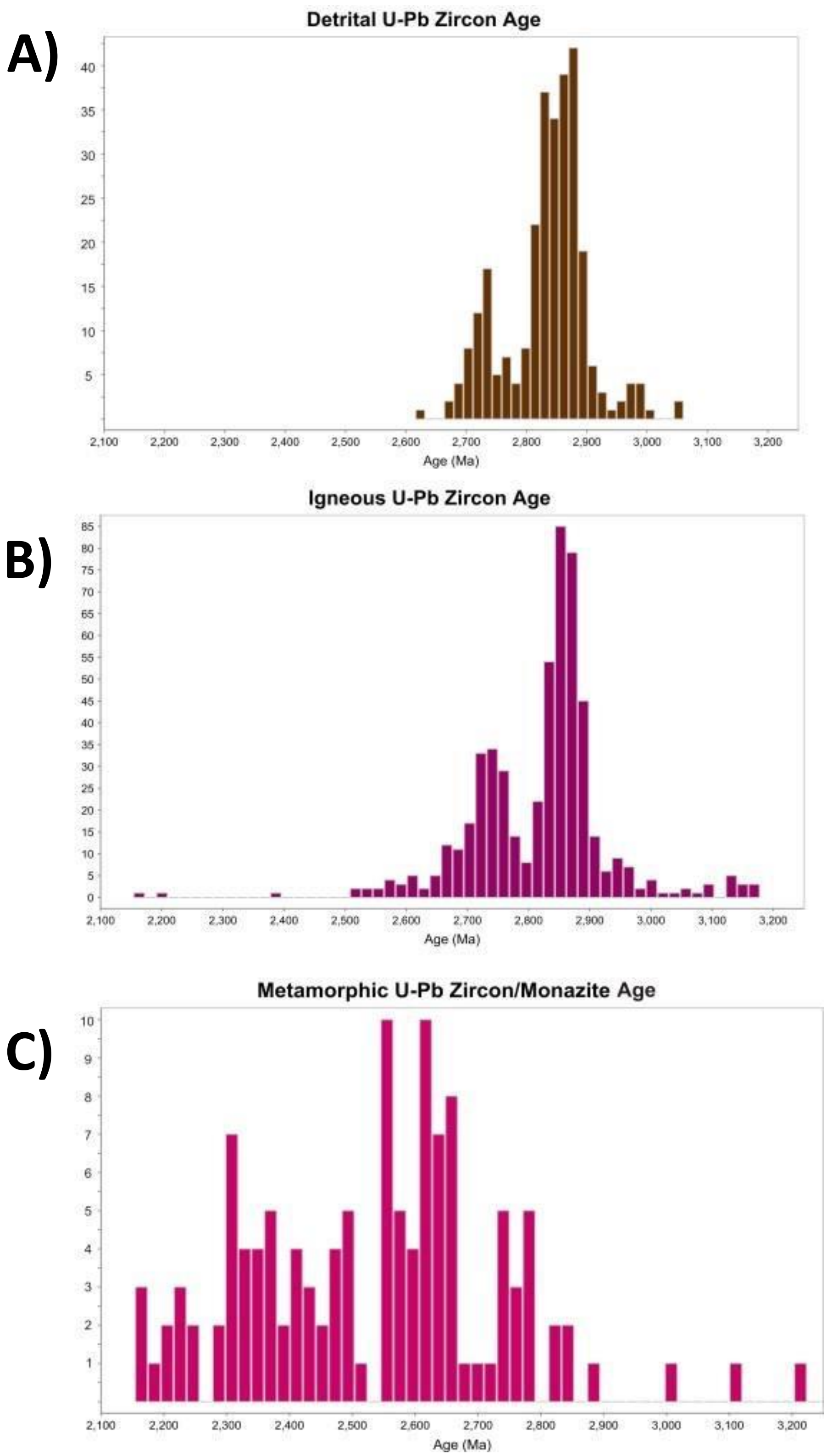

Figure 22: Histogram of U-Pb zircon ages from zircons and monazite A) Detrital U-Pb zircon dates from this study and Duff (2014). B) Igneous U-Pb dates from zircons sourced from batholiths by Van Lankvelt (2013). C) U-Pb dates from zircons and monazite interpreted to be hydrothermal from this study, Van Lankvelt (2013) and Kalbfleisch (2012).

Summary of the Evolution of the North Caribou greenstone belt and surrounding intrusions

1. Pre 2920 Ma: This period represents the oldest preserved magmatism in North Caribou greenstone belt including the volcanic packages of the North Rim volcanic rocks, South Rim volcanic rocks and Opapimiskan metavolcanic rocks. Zircons >3000 Ma have been interpreted to represent re-worked original continental crust of North Caribou core (VanLankvelt, 2013). An initial plutonic pulse may have initiated prior to 3002 ± 14 Ma as indicated as inherited by concordant detrital zircon grains and cores of igneous zircons present in the North Caribou Lake batholith, reported by Van Lankvelt (2013).

2. 2920-2820 Ma: A massive ~100 Ma pulse(s) of magmatic activity in which the major intrusive complexes (Schade Lake complex, Southern batholith, and North Caribou Lake batholith) formed. Consecutive detrital age populations (increasing by ~1-3 Ma) during this time indicate a long-lived period of magmatism. At 2860 Ma regional metamorphism associated with the docking of the Island Lake Domain and North Caribou greenstone belt has also been interpreted to have occurred (Van Lankvelt, 2013).

3. 2740-2660 Ma: Following a cessation in magmatism; southward subduction of the North Superior superterrane (**Figure 1**) and North Caribou superterrane and Northward subduction of the North Caribou superterrane and Winnipeg River terrane occurred causing a late Archean orogeny from 2720-2710 Ma. This likely triggered a period of magmatism across the Province. Partial melting of older rocks may have also contributed to this period of intrusive and magmatic activity (Libert Lake pluton, Southern batholith, Schade Lake complex). Similar aged magmatism is also noted in the Uchi, Bernes and Sachigo subprovinces (Percival et al., 2006a). Penetrative deformation at 2700-2669 Ma is noted in Island Lake Domain to the North of the North Caribou greenstone belt (Parks et al. 2006), which indicates the southern North Caribou superterrane amalgamation affected the northern area of this superterrane as well.

   During terrane amalgamation of the surrounding intrusions (Southern batholith, Schade Lake complex, Libert Lake pluton) are uplifted and rapidly eroded into a sedimentary basin along with syn-orogenic, magmatic, and volcanic units. These rapidly eroded (<10 Ma) sediments produce the Zeemal Heaton Lake 'Timiskaming-type' assemblage. As accretion continued throughout the Western Superior the rapidly buried sedimentary rocks were metamorphosed during Abukuma-type regional metamorphism and folded into the WSW-WNW orientation due to compressive deformation associated with the ~2700 Ma orogeny. Multiple phases of deformation beyond the four main noted (Breaks et al., 2001) are likely to have occurred to achieve the current variable orientations of the eastern limb. Evidence for horizontal tectonism (shallow dipping lineations) is recorded in shear zones that border the greenstone belt, indicating there was also a period of orogenic collapse (Gagnon et al. 2015).

Conclusions

- Metapelitic rocks and North-rim metasediments which occur near contacts with mafic volcanic rocks, display higher bulk rock Ni, Cr, Sc, and V than seen in the Central-belt sediments. The North-rim sediments also display whole-rock εNd (2680 Ma) from -1.2 to -0.9. These values overlap with that of the South Rim volcanics, Southern Batholith and Schade Lake complex at 2680 Ma. Trace elemental geochemistry of zircon from these rocks also shows similarities with those zircons recovered from the batholiths. Based on the whole rock geochemistry, and trace elemental geochemistry of zircon the North-rim rocks were sourced in-part, from nearby mafic volcanic rocks, as well the Southern Batholith, Schade Lake complex, and younger felsic volcanics.

- Central-belt metasediments display higher bulk rock La/Sm, Zr/Cr and Th/Sc than seen in the North-rim. The rocks display a bulk rock εNd (2800 Ma) =-1.8 to 0.1, which overlaps, but with slightly more negative values at 2800 Ma than those of the Southern batholith tonalite and Schade Lake complex reported by Wyman et al. (2011). Trace elemental geochemistry of zircons indicates an overlap with those of zircons from these batholiths. Overall, the Central-belt sediments were sourced primarily from granitic detritus.

- Overlapping zircon age populations occur between the North-rim and Central-belt sediments. However the North-rim contain a significantly younger zircon population with the youngest detrital zircon dated 2696 ± 39 Ma. This coincides with the youngest detrital age dated by Duff (2014) at 2674 ± 29 Ma. The Central-belt sediments youngest detrital zircon is dated 2798 ± 29 Ma.

- Based on similar deformation histories noted across the belt, interpreted from outcrop observations and inclusion trails noted in porphyroblasts, all sediments within the Zeemal Heaton Lake assemblage are interpreted to have undergone a minimum of D_2 deformation as defined by McNicoll et al. 2015. Based on the timing of deposition (2720-2680 Ma) the Zeemal Heaton Lake sediments are interpreted to "Timiskaming-type" and have all been deposited immaturely and rapidly. The variation in age of the youngest detrital zircons and sediment bulk rock chemistry between the North and Central-belt may be explained by Lin et al. (2013) "dome and keel sagduction" model which has been proven in the Borden Lake conglomerate. Younger volcanics and intrusions were rapidly eroded away first, and then later older intrusions were eroded to create variation in the zircon populations down stratigraphy. A rhyolite dated 2727.8 ± 2.4 Ma by McNicoll (personal communication in Janaury 2015) in contact with the North-rim sediments further indicates younger volcanism was also occurring at this time.

Future Work

To further delineate the provenance of the sediments in the North Caribou greenstone belt, geochemical analysis of the zircons from young (~2700 Ma) rhyolitic volcanics should be undertaken. This could be used for comparison purposes to solidify the link between the North-rim sediments and these younger igneous rocks in the belt. Dating of the conglomerate will also be useful to determine if the young zircons occur in any other units.

Beyond the scope of this study, deformation across the belt is poorly understood with qualitative descriptions of structures without orientation descriptions of clear-cut overprinting relationships. The lack of recognition of sub-horizontal fabrics associated with orogenic collapse is of concern when it is well known and documented that these processes occur in all orogens throughout geological time (Sanislav et al., 2011). It is, therefore, likely that more than the four main deformation events described by previous workers but not been recognized. To complete detailed microstructural analysis to determine the main deformation events, orientated thin sections are needed. A comprehensive study of the multiphase tectonic history would also help constrain the timing of gold mineralization related to deformation and therefore aid in regional exploration and a greater understanding of the amalgamation and history of the Western Superior Province.

References

Andrews, A.J., Sharpe, D.R. & Janes, D.A., 1981. Preliminary reconnaissance of the Weagamow-North Caribou Lake metavolcanic-metasedimentary belt, including the Opapimiskan Lake (Musselwhite) gold occurrence. Ontario Geological Survey, Miscellaneous Paper, 100, 196-202.

Bell, T. H., Rieuwers, M. T., Cihan, M., Evans, T. P., Ham, A. P., & Welch, P. W. 2013. Inter-relationships between deformation partitioning, metamorphism and tectonism. Tectonophysics, 587, 119-132.

Berman, R.G., 1991. Thermobarometry using multi-equilibrium calculations: a new technique, with petrological applications. Canadian Mineralogist, 29(4), 833-855.

Berman, R. G. 2007. winTWQ (version 2.3): a software package for performing internally-consistent thermobarometric calculations. Geological survey of Canada, Open File Report, 5462. p 41.

Bhatia, M. R., & Crook, K. A. 1986. Trace element characteristics of graywackes and tectonic setting discrimination of sedimentary basins. Contributions to Mineralogy and Petrology, 92(2), 181-193.

Bhattacharya, A., Mohanty, L., Maji, A., Sen, S. K., & Raith, M. 1992. Non-ideal mixing in the phlogopite-annite binary: constraints from experimental data on Mg− Fe partitioning and a reformulation of the biotite-garnet geothermometer. Contributions to Mineralogy and Petrology, 111(1), 87-93.

Biczok, J., Hollings, P., Klipfel, P., Heaman, L., Maas, R., Hamilton, M., Kamo, S. & Friedman, R. 2012. Geochronology of the North Caribou greenstone belt, Superior Province Canada: Implications for tectonic history and gold mineralization at the Musselwhite mine. Precambrian Research, 192, 209-230.

Bigot, L., & Jébrak, M. 2015. Gold mineralization at the syenite-hosted Beattie gold deposit, Duparquet, Neoarchean Abitibi Belt, Canada. Economic Geology, 110(2), 315-335.

Bleeker, W., 2012. Targeted Geoscience Initiative 4. Lode gold deposits in ancient deformed and metamorphosed terranes: the role of extension in the formation of Timiskaming basins and large gold deposits, Abitibi greenstone belt—a discussion. Ontario Geological Survey, Summary of Field Work and Other Activities, p 47.

Breaks, F.W., Osmani, I.A deKemp, E.A., 2001. Geology of the North Caribou Lakecarea, Northwestern Ontario. Ontario Geological Survey, Open File Report 6023, p 80.

Cao, H. and Fletcher, C., 2012. FIA trends along the Precambrian Rocky Mountains: a new approach to timing continental docking. Journal of Metamorphic Geology, 30(7), 639-650.

Carson, C. J., Ague, J. J., Grove, M., Coath, C. D., and Harrison, T. M. 2002. U–Pb isotopic behaviour of zircon during upper-amphibolite facies fluid infiltration in the Napier Complex, east Antarctica. Earth and Planetary Science Letters, 199(3), 287-310.

Corcoran, P. L., & Mueller, W. U. 2007. Time-Transgressive Archean Unconformities underlying molasse basin-fill successions of dissected oceanic arcs, Superior Province, Canada. The Journal of Geology, 115(6), 655-674.

Corfu, F., Jackson, S.L., & Sutcliffe, R.H. 1991. U-Pb geochronology in the southwestern Abitibi greenstone belt, Superior province. Canadian Journal of Earth Sciences. 28, 489-503.

Corfu, F. & Stone, D. 1998. Age structure & orogenic significance of the Berens River composite batholiths, western Superior Province. Canadian Journal of Earth Sciences 35, 1089-1109.

Corfu, F. & Lin, S. 2000. Geology and U-Pb geochronology of the Island Lake greenstone belt, Northwestern Superior Province, Manitoba. Canadian Journal of Earth Sciences 37, 1275-1286.

Corfu, F., Hanchar, J.M., Hoskin, P.W. & Kinny, P., 2003. Atlas of zircon textures. Reviews in Mineralogy and Geochemistry, 53(1), 469-500.

Corkery, M.T., Cameron, H.D.M., Lin, S., Skulski, T., Whalen, J.B., Stern, R.A., 2000. Geological investigations in the Knee Lake belt (Parts of NTS 53L). In: Report of Activities 2000. Manitoba Industry, Trade and Mines, Manitoba Geological Survey, 129–136.

Davis, D.W. and Stott, G.M. 2001. Geochronology of Several Greenstone Belts in the Sachigo Subprovince, Northwestern Ontario: Ontario Geological Survey Open File Report 6070-018, 18p.

de Kemp, E.A. 1987. Stratigraphy, provenance, and geochronology of Archean supracrustal rock of western Eyapamikama Lake area, Northwestern Ontario. Unpublished M.Sc. Thesis, Carleton University, Ottawa, ON, p 98.

Donaldson, J.A. & de Kemp, E.A., 1998. Archaean quartz arenites in the Canadian Shield: examples from the Superior and Churchill Provinces. Sedimentary Geology, 120(1), 153-176.

Driese, S. G., Jirsa, M. A., Ren, M., Brantley, S. L., Sheldon, N. D., Parker, D., & Schmitz, M. 2011. Neoarchean paleoweathering of tonalite and metabasalt: implications for reconstructions of 2.69 Ga early terrestrial ecosystems and paleoatmospheric chemistry. Precambrian Research, p 189.

Dube, B., & Gosselin, P. 2007. Greenstone-hosted quartz-carbonate vein deposits. Mineral Deposits of Canada: A synthesis of major deposit-types, district metallogeny, the evolution of geological provinces, and exploration methods: Geological Association of Canada, Mineral Deposits Division, Special Publication, 5, 49-73.

Duff, J., Hattori, K., Schneider, D.A., Cossette, E., Jackson S. & Biczok, J., 2012. Using garnet to record mineralization in a BIF-hosted orogenic Au deposit. 2012 Goldschmidt conference. Abstract.

Duff, J. 2014. A geochemical and isotopic investigation of metasedimentary rocks from the North Caribou greenstone belt, western Superior Province, Canada. Unpublished M.Sc. thesis, Department of Earth Science, University of Ottawa, Ottawa, ON, p 180.

Emslie, R.F. 1962. Wunnummin Lake (NTS 53A), Ontario. Geological Survey of Canada Map 1-1962

Feenstra, A., & Peters, T. 1996. Experimental determination of activities in $FeTiO_3$-$MnTiO_3$ ilmenite solid solution by redox reversals. Contributions to mineralogy and petrology, 126(1-2), 109-120.

Fu, B., Page, F.Z., Cavosie, A.J., Fournelle, J., Kita, N.T., Lackey, J.S., Wilde, S.A. & Valley, J.W., 2008. Ti-in-zircon thermometry: applications and limitations. Contributions to Mineralogy and Petrology, 156(2), 197-215.

Gagnon, É. 2015. Investigation of Transpressive Deformation Zones in the North Caribou Greenstone Belt (NW Superior) and Relationships with Regional Metamorphism: Implications for the Technothermal Evolution during Archean Cratonization. Unpublished M.Sc. thesis, Department of Earth Science, University of Ottawa, Ottawa, ON, p 205.

Gagnon, É., Schneider, D.A., Kalbfleisch, T., Habler, G. & Biczok, J., 2016. Characterization of transpressive deformation in shear zones of the Archean North Caribou greenstone belt (NW Superior Province) and the relationship with regional metamorphism. Tectonophysics.

Gehrels, G. 2012. Detrital zircon U-Pb geochronology: current methods and new opportunities. In Tectonics of Sedimentary Basins: Recent Advances, First Edition. Edited by Bubsy, C. and Azor, A. Blackwell Publishing Ltd., Hoboken, NJ. 47-62.

Goldstein, S. L., O'nions, R. K., & Hamilton, P. J. 1984. A Sm-Nd isotopic study of atmospheric dusts and particulates from major river systems. Earth and Planetary Science Letters, 70(2), 221-236.

Griffin, W. L., Powell, W. J., Pearson, N. J., & O'Reilly, S. Y. 2008. GLITTER: data reduction software for laser ablation ICP-MS. Laser Ablation-ICP-MS in the earth sciences. Mineralogical Association of Canada Short Course Series, 40, 204-207.

Groves, D. I., Goldfarb, R. J., Gebre-Mariam, M., Hagemann, S. G., & Robert, F. 1998. Orogenic gold deposits: a proposed classification in the context of their crustal distribution and relationship to other gold deposit types. Ore Geology Reviews, 13(1), 7-27.

Gulbin, Y.L., 2011. Optimization of the garnet-biotite geothermometer: I. Temperature trends. Geology of Ore Deposits, 53(7), 528-542.

Gürbüz, A. 2010. Geometric characteristics of pull-apart basins. Lithosphere,2(3), 199-206.

Haendel, D., Mühle, K., Nitzsche, H. M., Stiehl, G., & Wand, U. 1986. Isotopic variations of the fixed nitrogen in metamorphic rocks. Geochimica et Cosmochimica Acta, 50(5), 749-758.

Hawthorne, F.C., Oberti, R., Harlow, G.E., Maresch, W.V., Martin, R.F., Schumacher, J.C. and Welch, M.D., 2012. Nomenclature of the amphibole supergroup. American Mineralogist, 97 (11-12), 2031-2048.

Hellstrom, J., Paton, C., Woodhead, J., & Hergt, J. 2008. Iolite: software for spatially resolved LA-(quad and MC) ICPMS analysis. Mineralogical Association of Canada Short Course Series, 40, 343-348.

Henry, P., Stevenson, R. K., Larbi, Y., & Gariépy, C. 2000. Nd isotopic evidence for early to late Archean (3.4–2.7 Ga) crustal growth in the Western Superior Province (Ontario, Canada). Tectonophysics, 322(1), 135-151.

Hoisch, T. D. 1990. Empirical calibration of six geobarometers for the mineral assemblage quartz+ muscovite+ biotite+ plagioclase+ garnet. Contributions to Mineralogy and Petrology, 104(2), 225-234.

Hollings, P., Wyman, D.A., Kerrich, R., 1999. Komatiite - basalt - rhyolite volcanic associations in Northern Superior Province greenstone belts: Significance of plumearc interaction in the generation of the proto continental Superior Province. Lithos 46, 137–161.

Hollings, P., Isaac, C., Biczok, J., Maas, R., & Friedman, R., 2011. Nitrogen isotopes and geochronology of the Musselwhite Au mine, Canada. Goldschmidt conference abstracts, Mineralogical Magazine, 75 (3), 1039.

Hoskin, P. W., and Schaltegger, U. 2003. The composition of zircon and igneous and metamorphic petrogenesis. Reviews in Mineralogy and Geochemistry, 53(1), 27-62.

Issac, C. 2008. Stable isotope (N, O, H) geochemistry, petrology and compositions of biotite of the Musselwhite Mine, Ontario: implications for mineralisation. Unpublished M.Sc. thesis, Lakehead University, Thunder Bay, ON, 96 p.

Jackson, V.A., van Breemen, O., Ootes, L., Bleeker, W., Bennett, V., Davis, W.J., Ketchum, J.W.F. and Smar, L., 2013. U–Pb zircon ages and field relationships of Archean basement and Proterozoic intrusions, south-Central Wopmay Orogen, NWT: implications for tectonic assignments 1, 2. Canadian Journal of Earth Sciences, 50(10), 979-1006.

Jia, Y. & Kerrich, R. 2000. Giant quartz vein systems in accretionary orogenic belts: the evidence for a metamorphic fluid origin from $\delta^{15}N$ and $\delta^{13}C$ studies. Earth and Planetary Science Letters, 184, 211-224.

Jia, Y., 2006. Nitrogen isotope fractionations during progressive metamorphism: a case study from the Paleozoic Cooma metasedimentary complex, southeastern Australia. Geochimica et Cosmochimica Acta, 70, 5201-5214.

Kalbfleisch, T. 2012. Crustal-scale shear zones recording 400 M.Y. of tectonic activity in thNorth Caribou greenstone belt, western superior Province of Canada. Unpublished MSc.thesis, University of Ottawa 95 p.

Leclair, A.D., Ernst, R.E., Hattori, K., 1993, Crustal-scale auriferous shear zones in the Central Superior Province, Canada. Geology, 21, 399-402.

Legault, I.M., 1993. Petrology and geochemistry of Timiskaming Group sedimentary rocks, Kirkland Lake area, Abitibi greenstone belt. University of Ottawa, Canada.

Lin, S., Davis, D.W., Rotenberg, E., Corkery, M.T., & Bailes, A.H., 2006. Geological evolution of the Northwestern Superior Province: clues from geology, kinematics and geochronology in the Gods

Lake Narrows area, Oxford-Stull terrane, Manitoba. Canadian Journal of Earth Sciences 43, 749–765.

Lin, S., Parks, J., Heaman, L.M., Simonetti, A. & Corkery, M.T., 2013. Diapirism and sagduction as a mechanism for deposition and burial of “Timiskaming-type” sedimentary sequences, Superior Province: Evidence from detrital zircon geochronology and implications for the Borden Lake conglomerate in the exposed middle to lower crust in the Kapuskasing uplift. Precambrian Research, 238, 48-157.

Lobato, L.M., Santos, J.O.S., McNaughton, N.J., Fletcher, I.R. & Noce, C.M. 2007. U–Pb SHRIMP monazite ages of the giant Morro Velho and Cuiabá gold deposits, Rio das Velhas greenstone belt, Quadrilátero Ferrífero, Minas Gerais, Brazil. Ore Geology Reviews, 32 (3-4), 674-680.

Lodge, R.W., Gibson, H.L., Stott, G.M., Hudak, G.J., Jirsa, M.A. & Hamilton, M.A., 2013. New U–Pb geochronology from Timiskaming-type assemblages in the Shebandowan and Vermilion greenstone belts, Wawa subprovince, Superior Craton: Implications for the Neoarchean development of the southwestern Superior Province. Precambrian Research, 235, 264-277.

Longerich, H. P., Jackson, S. E., & Günther, D. 1996. Inter-laboratory note. Laser ablation inductively coupled plasma mass spectrometric transient signal data acquisition and analyte concentration calculation. Journal of Analytical Atomic Spectrometry, 11(9), 899-904.

Ludwig, K. R. 2003. User's manual for Isoplot 3.00: a geochronological toolkit for Microsoft Excel (No. 4). Kenneth R. Ludwig.

Marty, B., & Zimmerman, L., 1999. Volatiles (He, C, N, Ar) in mid-ocean ridge basalts: Assessment of shallow-level fractionation and characterization of source composition. Geochimica et Cosmochimica Acta, 63, 3619-3633.

McDonough, W. F., & Sun, S. S. 1995. The composition of the Earth. Chemical Geology, 120(3), 223-253.

McLennan, S.M. & Taylor, S.R., 1991. Sedimentary rocks and crustal evolution: tectonic setting and secular trends. The Journal of Geology, 99, 1-21.

McNicoll, V., Dubé, B., Castonguay, S., Oswald, W., Biczok, J., Mercier-Langevin, P., & Malo, M. (2016). The world-class Musselwhite BIF-hosted gold deposit, Superior Province, Canada: New high-precision U–Pb geochronology and implications for the geological setting of the deposit and gold exploration. Precambrian Research, 272, 133-149.

Michard, A., Gurriet, P., Soudant, M., & Albarede, F. 1985. Nd isotopes in French Phanerozoic shales: external vs. internal aspects of crustal evolution. Geochimica et Cosmochimica Acta, 49(2), 601-610.

Morelli, R. M., Bell, C. C., Creaser, R. A., and Simonetti, A. 2010. Constraints on the genesis of gold mineralization at the Homestake Gold Deposit, Black Hills, South Dakota from rhenium–osmium sulfide geochronology. Mineralium Deposita, 45(5), 461-480.

Mueller, W.U. and Corcoran, P.L., 1998. Late-orogenic basins in the Archaean Superior Province, Canada: characteristics and inferences. Sedimentary Geology, 120(1), 177-203.

Nishizawa, M., Sao, Y., Ueno, Y., Shigenori, M., 2007. Speciation and isotope ratios of nitrogen in fluid inclusions from seafloor hydrothermal deposits at ~3.5 Ga. Earth and Planetary Science Letters, 254, 332-344.

Ontario Geological Survey. 2001. 1:250,000 scale bedrock geology of Ontario. Ontario Geological Survey, Miscellaneous Relase, Data 126-Revision 1.

Oswald, W., Castonguay, S., Dubé, B., Malo, M., Mercier-Langevin, P., & Biczok, J. 2015. New insights on the geological and structural settings of the Musselwhite banded iron-formation–hosted gold deposit, North Caribou greenstone belt, Superior Province, Ontario. Geological Survey of Canada Current Research 2015-3, p 22.

Otto, A. 2002. Ore forming processes in BIF-hosted gold deposit Musselwhite Mine, Ontario, Canada. Unpublished M.Sc. thesis, Department of Economic Geology and Leibniz Laboratory for Applied Marine Research, Freiberg University of Mining and Technology, Freiberg, Germany. p 82.

Paces, J. B., & Miller, J. D. 1993. Precise U-Pb ages of Duluth complex and related mafic intrusions, Northeastern Minnesota: Geochronological insights to physical, petrogenetic, paleomagnetic, and tectonomagmatic processes associated with the 1.1 Ga midcontinent rift system. Journal of Geophysical Research: Solid Earth (1978–2012), 98(B8), 13997-14013.

Parks, J., Lin S., Davis, D.W., Corkery, M.T., 2006. New High precision U-Pb ages for the Island Lake greenstone belt, Northwestern Superior Province: implications for regional stratigraphy and the extent of the North Caribou terrane. Canadian Journal of Earth Sciences 43, 789–803.

Parmenter, A. C., Lin, S., & Corkery, M. T. 2006. Structural evolution of the Cross Lake greenstone belt in the Northwestern Superior Province, Manitoba: implications for relationship between vertical and horizontal tectonism. Canadian Journal of Earth Sciences, 43(7), 767-787.

Percival, J.A., Sandborn-Barrie, M., Skulski, T. Stott, G.M., Helmstaedt, H., & White, D.J., 2006a. Tectonic evolution of the western Superior Province from NATMAP and Lithoprobe studies. Canadian Journal of Earth Sciences 43, 1085–1117.

Percival, J.A., McNicoll, V. & Bailes, A.H., 2006b. Strike-slip juxtaposition of ca. 2.72 Ga juvenile arc and> 2.98 Ga continent margin sequences and its implications for Archean terrane accretion, western Superior Province, Canada. Canadian Journal of Earth Sciences, 43(7), 895-927..

Pettijohn, F.J., Potter, P.E., & Siever, R., 1987. Sand and sandstone: New York, Springer-Verlag, p 553.

Petrus, J. A., & Kamber, B. S. 2012. VizualAge: A novel approach to laser ablation ICP-MS U-Pb geochronology data Reduction. Geostandards and Geoanalytical Research, 36(3), 247-270.

Pitcairn, I. K., Teagle, D. A., Kerrich, R., Craw, D., & Brewer, T. S. 2005. The behavior of nitrogen and nitrogen isotopes during metamorphism and mineralization: evidence from the Otago and Alpine Schists, New Zealand.Earth and Planetary Science Letters, 233(1), 229-246.

Richard, P., Shimizu, N., & Allègre, C. J. 1976. ^{143} Nd/^{146} Nd, a natural tracer: an application to oceanic basalts. Earth and Planetary Science Letters, 31(2), 269-278.

Roser, B.P. and Korsch, R.J., 1988. Provenance signatures of sandstone-mudstone suites determined using discriminant function analysis of major-element data. Chemical geology, 67(1), 119-139.

Rubatto, D. 2002. Zircon trace element geochemistry: partitioning with garnet and the link between U–Pb ages and metamorphism. Chemical Geology, 184(1), 123-138.

Sage, R.P. & Breaks, F.W. 1982. Geology of the Cat Lake – Pickle Lake area, districts of Kenora and Thunder Bay. Ontario Geological Survey, Geological Report 207, p 238.

Sanislav, I.V. and Bell, T.H., 2011. The inter-relationships between long-lived metamorphism, pluton emplacement and changes in the direction of bulk shortening during orogenesis. Journal of Metamorphic Geology, 29(5), 513-536.

Satterly, J. 1941. Geology of the Windigo-North Caribou lakes area, Kenora District (Patricia Portion); Ontario Department of Mines. Annual Report of 1939 48, part 9: 1-32.

Sharp, Z. 2007. Principles of Stable Isotope Geochemistry. Upper Saddle River, NJ: Pearson Education. 344 p.

Shegelski, R. J. 1980. Archean cratonization, emergence and red bed development, Lake Shebandowan area, Canada. Precambrian Research, 12(1), 331-347.

Spear, F. S., & Daniel, C. G. 2001. Diffusion control of garnet growth, Harpswell Neck, Maine, USA. Journal of Metamorphic Geology, 19(2), 179-195.

Stevenson, R., 1995. Crust and mantle evolution in the Late Archean: Evidence from a Sm-Nd isotopic study of the North Spirit Lake greenstone belt, Northwestern Ontario, Canada. Geological Society of America Bulletin, 107(12), 1458-1467.

Stevenson, R. K., Henry, P., & Gariépy, C. 2009. Isotopic and geochemical evidence for differentiation and crustal contamination from granitoids of the Berens river subprovince, Superior province, Canada. Precambrian Research, 168(1), 123-133.

Stott, G. M., & Schnieders, B. R. 1983. Gold mineralization in the Shebandowan belt and its relation to regional deformation patterns. The geology of gold in Ontario. Edited by AC Colvine. Ontario Geological Survey, Miscellaneous Paper, 110, 181-193.

Stott, G.M., Biczok, J. 2010. North Caribou greenstone belt: gold and its possible relation to the North Caribou pluton emplacement - a belt wide contact strain aureole? In: Ayer, J.A., Easton, R.M., Beakhouse, G.P., Stott, G.M., Kelly, R.I., Debicki, E.J., Parker, J.R., Brown, T. (Eds.), Summary of Field Work and Other Activities 2010. Ontario Geological Survey, Open File Report 6260, 22-1 to 22-12.

Stott, G. M., Corkery, M. T., Percival, J. A., Simard, M. & Goutier, J. 2010. A Revised Terrane Subdivision of the Superior Province. Ontario Geological Survey, Open File Report 6260, 20-1-20-1.

Thurston, P.C., Chivers, K.M., 1990. Secular variation in greenstone sequence development emphasizing Superior Province, Canada. Precambrian Research 46, 21–58.

Thurston, P.C., Osmani, I. & Stone, D. 1991. Northwestern Superior Province: review and terrane analysis. *In* Geology of Ontario, Special Volume 4, Part 1. Ontario Geological Survey. Edited by Thurston, P.C., Williams, H.R., Sutcliffe, R.H. and Stott, G.M. 80-142.

Van Lankvelt A. 2013. Protracted magmatism within the North Caribou Terrane, Superior Province: petrology, geochronology, and geochemistry of Meso- to Neoarchean TTG suites. Unpublished MSc thesis, University of Ottawa, p 208.

Wyman, D.A., Hollings, P. & Biczok, J. 2011. Crustal evolution in a cratonic nucleus: Granitoids and felsic volcanic rocks of the North Caribou terrane, Superior Province Canada. Lithos, 123: 37-49.

Young, M.D., McNicoll, V., Helmstaedt, H., Skulski, T., & Percival, J.A., 2006. Pickle Lake revisited: new structural, geochronological and geochemical constraints on greenstone belt assembly, western Superior Province, Canada. Canadian Journal of Earth Sciences 43, 821–847.

Zhou, F. 1994. Ti-Mg-Fe biotites: formation, substitution, and thermodynamic properties at 650 to 900 C and 1.1 Kb with fO2 defined by the CH4-graphite buffer, Ph.D. thesis, State University of New York, Stony Brook.

Appendix I. EMPA Analysis of Garnet

Sample	Type	SiO2	ZrO2	TiO2	Al2O3	Cr2O3	FeO	MnO	MgO	CaO	Na2O	Total
ob-010-1-1	Garnet	36.645	0	0.015	21.038	0.03	23.11	16.338	1.56	1.544	0.043	100.323
ob-010-1-2	Garnet	36.586	0	0.024	20.937	0	23.008	16.182	1.376	1.536	0.023	99.672
ob-010-1-3	Garnet	36.679	0	0.076	20.828	0.009	22.342	16.779	1.453	2.004	0.018	100.188
ob-010-1-4	Garnet	36.492	0.041	0.084	20.859	0	22.268	16.685	1.463	2.113	0.029	100.034
ob-010-1-5	Garnet	36.636	0	0.047	20.91	0	22.592	16.956	1.491	1.778	0.018	100.428
ob-010-1-6	Garnet	36.6	0	0.065	20.842	0	22.296	16.595	1.49	1.835	0.039	99.762
ob-010-1-7	Garnet	36.69	0.011	0.04	21.071	0	22.855	16.485	1.487	1.674	0.026	100.339
ob-010-1-8	Garnet	36.637	0.004	0.037	20.915	0.016	23.27	15.811	1.49	1.64	0.019	99.839
ob-010-1-9	Garnet	36.947	0	0.104	20.846	0.024	22.591	16.381	1.301	1.62	0.027	99.841
ob-010-1-10	Garnet	36.632	0.01	0.016	20.855	0	23.033	16.454	1.33	1.486	0.01	99.826
ob-010-1-11	Garnet	36.555	0	0.023	21.1	0.019	22.914	16.066	1.334	1.85	0.032	99.893
ob-010-2-1	Garnet	36.79	0	0.0342	20.72	0.0041	22.89	16.24	1.5017	1.58	0.0264	99.7864
ob-010-2-2	Garnet	36.88	0.0029	0.0205	20.98	0.0247	22.59	16.49	1.5729	1.54	0	100.1009
ob-010-2-3	Garnet	36.9	0	0.0503	20.72	0	21.89	17.2	1.5562	1.74	0.0366	100.0931
ob-010-2-4	Garnet	36.74	0	0.0403	20.75	0.0363	21.97	16.82	1.556	1.79	0.0128	99.7155
ob-010-2-5	Garnet	36.79	0.0059	0.0664	20.7	0.0045	21.71	17.08	1.531	1.9	0.0229	99.8107
ob-010-2-6	Garnet	36.62	0.0147	0.0314	20.63	0	22.28	16.39	1.6106	1.6	0.0083	99.185
ob-010-2-7	Garnet	36.86	0	0.047	20.75	0	22.73	15.95	1.5361	1.9	0.0275	99.8006
ob-010-2-8	Garnet	36.96	0	0.0182	20.86	0.0232	22.47	16.54	1.4176	1.46	0.0137	99.7628
ob-010-3-1	Garnet	37.1	0	0.0105	20.59	0	22.05	16.94	1.3751	1.46	0.0459	99.5715
ob-010-3-2	Garnet	36.9	0.0044	0.0169	20.78	0.055	22.39	16.44	1.5702	1.5	0.0427	99.6993
ob-010-3-3	Garnet	36.86	0	0.0267	20.78	0.0547	22.18	16.64	1.5629	1.53	0.0294	99.6638
ob-010-3-4	Garnet	36.78	0.5212	0.123	20.13	0.1509	21.28	16.96	1.5021	1.7	0.0695	99.2167
ob-010-3-5	Garnet	36.96	0	0.0534	20.61	0.0715	21.21	17.52	1.4757	1.96	0.0196	99.8802
ob-010-3-6	Garnet	36.99	0	0.0729	20.55	0	20.99	16.52	1.4348	2.75	0	99.3078
ob-010-3-7	Garnet	36.6	0	0.053	20.6	0.0034	22.11	16.51	1.5632	1.75	0.0015	99.1912
ob-010-3-8	Garnet	36.56	0.0059	0.0411	20.77	0	22.12	16.33	1.3547	1.69	0.0406	98.9124

Sample	Type	SiO2	ZrO2	TiO2	Al2O3	Cr2O3	FeO	MnO	MgO	CaO	Na2O	Total
ob-023-1-1	Garnet	31.65	0.0151	0.8889	18.04	0.0585	6.51	18.66	5.51	0.3188	0.0427	81.6941
ob-023-1-2	Garnet	36.88	0.0148	0.0362	20.5	0.0435	14.62	22.44	1.71	1.79	0.03	98.0645
ob-023-1-3	Garnet	36.84	0.0577	0.0093	20.49	0	14.76	22.43	1.75	1.8	0.0226	98.1596
ob-023-1-4	Garnet	36.8	0.0517	0.0302	20.36	0.0725	14.75	22.4	1.76	1.76	0.037	98.0215
ob-023-1-5	Garnet	36.86	0	0.0492	20.56	0.0482	14.94	22.48	1.66	1.66	0.0408	98.2983
ob-023-1-6	Garnet	36.85	0	0.0253	20.51	0.0645	14.66	22.72	1.72	1.7	0.0377	98.2875
ob-023-1-7	Garnet	36.8	0	0	20.49	0.0448	15.74	22.06	1.4375	1.41	0.0003	97.9826
ob-023-1-8	Garnet	39.21	0	0.02	19.65	0.0149	16.3	21.44	1.4445	1.41	0	99.4894
ob-023-2-1	Garnet	36.88	0	0.0074	20.52	0.046	15.13	22.38	1.5998	1.42	0.0132	97.9964
ob-023-2-2	Garnet	36.77	0.0103	0.0359	20.45	0.004	14.6	22.34	1.76	1.93	0.0219	97.9222
ob-023-2-3	Garnet	36.96	0	0.0588	20.52	0.0346	14.77	22.6	1.78	1.74	0.0413	98.5047
ob-023-2-4	Garnet	36.76	0	0.0564	20.64	0.0513	14.69	22.11	1.7	1.98	0.025	98.0127
ob-023-2-5	Garnet	37.06	0.0326	0.0875	20.53	0.0509	14.83	22.38	1.68	2.01	0.0394	98.7005
ob-023-2-6	Garnet	36.7	0	0.0768	20.38	0.066	14.87	22.49	1.6378	1.94	0.015	98.1756
ob-023-2-7	Garnet	36.86	0.0044	0.0716	20.33	0.0785	14.66	22.36	1.5778	1.97	0.0461	97.9585
ob-023-2-8	Garnet	36.74	0.037	0	20.3	0.0244	15.45	21.88	1.4247	1.67	0.0106	97.5367
ob-001-1 -1	Garnet	37.11	0.0073	0.0731	21.03	0.0161	23.36	11.7	1.2576	5.44	0.0113	100.0054
ob-001-1 -2	Garnet	37.07	0.0102	0.0387	20.64	0.0866	21.94	13.68	1.3714	4.87	0	99.707
ob-001-1 -3	Garnet	37	0	0.0638	20.69	0.0711	21.37	14.28	1.2668	4.84	0	99.5818
ob-001-1 -4	Garnet	36.98	0.032	0.1031	20.63	0.1318	22.28	13.27	1.3565	5.15	0.0296	99.963
ob-001-1 -5	Garnet	37.23	0	0.0471	20.83	0.0299	23.34	11.64	1.2914	5.26	0.0079	99.6764
ob-001-1 -6	Garnet	37.18	0.0262	0.0528	20.84	0.0832	23.4	11.68	1.2762	5.22	0.011	99.7695
ob-001-1 -7	Garnet	37.16	0	0.0434	21.03	0.004	23.14	12.07	1.2322	5.01	0.0146	99.7043
ob-001-1 -8	Garnet	37.15	0	0.052	20.9	0.127	22.93	11.51	1.3668	5.71	0.0266	99.7724
ob-001-1 -9	Garnet	37.04	0.0437	0.0806	20.68	0	22.04	13.9	1.4127	4.78	0.0018	99.9789
ob-001-1 -10	Garnet	37.05	0	0.084	20.62	0	21.61	14.03	1.33	4.96	0.0039	99.6879
ob-001-1 -11	Garnet	37.18	0.0088	0.0207	20.83	0.0557	23.07	11.74	1.4025	5.54	0	99.8478
ob-001-1 -12	Garnet	37.27	0	0.0435	21.04	0.0829	23.68	11.54	1.4068	5.04	0.0081	100.1113
ob-001-1 -13	Garnet	37.3	0	0.0574	20.85	0.0349	23.6	11.52	1.3335	5.37	0.0034	100.0691
ob-001-2-1	Garnet	36.804	0	0.178	20.741	0.015	22.139	13.692	1.311	4.875	0	99.755
ob-001-2-2	Garnet	36.827	0	0.089	20.748	0.001	24.696	10.881	1.339	4.896	0.015	99.492

Sample	Type	SiO2	ZrO2	TiO2	Al2O3	Cr2O3	FeO	MnO	MgO	CaO	Na2O	Total
ob-001-2-3	Garnet	36.704	0	0.043	20.938	0	24.533	10.895	1.423	5.162	0.001	99.699
ob-001-2-4	Garnet	36.747	0	0.1	20.549	0	20.18	15.645	1.437	4.971	0.001	99.63
ob-001-2-5	Garnet	36.753	0	0.099	20.569	0	22.323	12.885	1.256	5.555	0	99.44
ob-001-2-6	Garnet	36.701	0	0.097	20.521	0.003	20.854	14.967	1.268	5.262	0	99.673
ob-001-2-7	Garnet	36.746	0.019	0.022	20.771	0	17.438	17.958	1.242	5.668	0.001	99.865
ob-001-2-8	Garnet	36.763	0	0.052	20.716	0	16.991	18.34	1.251	5.509	0.002	99.624
ob-001-2-9	Garnet	36.78	0.007	0.187	20.251	0.001	17.71	17.245	1.316	5.916	0.001	99.414
ob-001-2-10	Garnet	36.611	0.004	0.101	20.626	0.022	17.83	17.152	1.298	5.661	0.008	99.313
ob-001-2-11	Garnet	36.772	0.006	0.062	20.662	0.014	21.924	13.58	1.313	4.967	0.002	99.302
ob-001-2-12	Garnet	36.873	0	0.086	20.43	0.003	20.316	14.769	1.176	5.989	0.001	99.643
ob-001-2-13	Garnet	36.875	0.004	0.019	21.105	0	24.377	11.248	1.261	4.955	0.009	99.853
ob-001-2-14	Garnet	36.871	0.026	0.042	20.891	0	21.9	12.024	1.215	6.351	0.003	99.323
ob-001-3-1	Garnet	36.535	0.017	0.052	20.822	0	24.351	10.663	1.395	5.399	0.011	99.245
ob-001-3-2	Garnet	36.692	0	0.028	20.887	0	23.721	11.249	1.406	5.358	0	99.341
ob-001-3-3	Garnet	36.911	0	0.053	20.647	0	24.136	10.925	1.414	5.329	0.008	99.423
ob-001-3-4	Garnet	36.7	0.021	0.063	20.549	0	19.21	16.482	1.336	5.284	0.015	99.66
ob-001-3-5	Garnet	36.873	0	0.082	20.499	0	19.445	15.935	1.413	5.364	0	99.611
ob-001-3-6	Garnet	36.911	0	0.057	20.577	0.016	21.387	13.042	1.284	6.175	0.007	99.456
ob-001-3-7	Garnet	36.298	0	0.041	20.866	0	24.279	10.202	1.763	5.34	0.004	98.793
ob-001-3-8	Garnet	36.603	0.004	0.073	20.762	0.007	21.706	13.516	1.331	5.344	0	99.346
ob-001-3-9	Garnet	36.682	0	0.1	20.563	0	22.097	13.189	1.314	5.273	0.012	99.23
ob-001-3-10	Garnet	37.248	0.009	0.041	20.706	0.008	23.52	10.867	1.467	5.825	0	99.691
ob-001-4-1	Garnet	36.712	0.011	0.054	20.621	0	23.428	11.434	1.22	5.481	0.013	98.974
ob-001-4-2	Garnet	36.732	0	0.041	20.683	0.078	23.81	10.966	1.434	5.249	0.005	98.998
ob-001-4-3	Garnet	36.659	0.027	0.088	20.512	0.011	21.742	13.799	1.283	5.01	0	99.131
ob-001-4-4	Garnet	36.671	0.016	0.061	20.534	0.055	21.411	14.301	1.267	5.076	0.017	99.409
ob-001-4-5	Garnet	36.846	0.04	0.045	20.763	0	22.534	12.306	1.314	5.746	0.016	99.61
ob-001-4-6	Garnet	37.029	0	0.071	20.719	0.042	23.508	11.113	1.338	5.933	0.011	99.764
ob-001-4-7	Garnet	36.757	0	0.055	20.72	0.094	23.49	11.105	1.237	5.909	0.001	99.368
ob-035-1-1	Garnet	37.246	0.012	0.021	21.008	0	35.013	0.886	3.611	1.945	0.029	99.771
ob-035-1-2	Garnet	37.617	0	0.025	21.085	0.051	33.591	0.561	3.784	3.112	0.021	99.847
ob-035-1-3	Garnet	37.523	0	0.008	21.178	0.015	34.188	0.615	3.717	2.878	0.007	100.129

Sample	Type	SiO2	ZrO2	TiO2	Al2O3	Cr2O3	FeO	MnO	MgO	CaO	Na2O	Total
ob-035-1-4	Garnet	37.277	0.005	0.032	21.175	0.045	34.317	0.554	3.882	2.883	0.043	100.213
ob-035-1-5	Garnet	37.5	0	0.011	21.025	0.012	34.202	0.566	3.655	2.935	0.006	99.912
ob-035-1-6	Garnet	37.665	0	0.006	21.144	0	34.884	0.815	3.646	1.934	0.013	100.107
ob-035-1-7	Garnet	37.655	0	0.005	21.253	0.014	34.873	0.659	3.892	2.014	0.008	100.373
ob-035-1-8	Garnet	37.551	0.023	0.017	21.134	0.039	33.685	0.551	3.84	3.229	0	100.069
ob-035-1-9	Garnet	37.579	0	0.017	21.023	0.01	34.279	0.549	3.807	2.718	0.001	99.983
ob-035-1-10	Garnet	37.728	0	0.014	21.365	0	33.9	0.666	3.833	2.74	0.004	100.25
ob-035-2-1	Garnet	37.327	0.004	0.015	21.114	0	33.369	1.308	3.711	3.006	0.003	99.857
ob-035-2-2	Garnet	37.259	0.006	0.024	21.179	0.032	33.005	1.677	3.697	2.919	0	99.798
ob-035-2-3	Garnet	37.472	0.696	0.029	20.829	0	32.294	1.634	3.562	3.606	0	100.122
ob-035-2-4	Garnet	37.478	0	0.029	21.206	0	32.59	1.573	3.569	3.516	0.011	99.972
ob-035-2-5	Garnet	37.284	0.013	0.044	21.083	0.012	33.135	1.672	3.62	2.834	0.004	99.701
ob-035-2-6	Garnet	37.422	0.019	0.013	20.947	0.055	33.556	1.516	3.691	2.871	0.011	100.101
ob-035-2-7	Garnet	37.369	0	0.015	21.049	0.052	33.362	1.357	3.716	2.874	0	99.794
ob-035-2-8	Garnet	37.485	0.006	0.035	20.702	0.09	33.979	1.308	3.341	2.805	0.002	99.753
ob-035-2-9	Garnet	37.258	0	0.008	20.938	0.024	33.33	1.34	3.618	2.815	0.014	99.345
ob-035-2-10	Garnet	37.254	0	0.006	21.124	0.018	34.032	1.233	3.49	2.783	0.009	99.949
ob-035-3-1	Garnet	37.234	0	0	21.036	0.062	33.307	1.231	4.266	2.174	0.01	99.32
ob-035-3-2	Garnet	37.285	0	0.039	21.07	0	32.753	0.852	4.056	3.051	0	99.106
ob-035-3-3	Garnet	37.103	0	0.033	21.115	0	32.646	1.269	3.909	3.225	0.008	99.308
ob-035-3-4	Garnet	37.622	0.012	0.02	20.859	0	32.362	0.941	3.973	3.344	0	99.133
ob-035-3-5	Garnet	37.305	0.015	0.015	21.186	0.009	32.851	1.303	3.713	2.994	0.001	99.392
ob-035-3-6	Garnet	37.276	0.002	0.024	21.08	0.027	31.678	1.238	3.523	3.989	0.003	98.84
ob-035-3-7	Garnet	37.098	0.012	0.042	21.175	0	33.452	1.291	3.503	2.951	0	99.524
ob-035-3-8	Garnet	38.15	0.019	0.011	20.165	0.114	33.301	1.454	3.805	2.836	0.003	99.858
ob-035-3-9	Garnet	37.456	0	0.033	21.226	0.02	32.779	1.249	3.737	3.598	0.006	100.104
ob-035-3-10	Garnet	37.329	0.004	0.029	21.09	0.02	33.186	1.808	3.275	3.164	0.02	99.925
ob-035-3-11	Garnet	37.441	0	0.021	21.017	0	32.558	1.375	3.868	3.283	0.015	99.578
ob-035-3-12	Garnet	37.458	0	0.039	21.161	0	32.359	1.261	4.066	3.169	0.006	99.519
ob-035-3-13	Garnet	37.166	0	0.004	20.879	0.014	33.557	3.038	2.568	2.497	0.004	99.727
ob-035-3-14	Garnet	37.294	0.017	0.005	21.022	0.042	32.882	1.972	3.606	2.67	0.01	99.52
ob-035-3-15	Garnet	37.5	0.008	0.009	21.208	0.022	33.138	1.482	4.149	2.044	0.012	99.572

Sample	Type	SiO2	ZrO2	TiO2	Al2O3	Cr2O3	FeO	MnO	MgO	CaO	Na2O	Total
ob-035-3-16	Garnet	37.568	0	0.046	20.979	0.232	32.238	1.045	3.893	3.806	0	99.807
jd-033-1-1	Garnet	36.327	0.006	0.012	20.676	0.078	27.893	10.116	0.869	3.194	0.023	99.194
jd-033-1-2	Garnet	36.443	0	0.006	20.538	0.116	28.471	7.945	1.14	4.388	0.02	99.067
jd-033-1-3	Garnet	37.049	0	0.134	20.78	0	26.727	6.769	1.095	7.26	0.023	99.837
jd-033-1-4	Garnet	36.91	0.014	0.122	20.757	0.062	26.475	6.817	1.11	7.301	0.008	99.576
jd-033-1-5	Garnet	36.663	0	0.077	20.672	0.054	27.55	7.069	1.126	6.202	0	99.413
jd-033-1-6	Garnet	36.719	0.011	0.163	20.642	0.105	27.289	7.021	1.08	6.556	0.018	99.604
jd-033-1-7	Garnet	36.844	0.008	0.115	20.72	0.062	26.693	7.192	1.095	7.062	0.017	99.808
jd-033-1-8	Garnet	36.898	0	0.11	20.718	0.042	26.59	7.062	1.099	7.186	0.02	99.725
jd-033-1-9	Garnet	36.664	0	0.051	20.693	0.057	28.182	7.073	1.209	5.763	0.008	99.7
jd-033-1-10	Garnet	36.993	0	0.082	20.798	0.091	26.62	6.672	1.132	7.331	0.015	99.734
jd-033-1-11	Garnet	36.831	0.002	0.089	20.679	0.055	26.629	7.146	0.993	7.137	0.008	99.569
jd-033-1-12	Garnet	36.549	0.012	0	20.836	0	29.202	7.529	1.225	4.214	0.007	99.574
jd-033-1-13	Garnet	36.657	0.01	0.011	20.705	0.074	29.318	8.224	1.238	3.541	0.017	99.795
jd-033-1-14	Garnet	36.563	0	0.013	20.703	0.067	28.058	9.976	0.919	3.377	0.033	99.709
jd-033-1-15	Garnet	36.442	0	0.005	20.75	0	27.831	9.829	0.931	3.757	0.002	99.547
jd-033-1-16	Garnet	37.53	0.024	0.279	20.611	0.083	27.239	6.673	1.111	6.955	0.008	100.513
jd-033-1-17	Garnet	36.528	0.004	0.006	20.825	0.062	26.785	9.81	0.817	4.54	0.009	99.386
jd-033-2-1	Garnet	36.488	0.009	0.012	20.723	0.124	27.942	7.365	1.069	5.312	0.088	99.132
jd-033-2-2	Garnet	36.641	0.009	0	20.849	0.091	30.029	5.671	1.395	4.833	0.086	99.604
jd-033-2-3	Garnet	36.699	0.002	0.01	20.668	0.089	29.791	5.552	1.408	4.955	0.016	99.19
jd-033-2-4	Garnet	36.69	0.016	0.005	20.666	0.102	29.051	6.013	1.313	5.395	0.014	99.265
jd-033-2-5	Garnet	36.645	0	0.012	20.682	0.034	28.15	6.261	1.248	5.851	0.055	98.938
jd-033-2-6	Garnet	36.796	0.015	0.015	20.717	0.071	27.913	6.333	1.135	6.061	0.014	99.07
jd-033-2-7	Garnet	36.727	0	0.007	20.676	0.085	27.867	6.557	1.095	5.876	0.025	98.915
jd-033-2-8	Garnet	36.626	0.025	0.121	20.616	0.048	26.688	6.85	1.082	6.807	0.016	98.879
jd-033-2-9	Garnet	36.454	0.007	0.048	20.605	0.039	26.769	6.591	1.145	6.741	0.028	98.427
jd-033-2-10	Garnet	36.751	0	0.021	20.76	0.086	28.341	6.305	1.261	5.793	0.02	99.338
jd-033-2-11	Garnet	36.803	0.019	0.012	20.76	0.088	30.314	5.744	1.387	4.749	0.005	99.881

Sample	Type	SiO2	ZrO2	TiO2	Al2O3	Cr2O3	FeO	MnO	MgO	CaO	Na2O	Total
jd-033-2-12	Garnet	36.825	0.003	0.007	20.915	0.077	29.238	6.147	1.229	5.364	0.008	99.813
jd-033-2-13	Garnet	36.958	0.025	0.01	20.601	0.108	27.544	7.819	0.946	5.334	0.013	99.358
jd-033-2-14	Garnet	36.781	0.028	0.01	20.697	0.087	28.089	7.54	1.072	5.014	0.011	99.329
jd-033-2-15	Garnet	36.842	0	0.016	20.896	0.073	28.381	6.974	1.099	5.144	0.033	99.458
jd-033-3-1	Garnet	36.672	0.009	0.021	20.783	0.087	28.719	8.055	0.96	4.134	0.001	99.441
jd-033-3-2	Garnet	36.797	0	0.007	20.928	0.088	28.789	6.356	1.16	5.517	0.009	99.651
jd-033-3-3	Garnet	37.063	0.02	0.095	20.845	0.053	26.842	6.942	1.051	7.017	0	99.928
jd-033-3-4	Garnet	36.955	0	0.095	20.82	0.075	26.951	7.269	1.027	6.87	0.009	100.071
jd-033-3-5	Garnet	37.019	0	0.089	20.851	0.07	26.601	7.284	1.047	7.034	0.014	100.009
jd-033-3-6	Garnet	36.746	0.023	0.013	20.85	0.099	28.193	6.005	1.134	6.328	0.029	99.42
jd-033-3-7	Garnet	36.597	0.018	0.017	20.853	0.075	30.208	6.828	1.244	3.934	0.007	99.781
jd-033-3-8	Garnet	36.823	0	0.007	20.867	0.096	29.678	7.408	1.146	3.978	0	100.003
jd-033-3-9	Garnet	40.143	0	0.026	20.098	0.118	25.344	8.37	1.153	6.259	0.018	101.529
jd-033-3-10	Garnet	36.848	0	0	20.951	0.011	29.636	6.92	1.151	4.335	0.008	99.86
jd-033-3-11	Garnet	36.884	0	0.003	20.943	0.049	27.394	7.7	0.851	5.832	0.02	99.676
jd-100-1-1	Garnet	36.35	0	0.0322	20.72	0	11.2	26.26	1.4443	1.7	0.0283	97.7348
jd-100-1-2	Garnet	36.66	0.071	0.0685	20.53	0.0173	11.31	25.94	1.5007	1.79	0.025	97.9125
jd-100-1-3	Garnet	36.92	0.0074	0.0206	20.31	0.0475	11.28	25.84	1.5248	1.71	0.0697	97.73
jd-100-1-4	Garnet	37.03	0	0.0201	20.32	0	11.17	26.09	1.4479	1.8	0.041	97.919
jd-100-1-5	Garnet	36.99	0.0148	0.0246	20.27	0.0092	11.37	26.24	1.479	1.93	0.0155	98.3432
jd-100-1-6	Garnet	36.56	0.0029	0.041	20.57	0	11.11	26.32	1.3705	1.9	0.0156	97.89
jd-100-1-7	Garnet	34.42	0	0.0392	20.05	0.0228	10.09	26.71	2.26	1.91	0.042	95.544
jd-100-1-8	Garnet	36.81	0	0.0131	20.21	0	11.9	26	1.2992	1.62	0.0244	97.8768
jd-100-1-9	Garnet	36.81	0	0.0402	20.22	0	10.93	26.03	1.4121	1.89	0.038	97.3704
jd-100-1-10	Garnet	36.9	0	0.0131	20.25	0	11.45	26.47	1.3462	1.61	0.0465	98.0859
jd-100-1-11	Garnet	36.83	0.0088	0.329	20.05	0.0296	11.07	25.65	1.1076	3.3	0.0308	98.4058
jd-100-1-12	Garnet	36.92	0	0.1283	19.88	0.1424	11.09	25.83	1.1356	3.02	0.0264	98.1727
jd-100-1-13	Garnet	36.93	0	0.1719	20.11	0.1337	11.19	25.46	0.9482	3.8	0.0224	98.7662
jd-100-1-14	Garnet	37.01	0.0088	0.11	20.3	0	10.98	26.68	1.2827	2.32	0.0203	98.7118
jd-100-1-15	Garnet	34.85	0.0029	0.0452	18.35	0.0056	10.83	24.68	1.1401	2	0.276	92.1799
jd-100-1-16	Garnet	36.81	0	0.0281	20.43	0	11.52	26.5	1.1626	2.06	0.0055	98.5163
jd-100-1-17	Garnet	95.84	0	0.0206	2.12	0	1.84	3.69	0.1186	0.3542	0.0154	103.9987

Sample	Type	Si	Zr	Ti	Al	Cr	Fe	Mn	Mg	Ca	Na	Total
ob-010-1-1	Garnet	5.9532	0	0.0018	4.0286	0.0038	3.1399	2.2483	0.3777	0.2687	0.0136	16.0357
ob-010-1-2	Garnet	5.9776	0	0.0029	4.0321	0	3.1439	2.2395	0.335	0.2689	0.0073	16.0072
ob-010-1-3	Garnet	5.9666	0	0.0092	3.9935	0.0011	3.0396	2.312	0.3524	0.3493	0.0058	16.0296
ob-010-1-4	Garnet	5.9473	0.0033	0.0103	4.0071	0	3.0352	2.3034	0.3554	0.369	0.009	16.0401
ob-010-1-5	Garnet	5.9524	0	0.0057	4.0045	0	3.0698	2.3335	0.3612	0.3096	0.0058	16.0426
ob-010-1-6	Garnet	5.9725	0	0.008	4.0088	0	3.0428	2.2938	0.3623	0.3209	0.0122	16.0213
ob-010-1-7	Garnet	5.957	0.0009	0.0049	4.0324	0	3.1034	2.2671	0.36	0.2912	0.0083	16.0252
ob-010-1-8	Garnet	5.9741	0.0003	0.0045	4.0199	0.0021	3.1734	2.1839	0.3621	0.2865	0.006	16.0128
ob-010-1-9	Garnet	6.0156	0	0.0127	4.0005	0.0031	3.0762	2.2592	0.3157	0.2826	0.0086	15.9743
ob-010-1-10	Garnet	5.9825	0.0008	0.0019	4.0145	0	3.1459	2.2762	0.3238	0.2601	0.0031	16.0089
ob-010-1-11	Garnet	5.9581	0	0.0028	4.0537	0.0024	3.1235	2.2182	0.3241	0.323	0.0102	16.0161
ob-010-2-1	Garnet	6.001	0	0.0042	3.984	0.0005	3.123	2.244	0.3651	0.276	0.0083	16.0061
ob-010-2-2	Garnet	5.989	0.0002	0.0025	4.017	0.0032	3.068	2.269	0.3808	0.268	0	15.9977
ob-010-2-3	Garnet	6	0	0.0062	3.971	0	2.976	2.369	0.3772	0.302	0.0115	16.0129
ob-010-2-4	Garnet	5.993	0	0.0049	3.989	0.0047	2.997	2.324	0.3783	0.312	0.004	16.0069
ob-010-2-5	Garnet	5.996	0.0005	0.0081	3.976	0.0006	2.959	2.358	0.372	0.332	0.0072	16.0094
ob-010-2-6	Garnet	6.003	0.0012	0.0039	3.987	0	3.054	2.275	0.3935	0.28	0.0026	16.0003
ob-010-2-7	Garnet	6.003	0	0.0058	3.983	0	3.097	2.201	0.373	0.332	0.0087	16.0035
ob-010-2-8	Garnet	6.02	0	0.0022	4.005	0.003	3.06	2.282	0.3442	0.254	0.0043	15.9748
ob-010-3-1	Garnet	6.054	0	0.0013	3.961	0	3.009	2.341	0.3345	0.256	0.0145	15.9714
ob-010-3-2	Garnet	6.013	0.0003	0.0021	3.991	0.0071	3.051	2.27	0.3815	0.262	0.0135	15.9916
ob-010-3-3	Garnet	6.009	0	0.0033	3.993	0.007	3.025	2.298	0.3799	0.268	0.0093	15.9925
ob-010-3-4	Garnet	6.033	0.0417	0.0152	3.892	0.0196	2.92	2.357	0.3673	0.298	0.0221	15.966
ob-010-3-5	Garnet	6.016	0	0.0065	3.955	0.0092	2.888	2.416	0.3581	0.342	0.0062	15.997
ob-010-3-6	Garnet	6.037	0	0.009	3.954	0	2.865	2.283	0.349	0.481	0	15.9781
ob-010-3-7	Garnet	6.001	0	0.0065	3.981	0.0004	3.031	2.292	0.382	0.308	0.0005	16.0024
ob-010-3-8	Garnet	6.006	0.0005	0.0051	4.021	0	3.039	2.272	0.3317	0.298	0.0129	15.9863

Sample	Type	Si	Zr	Ti	Al	Cr	Fe	Mn	Mg	Ca	Na	Total
ob-023-1-1	Garnet	6.013	0.0014	0.127	4.04	0.0088	1.048	2.964	1.56	0.0649	0.0157	15.8429
ob-023-1-2	Garnet	6.072	0.0012	0.0045	3.979	0.0057	2.039	3.09	0.419	0.315	0.0096	15.935
ob-023-1-3	Garnet	6.064	0.0046	0.0012	3.976	0	2.058	3.088	0.43	0.317	0.0072	15.9461
ob-023-1-4	Garnet	6.068	0.0042	0.0037	3.958	0.0095	2.06	3.089	0.432	0.311	0.0118	15.9472
ob-023-1-5	Garnet	6.061	0	0.0061	3.985	0.0063	2.081	3.091	0.408	0.292	0.013	15.9434
ob-023-1-6	Garnet	6.061	0	0.0031	3.976	0.0084	2.042	3.125	0.422	0.3	0.012	15.9496
ob-023-1-7	Garnet	6.077	0	0	3.99	0.0058	2.202	3.047	0.3539	0.249	0.0001	15.9248
ob-023-1-8	Garnet	6.332	0	0.0024	3.741	0.0019	2.23	2.896	0.3478	0.243	0	15.7942
ob-023-2-1	Garnet	6.081	0	0.0009	3.988	0.006	2.113	3.087	0.3932	0.251	0.0042	15.9243
ob-023-2-2	Garnet	6.064	0.0008	0.0044	3.976	0.0005	2.04	3.081	0.433	0.341	0.007	15.9478
ob-023-2-3	Garnet	6.063	0	0.0073	3.967	0.0045	2.053	3.1	0.436	0.305	0.0131	15.949
ob-023-2-4	Garnet	6.052	0	0.007	4.004	0.0067	2.049	3.045	0.418	0.35	0.008	15.9398
ob-023-2-5	Garnet	6.067	0.0026	0.0108	3.962	0.0066	2.056	3.063	0.409	0.352	0.0125	15.9415
ob-023-2-6	Garnet	6.05	0	0.0095	3.961	0.0086	2.077	3.102	0.4025	0.342	0.0048	15.9575
ob-023-2-7	Garnet	6.081	0.0004	0.0089	3.952	0.0102	2.048	3.084	0.388	0.348	0.0147	15.9352
ob-023-2-8	Garnet	6.092	0.003	0	3.967	0.0032	2.17	3.034	0.3521	0.297	0.0034	15.9218
ob-001-1 -1	Garnet	5.99	0.0006	0.0089	4.001	0.0021	3.153	1.599	0.3026	0.941	0.0035	16.0017
ob-001-1 -2	Garnet	6.012	0.0008	0.0047	3.945	0.0111	2.975	1.879	0.3315	0.847	0	16.0061
ob-001-1 -3	Garnet	6.007	0	0.0078	3.96	0.0091	2.902	1.965	0.3066	0.843	0	16.0005
ob-001-1 -4	Garnet	5.988	0.0025	0.0126	3.937	0.0169	3.017	1.821	0.3274	0.894	0.0093	16.0257
ob-001-1 -5	Garnet	6.024	0	0.0057	3.973	0.0038	3.158	1.595	0.3114	0.911	0.0025	15.9845
ob-001-1 -6	Garnet	6.014	0.0021	0.0064	3.973	0.0106	3.165	1.6	0.3077	0.905	0.0035	15.9874
ob-001-1 -7	Garnet	6.011	0	0.0053	4.01	0.0005	3.131	1.653	0.2971	0.869	0.0046	15.9816
ob-001-1 -8	Garnet	6	0	0.0063	3.979	0.0162	3.098	1.574	0.3291	0.989	0.0083	15.9999
ob-001-1 -9	Garnet	5.996	0.0034	0.0098	3.947	0	2.984	1.906	0.341	0.828	0.0006	16.0158
ob-001-1 -10	Garnet	6.011	0	0.0103	3.943	0	2.932	1.928	0.3217	0.862	0.0012	16.0093
ob-001-1 -11	Garnet	6.006	0.0007	0.0025	3.967	0.0071	3.117	1.607	0.3377	0.959	0	16.004
ob-001-1 -12	Garnet	6.004	0	0.0053	3.995	0.0106	3.189	1.575	0.3378	0.871	0.0025	15.9903
ob-001-1 -13	Garnet	6.015	0	0.007	3.962	0.0044	3.183	1.573	0.3205	0.928	0.0011	15.994
ob-001-2-1	Garnet	5.9741	0	0.0217	3.9683	0.0019	3.0054	1.8826	0.3171	0.8478	0	16.0189
ob-001-2-2	Garnet	5.9882	0	0.0109	3.9765	0.0001	3.3584	1.4986	0.3247	0.853	0.0046	16.0151

Sample	Type	Si	Zr	Ti	Al	Cr	Fe	Mn	Mg	Ca	Na	Total
ob-001-2-3	Garnet	5.9563	0	0.0052	4.0051	0	3.3296	1.4976	0.3443	0.8976	0.0004	16.0361
ob-001-2-4	Garnet	5.9761	0	0.0123	3.939	0	2.7446	2.1552	0.3485	0.8662	0.0003	16.0422
ob-001-2-5	Garnet	5.983	0	0.0121	3.9468	0	3.0392	1.7767	0.3047	0.9689	0	16.0315
ob-001-2-6	Garnet	5.9724	0	0.0119	3.9362	0.0004	2.8382	2.063	0.3076	0.9176	0	16.0473
ob-001-2-7	Garnet	5.9593	0.0015	0.0027	3.9704	0	2.3652	2.4668	0.3003	0.9849	0.0003	16.0514
ob-001-2-8	Garnet	5.9718	0	0.0063	3.9665	0	2.3083	2.5234	0.303	0.9589	0.0005	16.0387
ob-001-2-9	Garnet	5.9896	0.0006	0.0229	3.8873	0.0001	2.4121	2.3788	0.3195	1.0323	0.0002	16.0435
ob-001-2-10	Garnet	5.9643	0.0003	0.0124	3.9606	0.0028	2.4293	2.3669	0.3152	0.9881	0.0024	16.0423
ob-001-2-11	Garnet	5.9909	0.0005	0.0076	3.9678	0.0019	2.9872	1.8741	0.3189	0.8671	0.0006	16.0166
ob-001-2-12	Garnet	5.9927	0	0.0105	3.9136	0.0004	2.7614	2.0332	0.2848	1.0429	0.0004	16.0399
ob-001-2-13	Garnet	5.9712	0.0003	0.0023	4.0284	0	3.3013	1.5429	0.3044	0.8597	0.0029	16.0134
ob-001-2-14	Garnet	5.9837	0.0021	0.0052	3.9961	0	2.9723	1.6528	0.2938	1.1044	0.001	16.0114
ob-001-3-1	Garnet	5.9547	0.0014	0.0064	4.0002	0	3.3193	1.4721	0.3389	0.9429	0.0034	16.0394
ob-001-3-2	Garnet	5.9679	0	0.0034	4.0042	0	3.2267	1.5498	0.341	0.9337	0	16.0267
ob-001-3-3	Garnet	5.9988	0	0.0065	3.9552	0	3.2805	1.504	0.3426	0.928	0.0026	16.0182
ob-001-3-4	Garnet	5.9698	0.0017	0.0077	3.9399	0	2.6134	2.271	0.324	0.9209	0.0049	16.0533
ob-001-3-5	Garnet	5.9904	0	0.01	3.9255	0	2.6421	2.1929	0.3421	0.9337	0	16.0367
ob-001-3-6	Garnet	5.9946	0	0.007	3.939	0.002	2.9048	1.7942	0.3108	1.0745	0.0022	16.0291
ob-001-3-7	Garnet	5.9323	0	0.005	4.0196	0	3.3185	1.4124	0.4295	0.935	0.0013	16.0536
ob-001-3-8	Garnet	5.9619	0.0003	0.0089	3.9859	0.001	2.9567	1.8648	0.3231	0.9327	0	16.0354
ob-001-3-9	Garnet	5.9831	0	0.0123	3.9534	0	3.0142	1.8222	0.3194	0.9215	0.0038	16.0299
ob-001-3-10	Garnet	6.0203	0.0007	0.005	3.9447	0.001	3.1793	1.4878	0.3535	1.0088	0	16.0012
ob-001-4-1	Garnet	5.9956	0.0009	0.0066	3.9694	0	3.1999	1.5817	0.297	0.9591	0.0042	16.0145
ob-001-4-2	Garnet	5.9907	0	0.005	3.9761	0.01	3.2476	1.515	0.3487	0.9173	0.0014	16.0119
ob-001-4-3	Garnet	5.9888	0.0021	0.0108	3.9499	0.0015	2.9705	1.9095	0.3124	0.877	0	16.0226
ob-001-4-4	Garnet	5.9797	0.0013	0.0075	3.9467	0.007	2.9199	1.9753	0.3079	0.8869	0.0054	16.0376
ob-001-4-5	Garnet	5.9787	0.0032	0.0054	3.9712	0	3.058	1.6914	0.3177	0.999	0.0052	16.0299
ob-001-4-6	Garnet	5.9933	0	0.0086	3.9527	0.0054	3.1821	1.5236	0.3228	1.0289	0.0034	16.0208
ob-001-4-7	Garnet	5.9779	0	0.0068	3.972	0.012	3.195	1.5298	0.2999	1.0297	0.0002	16.0233
ob-035-1-1	Garnet	5.991	0.001	0.0026	3.9831	0	4.7101	0.1207	0.8657	0.3353	0.0089	16.0184
ob-035-1-2	Garnet	6.0117	0	0.003	3.9718	0.0064	4.4897	0.076	0.9015	0.5329	0.0064	15.9994
ob-035-1-3	Garnet	5.9932	0	0.001	3.987	0.0019	4.5667	0.0832	0.8849	0.4925	0.0021	16.0125

Sample	Type	Si	Zr	Ti	Al	Cr	Fe	Mn	Mg	Ca	Na	Total
ob-035-1-4	Garnet	5.9569	0.0004	0.0038	3.9886	0.0057	4.5863	0.075	0.9247	0.4936	0.0134	16.0484
ob-035-1-5	Garnet	6.0046	0	0.0013	3.9681	0.0015	4.5802	0.0767	0.8724	0.5036	0.0018	16.0103
ob-035-1-6	Garnet	6.0221	0	0.0007	3.9847	0	4.6645	0.1104	0.8691	0.3314	0.0039	15.9868
ob-035-1-7	Garnet	6.0007	0	0.0006	3.9922	0.0018	4.6478	0.089	0.9245	0.344	0.0025	16.0031
ob-035-1-8	Garnet	5.9928	0.0018	0.0021	3.9754	0.0049	4.4959	0.0745	0.9136	0.5522	0	16.0133
ob-035-1-9	Garnet	6.0091	0	0.0021	3.9625	0.0013	4.5842	0.0744	0.9075	0.4656	0.0002	16.0069
ob-035-1-10	Garnet	6.0037	0	0.0016	4.0073	0	4.5116	0.0898	0.9093	0.4672	0.0011	15.9916
ob-035-2-1	Garnet	5.9809	0.0003	0.0018	3.9877	0	4.4717	0.1776	0.8864	0.5161	0.0011	16.0237
ob-035-2-2	Garnet	5.9732	0.0005	0.0029	4.002	0.0041	4.4252	0.2277	0.8835	0.5014	0.0001	16.0206
ob-035-2-3	Garnet	5.9931	0.0543	0.0035	3.9265	0	4.3196	0.2213	0.8492	0.618	0.0001	15.9857
ob-035-2-4	Garnet	5.9893	0	0.0035	3.9945	0	4.3557	0.2129	0.8501	0.6021	0.0035	16.0117
ob-035-2-5	Garnet	5.9853	0.001	0.0054	3.9893	0.0016	4.4487	0.2273	0.8663	0.4875	0.0014	16.0138
ob-035-2-6	Garnet	5.9907	0.0015	0.0016	3.9524	0.0069	4.4925	0.2056	0.8809	0.4925	0.0035	16.0281
ob-035-2-7	Garnet	5.9907	0	0.0018	3.9774	0.0066	4.4729	0.1842	0.888	0.4937	0	16.0154
ob-035-2-8	Garnet	6.0276	0.0005	0.0042	3.9239	0.0115	4.5697	0.1782	0.801	0.4833	0.0007	16.0006
ob-035-2-9	Garnet	6.0009	0	0.001	3.975	0.0031	4.4896	0.1829	0.8686	0.4858	0.0043	16.0112
ob-035-2-10	Garnet	5.9772	0	0.0007	3.9949	0.0023	4.5665	0.1675	0.8347	0.4784	0.0027	16.025
ob-035-3-1	Garnet	5.9842	0	0	3.9849	0.0078	4.4768	0.1676	1.0222	0.3744	0.0032	16.0211
ob-035-3-2	Garnet	5.9931	0	0.0047	3.992	0	4.403	0.116	0.9719	0.5256	0	16.0063
ob-035-3-3	Garnet	5.966	0	0.0039	4.0021	0	4.3902	0.1728	0.9369	0.5557	0.0026	16.0302
ob-035-3-4	Garnet	6.0383	0.0009	0.0024	3.9461	0	4.344	0.128	0.9505	0.5751	0	15.9853
ob-035-3-5	Garnet	5.9913	0.0012	0.0019	4.0105	0.0011	4.4124	0.1772	0.889	0.5152	0.0004	16.0002
ob-035-3-6	Garnet	6.0057	0.0002	0.0028	4.0032	0.0035	4.2684	0.1689	0.8461	0.6886	0.001	15.9884
ob-035-3-7	Garnet	5.9691	0.0009	0.0051	4.0158	0	4.5014	0.1759	0.8401	0.5087	0	16.017
ob-035-3-8	Garnet	6.1073	0.0015	0.0013	3.805	0.0144	4.4585	0.1972	0.908	0.4864	0.001	15.9806
ob-035-3-9	Garnet	5.9764	0	0.004	3.9919	0.0026	4.3741	0.1688	0.8888	0.6151	0.0018	16.0236
ob-035-3-10	Garnet	5.9888	0.0003	0.0035	3.9882	0.0025	4.4528	0.2456	0.7833	0.5439	0.0062	16.0152
ob-035-3-11	Garnet	6	0	0.0025	3.97	0	4.3634	0.1867	0.9239	0.5637	0.0047	16.0149
ob-035-3-12	Garnet	5.9941	0	0.0047	3.9912	0	4.3305	0.1709	0.9699	0.5433	0.0017	16.0063
ob-035-3-13	Garnet	6.0102	0	0.0005	3.9796	0.0017	4.5384	0.4162	0.6189	0.4326	0.0011	15.9993
ob-035-3-14	Garnet	5.9972	0.0013	0.0007	3.9846	0.0053	4.4222	0.2686	0.8644	0.4601	0.0031	16.0075
ob-035-3-15	Garnet	6.004	0.0006	0.0011	4.0023	0.0028	4.4372	0.2009	0.9902	0.3507	0.0036	15.9935

Sample	Type	Si	Zr	Ti	Al	Cr	Fe	Mn	Mg	Ca	Na	Total
ob-035-3-16	Garnet	5.9988	0	0.0055	3.9486	0.0293	4.3051	0.1414	0.9267	0.6512	0	16.0066
jd-033-1-1	Garnet	5.9731	0.0005	0.0015	4.0072	0.0101	3.8357	1.4089	0.213	0.5627	0.0072	16.02
jd-033-1-2	Garnet	5.9781	0	0.0007	3.9711	0.015	3.906	1.104	0.2788	0.7713	0.0063	16.0313
jd-033-1-3	Garnet	5.9853	0	0.0162	3.957	0	3.611	0.9263	0.2638	1.2567	0.0071	16.0234
jd-033-1-4	Garnet	5.9777	0.0011	0.0148	3.9623	0.008	3.5859	0.9352	0.268	1.267	0.0027	16.0228
jd-033-1-5	Garnet	5.9693	0	0.0094	3.9671	0.007	3.7513	0.9749	0.2733	1.082	0	16.0343
jd-033-1-6	Garnet	5.965	0.0009	0.0199	3.9526	0.0135	3.7075	0.9661	0.2616	1.1412	0.0058	16.0341
jd-033-1-7	Garnet	5.9662	0.0006	0.014	3.9549	0.0079	3.615	0.9865	0.2643	1.2254	0.0054	16.0402
jd-033-1-8	Garnet	5.9746	0	0.0134	3.9541	0.0054	3.6008	0.9686	0.2653	1.2468	0.0062	16.0352
jd-033-1-9	Garnet	5.9615	0	0.0062	3.9658	0.0073	3.8324	0.9741	0.2929	1.0041	0.0027	16.0471
jd-033-1-10	Garnet	5.9802	0	0.0099	3.963	0.0117	3.599	0.9136	0.2729	1.2698	0.0048	16.025
jd-033-1-11	Garnet	5.9773	0.0002	0.0108	3.9557	0.0071	3.6144	0.9824	0.2402	1.2411	0.0025	16.0317
jd-033-1-12	Garnet	5.9632	0.0009	0	4.0071	0	3.9847	1.0406	0.2979	0.7367	0.0023	16.0334
jd-033-1-13	Garnet	5.9777	0.0008	0.0013	3.9797	0.0095	3.9984	1.1359	0.301	0.6187	0.0053	16.0283
jd-033-1-14	Garnet	5.979	0	0.0016	3.9905	0.0087	3.8372	1.3818	0.224	0.5918	0.0104	16.0251
jd-033-1-15	Garnet	5.9661	0	0.0006	4.0041	0	3.8106	1.363	0.2272	0.6591	0.0007	16.0315
jd-033-1-16	Garnet	6.0212	0.0019	0.0337	3.8977	0.0105	3.6549	0.9069	0.2657	1.1956	0.0024	15.9906
jd-033-1-17	Garnet	5.9733	0.0003	0.0007	4.014	0.0081	3.6632	1.3589	0.1992	0.7955	0.0027	16.0159
jd-033-2-1	Garnet	5.9667	0.0007	0.0014	3.9944	0.016	3.8214	1.0202	0.2605	0.9307	0.028	16.04
jd-033-2-2	Garnet	5.9611	0.0007	0	3.9981	0.0118	4.0858	0.7815	0.3382	0.8425	0.0272	16.0469
jd-033-2-3	Garnet	5.9874	0.0002	0.0012	3.9746	0.0115	4.0649	0.7673	0.3424	0.8662	0.0052	16.0209
jd-033-2-4	Garnet	5.9818	0.0013	0.0007	3.9714	0.0132	3.9612	0.8304	0.3191	0.9425	0.0045	16.0261
jd-033-2-5	Garnet	5.9851	0	0.0015	3.9815	0.0045	3.8451	0.8661	0.3039	1.024	0.0176	16.0293
jd-033-2-6	Garnet	5.9973	0.0012	0.0018	3.98	0.0092	3.8048	0.8744	0.2758	1.0584	0.0043	16.0072
jd-033-2-7	Garnet	5.9989	0	0.0008	3.9806	0.011	3.8067	0.9072	0.2667	1.0283	0.008	16.0082
jd-033-2-8	Garnet	5.9794	0.002	0.0148	3.967	0.0062	3.6439	0.9473	0.2634	1.1907	0.0052	16.0199
jd-033-2-9	Garnet	5.9764	0.0006	0.006	3.9817	0.0051	3.6703	0.9153	0.2798	1.1841	0.0089	16.0282
jd-033-2-10	Garnet	5.9802	0	0.0025	3.9818	0.0111	3.8569	0.869	0.306	1.01	0.0064	16.0239
jd-033-2-11	Garnet	5.9749	0.0015	0.0015	3.9727	0.0112	4.1159	0.7899	0.3357	0.8261	0.0014	16.0308

Sample	Type	Si	Zr	Ti	Al	Cr	Fe	Mn	Mg	Ca	Na	Total
jd-033-2-12	Garnet	5.9724	0.0002	0.0009	3.9983	0.0098	3.9658	0.8445	0.2971	0.9321	0.0025	16.0236
jd-033-2-13	Garnet	6.0214	0.002	0.0012	3.9564	0.0139	3.7531	1.0791	0.2299	0.9311	0.0041	15.9922
jd-033-2-14	Garnet	5.9985	0.0022	0.0012	3.9786	0.0112	3.8312	1.0417	0.2606	0.8763	0.0033	16.0049
jd-033-2-15	Garnet	5.992	0	0.002	4.0058	0.0093	3.8604	0.9608	0.2665	0.8964	0.0105	16.0037
jd-033-3-1	Garnet	5.9898	0.0007	0.0026	4.0013	0.0113	3.923	1.1145	0.2338	0.7235	0.0004	16.0009
jd-033-3-2	Garnet	5.9743	0	0.0009	4.005	0.0113	3.9092	0.8742	0.2806	0.9598	0.003	16.0183
jd-033-3-3	Garnet	5.9852	0.0016	0.0115	3.9677	0.0068	3.6251	0.9496	0.2531	1.2141	0	16.0147
jd-033-3-4	Garnet	5.9705	0	0.0116	3.9647	0.0095	3.6416	0.9948	0.2474	1.1893	0.0029	16.0323
jd-033-3-5	Garnet	5.9769	0	0.0108	3.9681	0.009	3.5918	0.9962	0.2519	1.2169	0.0045	16.0261
jd-033-3-6	Garnet	5.9718	0.0018	0.0015	3.9939	0.0127	3.8319	0.8266	0.2747	1.1019	0.0091	16.0259
jd-033-3-7	Garnet	5.9621	0.0014	0.0021	4.0042	0.0097	4.1157	0.9423	0.3021	0.6867	0.0023	16.0287
jd-033-3-8	Garnet	5.9822	0	0.0009	3.9958	0.0123	4.0323	1.0194	0.2776	0.6925	0	16.013
jd-033-3-9	Garnet	6.3082	0	0.003	3.7226	0.0147	3.3308	1.1141	0.2701	1.0539	0.0056	15.823
jd-033-3-10	Garnet	5.9849	0	0	4.0109	0.0014	4.0256	0.952	0.2786	0.7544	0.0026	16.0104
jd-033-3-11	Garnet	5.9881	0	0.0004	4.0078	0.0063	3.7195	1.059	0.2059	1.0145	0.0064	16.0079
jd-100-1-1	Garnet	6.024	0	0.004	4.047	0	1.572	3.64	0.3568	0.301	0.0091	15.954
jd-100-1-2	Garnet	6.056	0.0057	0.0085	3.999	0.0023	1.583	3.585	0.3696	0.317	0.008	15.9342
jd-100-1-3	Garnet	6.103	0.0006	0.0026	3.958	0.0062	1.579	3.573	0.3757	0.303	0.0223	15.9234
jd-100-1-4	Garnet	6.111	0	0.0025	3.952	0	1.562	3.602	0.3562	0.318	0.0131	15.9169
jd-100-1-5	Garnet	6.091	0.0012	0.0031	3.934	0.0012	1.586	3.614	0.363	0.341	0.0049	15.9394
jd-100-1-6	Garnet	6.048	0.0002	0.0051	4.011	0	1.557	3.641	0.338	0.337	0.005	15.9424
jd-100-1-7	Garnet	5.87	0	0.005	4.032	0.0031	1.458	3.81	0.576	0.349	0.0139	16.1171
jd-100-1-8	Garnet	6.097	0	0.0016	3.946	0	1.67	3.602	0.3208	0.288	0.0078	15.9333
jd-100-1-9	Garnet	6.108	0	0.005	3.955	0	1.536	3.612	0.3493	0.337	0.0122	15.9146
jd-100-1-10	Garnet	6.097	0	0.0016	3.945	0	1.603	3.659	0.3316	0.284	0.0149	15.9362
jd-100-1-11	Garnet	6.067	0.0007	0.0408	3.893	0.0039	1.545	3.534	0.272	0.583	0.0098	15.9492
jd-100-1-12	Garnet	6.098	0	0.0159	3.87	0.0186	1.552	3.568	0.2796	0.535	0.0084	15.9455
jd-100-1-13	Garnet	6.066	0	0.0212	3.893	0.0174	1.557	3.498	0.2322	0.669	0.0071	15.961
jd-100-1-14	Garnet	6.079	0.0007	0.0136	3.93	0	1.528	3.666	0.3141	0.408	0.0065	15.9459
jd-100-1-15	Garnet	6.143	0.0003	0.006	3.813	0.0008	1.618	3.638	0.2996	0.377	0.0943	15.99
jd-100-1-16	Garnet	6.065	0	0.0035	3.968	0	1.608	3.653	0.2856	0.364	0.0018	15.949
jd-100-1-17	Garnet	11.462	0	0.0019	0.299	0	0.187	0.369	0.0211	0.0454	0.0036	12.389

Appendix II. 2013 Whole Rock Geochemistry

Analyte Symbol	SiO2	Al2O3	Fe2O3	MgO	CaO	Na2O	K2O	TiO2	P2O5	MnO	Cr2O3	LOI	Sum
Unit Symbol	%	%	%	%	%	%	%	%	%	%	%	%	%
Detection Limit	0.01	0.01	0.04	0.01	0.01	0.01	0.01	0.01	0.01	0.01	0.002	-5.1	0.01
OB-001	84.63	6.65	2.82	1.22	1.53	0.54	0.68	0.17	0.04	0.14	0.008	1.5	99.92
OB-003	77.46	11.22	2.3	1.27	1.1	4.33	0.96	0.24	0.03	0.02	0.007	0.9	99.92
OB-004	83.21	8.38	1.56	0.79	0.31	2.75	1.94	0.19	0.04	0.02	0.004	0.7	99.91
OB-005													
OB-006	59.4	17.34	7.48	4.29	3.25	3.04	1.84	0.64	0.14	0.11	0.016	2.3	99.9
OB-007	80.87	7.71	3.98	2.3	1.05	1.25	0.78	0.26	0.09	0.11	0.02	1.5	99.92
OB-009	76.87	10.51	3.65	1.78	1.11	2.72	1.47	0.31	0.06	0.05	0.021	1.3	99.9
OB-010	78.79	9.86	3.12	1.49	1.28	2.58	1.21	0.29	0.06	0.06	0.016	1.1	99.91
OB-012	76.5	11.34	3.39	1.44	0.95	2.65	1.73	0.33	0.06	0.06	0.016	1.4	99.93
OB-013	68.43	16.88	3.02	0.65	3.78	2.41	2.3	0.4	0.11	0.05	0.004	1.7	99.9
OB-016	71.22	15.71	2.03	0.83	2.41	5.81	0.99	0.31	0.13	0.02	<0.002	0.3	99.93
OB-017	59.43	15.8	6.18	5.01	6.22	3.81	1.65	0.6	0.16	0.11	0.027	0.8	99.9
OB-018	61.9	14.7	6.35	4.81	7.53	3.23	0.3	0.53	0.14	0.13	0.025	0.2	99.89
OB-021	68.74	15.33	3.14	1.36	2.5	4.85	1.51	0.36	0.12	0.06	0.002	1.9	99.91
OB-022													
OB-023	70.44	13.77	4.82	2.15	1.3	2.38	2.93	0.44	0.08	0.08	0.024	1.4	99.91
OB-024													
OB-026	71.05	14.26	3.54	0.9	3.59	2.44	2.36	0.32	0.08	0.05	<0.002	1.2	99.9
OB-027	70.35	13.78	3.56	0.82	4.18	2.1	2.66	0.29	0.07	0.05	<0.002	1.9	99.91
OB-028	72.45	13.39	1.97	1.03	1.73	3.63	3.61	0.28	0.06	0.03	0.007	1.6	99.92
OB-031	68.05	16	4.63	0.78	3.9	3.48	0.78	0.38	0.19	0.1	0.003	1.5	99.91
OB-032	70.72	14.72	2.91	0.87	1.32	4.71	3.32	0.59	0.13	0.04	<0.002	0.4	99.9
OB-033	58.69	14.25	6.43	7.2	4.92	3.72	1.18	0.62	0.19	0.1	0.048	2.4	99.9
OB-034	58.93	16.94	8.49	3.31	4.86	4.4	0.59	1.12	0.32	0.11	0.013	0.7	99.87
OB-035	58.01	17.45	8.98	3.52	4.14	3.03	2	0.78	0.2	0.13	0.027	1.5	99.89
OB-036	57.73	15.05	10.67	5.72	3.59	2.17	1.48	0.64	0.08	0.17	0.052	2.4	99.89

Analyte Symbol	Au	Ag	Cu	Cd	Mo	Mn	Pb	Ni	Zn	As	Ba	Be	Bi	Br
Unit Symbol	ppb	ppm	ppm	ppm	ppm	ppm	ppm	ppm	ppm	ppm	ppm	ppm	ppm	ppm
Detection Limit	2	0.05	0.2	0.1	0.2	1	0.5	0.5	0.5	0.5	1	0.1	0.02	0.5
OB-001	< 2	0.18	13.8	0.3	0.6	964	11.6	29.2	50.8	3	127	0.3	0.1	2.3
OB-003	< 2	0.17	4.7	< 0.1	< 0.2	162	5.3	29.7	19.4	< 0.5	265	0.8	0.08	< 0.5
OB-004	< 2	0.13	10.1	< 0.1	0.4	138	6.8	25.7	12	< 0.5	524	0.4	0.03	< 0.5
OB-005	< 2	0.27	6.8	< 0.1	0.5	119	11.3	1	20.1	2.2	702	0.8	0.24	< 0.5
OB-006	< 2	0.1	43.3	< 0.1	0.2	801	10	106	95.8	4.2	283	1.1	0.13	< 0.5
OB-007	< 2	0.13	10.1	0.1	0.3	779	10.3	89.5	67.3	22.7	144	0.7	0.15	< 0.5
OB-009	< 2	0.09	12.6	< 0.1	0.5	377	13	50.3	54.3	6.5	403	0.6	0.15	< 0.5
OB-010	< 2	0.13	4	< 0.1	0.8	448	12.8	38.4	50	957	265	0.7	0.21	< 0.5
OB-012	< 2	0.16	10.2	< 0.1	1.4	461	10.3	28.9	37.8	38.2	446	0.7	0.11	< 0.5
OB-013	< 2	0.13	8.3	< 0.1	0.2	388	17.7	27.5	69.8	7.5	570	1.4	0.11	< 0.5
OB-016	< 2	0.17	18.6	< 0.1	0.5	221	18.7	6.9	37.5	< 0.5	763	1.4	0.09	< 0.5
OB-017	< 2	0.14	43.2	0.1	0.2	869	7.5	168	84.4	< 0.5	716	0.9	0.25	10.9
OB-018	< 2	0.14	70	< 0.1	0.2	1050	6.7	156	72.9	< 0.5	74	0.8	0.48	< 0.5
OB-021	< 2	0.1	17.3	< 0.1	0.2	419	7.8	12.7	53.1	2.2	289	0.8	0.1	< 0.5
OB-022	< 2	0.13	15.1	0.2	0.3	1160	5.6	154	135	56.9	114	0.6	0.06	< 0.5
OB-023	< 2	0.11	41.7	< 0.1	0.5	575	13.3	104	88.5	16.7	682	0.9	0.19	< 0.5
OB-024	< 2	0.19	121	0.2	0.7	1600	5.2	525	110	< 0.5	110	0.6	0.19	< 0.5
OB-026	< 2	0.17	26.3	< 0.1	0.2	392	15.5	17.2	52.4	< 0.5	704	0.9	0.23	< 0.5
OB-027	< 2	0.13	27.6	< 0.1	< 0.2	347	8.8	24.8	31.3	4.3	745	0.7	0.13	5.8
OB-028	< 2	0.17	9.9	< 0.1	0.3	236	6.8	22.1	51.1	12.4	441	0.8	0.07	< 0.5
OB-031	36	0.26	32.1	< 0.1	0.9	677	20.8	24.1	82.9	58.3	346	1.6	0.18	< 0.5
OB-032	< 2	0.14	2.8	< 0.1	0.3	273	19	10.1	72.5	3.6	909	1.6	0.23	< 0.5
OB-033	< 2	0.23	90.7	< 0.1	0.7	757	5.9	248	81.4	< 0.5	381	0.9	0.06	< 0.5
OB-034	< 2	0.22	111	< 0.1	< 0.2	847	7.9	68.5	123	< 0.5	221	1.1	0.12	6.1
OB-035	< 2	0.28	92.9	< 0.1	0.3	936	8.9	106	81.6	3	304	1.3	0.21	< 0.5
OB-036	< 2	0.2	28.2	< 0.1	14.1	1240	8.5	87	99.6	< 0.5	358	0.8	0.68	< 0.5

Analyte Symbol	Ca	Co	Cr	Cs	Fe	Hf	Ga	Ge	In	Li	Mg	Na	Nb	Rb	Re
Unit Symbol	%	ppm	ppm	ppm	%	ppm	ppm	ppm	ppm	ppm	%	%	ppm	ppm	ppm
Detection Limit	0.01	1	2	0.05	0.01	1	0.1	0.1	0.1	0.5	0.01	0.01	0.1	0.2	0.001
OB-001	1.23	7	59	2.22	2.15	2	7.8	< 0.1	< 0.1	13.7	0.69	0.42	1.8	31	< 0.001
OB-003	0.93	7	74	0.96	1.79	2	15.6	0.2	< 0.1	27.1	0.73	3.28	0.6	29.5	< 0.001
OB-004	0.28	4	39	1.16	1.47	2	11.1	< 0.1	< 0.1	21.1	0.47	2.1	2.1	40.4	0.001
OB-005	0.19	< 1	< 2	2.97	1.45	4	22.3	0.2	< 0.1	23.9	0.29	0.35	6.2	104	< 0.001
OB-006	2.61	24	105	2.97	4.79	3	20.7	0.3	< 0.1	54.2	2.45	2.32	0.9	74.2	0.001
OB-007	0.9	13	144	1.66	2.99	2	10.1	0.5	< 0.1	30.5	1.37	0.98	1.1	30.8	0.003
OB-009	0.87	9	144	2.52	2.61	2	13	0.3	< 0.1	16.3	0.98	1.97	0.6	52	0.004
OB-010	1.08	6	113	2.53	2.33	2	12.8	< 0.1	< 0.1	13.7	0.85	1.94	3.3	51	0.002
OB-012	0.55	6	133	1.25	2.87	3	14.2	0.1	< 0.1	19.7	0.77	2.08	4.9	35.2	0.001
OB-013	3	6	42	2.99	2.13	3	21.4	0.2	< 0.1	11.6	0.38	1.75	3.6	77.4	< 0.001
OB-016	2.11	6	< 2	1.9	1.52	3	22.8	0.1	< 0.1	36.6	0.51	4.44	2.6	32.4	0.003
OB-017	5.09	25	191	3.32	4.18	3	17.8	0.3	< 0.1	46.5	2.98	2.94	0.3	86.1	0.002
OB-018	6.38	22	190	0.32	4.64	2	18.2	0.3	< 0.1	10.9	2.87	2.47	0.5	6.4	< 0.001
OB-021	1.94	8	22	1.1	2.26	5	19.5	0.3	< 0.1	24.5	0.76	3.72	0.8	43.1	0.002
OB-022	5.18	30	240	0.78	8.09	3	19.7	0.4	< 0.1	9.8	3.8	2.13	1.6	9.8	0.001
OB-023	1.05	19	180	2.73	3.39	2	17.4	0.5	< 0.1	30.8	1.24	1.8	0.9	78	0.001
OB-024	6.42	54	883	0.44	7.96	2	14.8	0.2	< 0.1	16.5	4.32	1.12	3.6	16.9	0.001
OB-026	3.02	6	9	1.63	2.46	3	17.3	0.4	< 0.1	15.3	0.54	1.79	2.4	100	< 0.001
OB-027	3.41	9	16	0.88	2.55	3	15.3	0.5	< 0.1	12.4	0.48	1.57	2.6	95.6	< 0.001
OB-028	1.12	3	56	1.95	1.47	2	14.9	< 0.1	< 0.1	19.5	0.56	2.69	5.6	81.6	0.003
OB-031	3.07	15	38	2.27	3.28	4	18	0.2	< 0.1	19.5	0.46	2.7	7.7	44.3	< 0.001
OB-032	1.05	< 1	< 2	2.46	2.12	6	19.8	0.3	< 0.1	15.6	0.5	3.57	0.3	90.6	0.002
OB-033	3.85	30	332	5.15	4.39	4	18	0.3	< 0.1	38.2	4.11	2.87	5.5	40.8	< 0.001
OB-034	3.85	27	93	2.71	5.66	5	19.7	0.5	< 0.1	68.8	1.88	3.41	1.3	19	0.003
OB-035	3.26	31	192	8.52	6.02	4	19	0.5	< 0.1	131	1.95	2.27	1.1	69	< 0.001
OB-036	2.77	20	335	3.62	6.9	3	18.9	0.6	< 0.1	47.2	3.21	1.61	3.5	53.1	< 0.001

Analyte Symbol	Sb	Sc	Se	Sn	Sr	Ta	Te	Th	Tl	U	V	W	Y	Zr	La
Unit Symbol	ppm	ppm	ppm	ppm	ppm	ppm	ppm	ppm	ppm	ppm	ppm	ppm	ppm	ppm	ppm
Detection Limit	0.1	0.1	0.1	1	0.2	0.1	0.1	0.1	0.05	0.1	1	1	0.1	1	0.1
OB-001	0.2	4.2	0.5	< 1	80.4	< 0.1	< 0.1	3.3	0.22	1.1	38	< 1	8	41	9.9
OB-003	< 0.1	3.3	0.1	< 1	71.5	< 0.1	< 0.1	7.8	0.19	1.6	23	< 1	7.8	35	21.3
OB-004	< 0.1	3.1	< 0.1	< 1	72.2	0.1	< 0.1	5.3	0.31	1	25	< 1	6	25	8.1
OB-005	1	3.9	0.5	7	42.3	0.5	< 0.1	11	0.87	2.2	5	< 1	11.5	160	2.5
OB-006	2.7	18.2	0.3	1	197	< 0.1	< 0.1	5.6	0.51	1.5	99	< 1	15.4	112	14.9
OB-007	4.6	6.9	0.3	< 1	97.5	< 0.1	< 0.1	4.5	0.25	1	50	< 1	12.3	22	23.1
OB-009	1	6.5	< 0.1	< 1	144	< 0.1	< 0.1	5.4	0.34	1.9	36	< 1	6.6	69	15.4
OB-010	2.1	6	0.3	< 1	191	< 0.1	0.1	5	0.38	1.2	52	< 1	7.5	66	12.7
OB-012	0.9	6.8	0.2	< 1	145	0.4	< 0.1	5.6	0.3	1.4	55	< 1	5.8	99	8.5
OB-013	3.9	4.2	0.2	< 1	521	0.3	< 0.1	6.8	0.68	2.2	43	< 1	7.6	148	20.3
OB-016	< 0.1	3.2	0.4	1	562	0.2	< 0.1	8.2	0.2	1.8	43	< 1	5.1	156	32.2
OB-017	< 0.1	17.2	0.5	< 1	233	< 0.1	< 0.1	4.7	0.51	1.1	78	< 1	18	90	12.2
OB-018	< 0.1	16.6	0.6	< 1	224	< 0.1	< 0.1	3.8	< 0.05	0.9	81	< 1	17	72	8.4
OB-021	< 0.1	5.5	0.1	< 1	191	< 0.1	< 0.1	4.1	0.23	1	43	< 1	10.8	80	24.9
OB-022	1.8	20	0.5	< 1	269	< 0.1	< 0.1	2.3	0.09	0.7	153	< 1	23.6	116	11.1
OB-023	0.6	8.9	0.2	< 1	161	< 0.1	< 0.1	6	0.61	2.6	66	< 1	7.1	103	23.2
OB-024	1.2	25.6	0.8	1	91.4	0.2	< 0.1	2.2	0.11	0.7	199	< 1	19.2	77	7
OB-026	0.4	6.1	0.4	1	189	0.1	< 0.1	15	0.57	2.3	44	< 1	14.2	127	35.4
OB-027	0.5	8.2	0.2	1	181	0.2	< 0.1	15.3	0.51	2.8	41	< 1	14.7	123	37.5
OB-028	0.5	3.7	0.1	< 1	143	0.4	< 0.1	6.6	0.72	1.1	38	< 1	5.7	98	10.4
OB-031	0.4	6.6	0.2	< 1	430	0.4	< 0.1	10.9	0.33	3.5	68	< 1	12	168	36.9
OB-032	7.6	5.6	0.3	< 1	319	0.1	< 0.1	9.9	0.71	2.1	19	< 1	20	109	36.1
OB-033	< 0.1	13.4	0.5	1	420	0.3	< 0.1	4.2	0.26	1.1	102	< 1	13.6	140	24.2
OB-034	< 0.1	20.2	0.7	1	258	< 0.1	< 0.1	4.3	0.09	1.1	104	< 1	27.6	157	25.1
OB-035	< 0.1	17.2	0.5	< 1	235	< 0.1	< 0.1	4.8	0.33	1.1	77	< 1	17.7	112	26.1
OB-036	0.8	24.6	0.4	2	168	0.2	< 0.1	3.7	0.35	1.2	173	< 1	16.7	94	6.2

Analyte Symbol	K	Ce	Pr	Nd	Sm	Eu	Gd	Dy	Tb	Ho	Hg	Er	Tm	Yb	Lu	Mass
Unit Symbol	%	ppm	ppm	ppm	ppm	ppm	ppm	ppm	ppm	ppm	ppb	ppm	ppm	ppm	ppm	g
Detection Limit	0.01	0.1	0.1	0.1	0.1	0.05	0.1	0.1	0.1	0.1	10	0.1	0.1	0.1	0.1	
OB-001	0.58	17.6	2	6.2	1.1	0.34	1.2	1.2	0.2	0.3	< 10	0.7	0.1	0.6	0.1	25.2
OB-003	0.86	38.5	4.1	12.6	2	0.32	1.6	1.3	0.2	0.3	< 10	0.7	0.1	0.7	0.1	26.6
OB-004	1.58	17.1	1.7	5.3	1	0.2	1	1	0.2	0.2	< 10	0.6	< 0.1	0.5	< 0.1	28.7
OB-005	3.84	6.5	0.5	1.7	0.5	0.12	0.7	1.5	0.2	0.4	< 10	1.4	0.2	1.6	0.3	26
OB-006	1.58	30.4	3.6	12.1	2.4	0.69	2.6	2.6	0.4	0.6	< 10	1.6	0.2	1.4	0.3	28.6
OB-007	0.71	37.3	4.5	14.7	2.5	0.7	2.6	2	0.4	0.4	< 10	1	0.1	0.8	0.1	27.3
OB-009	1.19	28.8	3.3	10.7	1.8	0.49	1.5	1.2	0.2	0.2	< 10	0.7	0.1	0.6	0.1	28.8
OB-010	1.03	24	2.7	8.8	1.5	0.47	1.4	1.3	0.2	0.3	< 10	0.7	0.1	0.7	0.1	26.9
OB-012	1.12	18.7	2	6.7	1.3	0.38	1.1	1.1	0.2	0.2	< 10	0.6	< 0.1	0.6	< 0.1	26.8
OB-013	1.65	38.7	4.3	13.4	2.2	0.66	1.8	1.3	0.2	0.2	< 10	0.7	< 0.1	0.6	< 0.1	25.7
OB-016	0.89	57.4	6.5	20	2.7	0.74	1.8	0.9	0.2	0.2	< 10	0.4	< 0.1	0.3	< 0.1	26.2
OB-017	1.45	25.6	3.1	11.5	2.7	0.84	3	2.9	0.5	0.6	< 10	1.9	0.3	1.6	0.3	25.8
OB-018	0.28	18	2.3	9.3	2.5	0.82	2.8	2.7	0.5	0.6	< 10	1.8	0.3	1.6	0.3	26.6
OB-021	1.23	41.8	4.9	16.4	2.7	0.94	2.3	1.8	0.3	0.3	< 10	1	0.1	0.8	0.1	27.5
OB-022	0.26	25.2	3.3	12.4	3.1	1.16	3.8	4	0.6	0.8	< 10	2.3	0.3	1.9	0.3	24.9
OB-023	2.06	42.9	5	16.1	2.7	0.68	2.1	1.4	0.3	0.3	< 10	0.7	< 0.1	0.6	0.1	27.6
OB-024	0.46	14.9	2	7.7	2	0.81	2.7	3	0.5	0.7	< 10	2	0.3	1.7	0.3	28
OB-026	1.94	61.1	6.5	19.4	3	0.6	2.6	2.2	0.4	0.5	< 10	1.4	0.2	1.3	0.2	26.9
OB-027	1.61	65.3	7	20.7	3.2	0.63	2.8	2.3	0.4	0.5	< 10	1.4	0.2	1.2	0.2	27.3
OB-028	1.9	26.4	2.2	7.1	1.2	0.33	1.1	1	0.2	0.2	< 10	0.6	< 0.1	0.5	< 0.1	26.4
OB-031	0.68	73.3	8.2	26.5	4.3	1.14	3.3	2.1	0.4	0.4	< 10	1.1	0.2	0.9	0.2	26.5
OB-032	1.99	69	8.2	26.7	4.4	1.02	3.8	3.3	0.6	0.7	< 10	1.9	0.3	1.6	0.3	27
OB-033	1.02	47.7	5.9	20.1	3.5	1	3.1	2.4	0.4	0.5	< 10	1.3	0.2	1	0.2	25.9
OB-034	0.5	49.4	6.4	23.4	4.9	1.47	5.1	5	0.8	1	< 10	3	0.5	2.8	0.5	28.2
OB-035	1.67	52.5	6.4	21.7	3.9	1.17	3.6	3.2	0.5	0.6	< 10	1.8	0.3	1.6	0.3	28
OB-036	1.25	10.6	1.1	3.8	1.1	0.52	1.9	2.5	0.4	0.6	< 10	1.7	0.2	1.5	0.2	27.9

Appendix III. Whole Rock Geochemistry 2014

Analyte Symbol	SiO2	Al2O3	Fe2O3(T)	MnO	MgO	CaO	Na2O	K2O	TiO2	P2O5	LOI	Total
Unit Symbol	%	%	%	%	%	%	%	%	%	%	%	%
Detection Limit	0.01	0.01	0.01	0.001	0.01	0.01	0.01	0.01	0.001	0.01		0.01
Analysis Method	FUS-ICP	FUS-ICP	FUS-ICP	FUS-ICP	FUS-ICP	FUS-ICP	FUS-ICP	FUS-ICP	FUS-ICP	FUS-ICP	FUS-ICP	FUS-ICP
OB-100	66.65	18.17	2.4	0.052	2.02	3.63	2.09	3.07	0.492	0.12	2.06	100.7
OB-101	73.45	13.82	2.38	0.066	1.93	3.5	1.14	2.13	0.332	0.07	1.71	100.5
OB-102	80.59	9.59	4.45	0.068	1.26	0.8	0.73	1.11	0.284	0.05	1.63	100.6
OB-103	63.82	17.35	5.44	0.117	3.07	6.34	2.03	0.73	0.989	0.08	0.88	100.8
OB-104	71.8	11.81	5.86	0.111	2.07	3.13	0.77	1.71	0.7	0.07	2.6	100.6
OB-106	81.66	10	1.71	0.021	1	0.51	2.47	2	0.207	0.04	1.05	100.7
OB-107	70.65	15.52	2.72	0.047	1.29	1.49	3.53	3.25	0.297	0.06	1.36	100.2
OB-108	72.17	15.23	2.08	0.033	0.29	0.86	3.65	4.26	0.093	< 0.01	1.68	100.3
OB-109	83.54	7.09	4.73	0.047	1.46	0.15	0.1	0.57	0.221	0.05	2.53	100.5
OB-110	70.05	12.44	4.12	0.13	2.95	4.84	2.98	1.33	0.354	0.08	1.35	100.6
OB-111	72	15.03	2.14	0.027	0.71	1.85	4.35	3.08	0.307	0.09	1.1	100.7

Analyte Symbol	Sc	Be	V	Ba	Sr	Y	Zr	Cr	Co	Ni	Cu	Zn
Unit Symbol	ppm	ppm	ppm	ppm	ppm	ppm	ppm	ppm	ppm	ppm	ppm	ppm
Detection Limit	1	1	5	3	2	2	4	20	1	20	10	30
Analysis Method	FUS-ICP	FUS-ICP	FUS-ICP	FUS-ICP	FUS-ICP	FUS-ICP	FUS-ICP	FUS-MS	FUS-MS	FUS-MS	FUS-MS	FUS-MS
OB-100	8	< 1	62	130	110	5	114	40	11	30	10	40
OB-101	8	< 1	56	125	115	7	113	110	9	30	30	80
OB-102	5	< 1	46	133	75	7	71	130	10	30	20	50
OB-103	46	< 1	406	284	181	16	59	310	51	80	120	60
OB-104	12	< 1	107	295	78	19	164	250	15	50	30	80
OB-106	3	< 1	20	428	107	5	84	50	3	< 20	10	40
OB-107	5	1	35	607	183	8	132	100	7	30	30	60
OB-108	6	2	< 5	1045	84	29	739	20	< 1	< 20	< 10	40
OB-109	7	< 1	61	129	18	5	60	90	13	40	20	50
OB-110	8	< 1	58	349	149	10	126	330	18	140	30	50
OB-111	3	1	23	788	234	5	190	30	4	< 20	< 10	50

Analyte Symbol	Ga	Ge	As	Rb	Nb	Mo	Ag	In	Sn	Sb	Cs	La
Unit Symbol	ppm	ppm	ppm	ppm	ppm	ppm	ppm	ppm	ppm	ppm	ppm	ppm
Detection Limit	1	1	5	2	1	2	0.5	0.2	1	0.5	0.5	0.1
Analysis Method	FUS-MS	FUS-MS	FUS-MS	FUS-MS	FUS-MS	FUS-MS	FUS-MS	FUS-MS	FUS-MS	FUS-MS	FUS-MS	FUS-MS
OB-100	21	< 1	< 5	70	3	< 2	0.7	< 0.2	< 1	< 0.5	4.7	17.8
OB-101	17	1	< 5	62	5	< 2	0.6	< 0.2	1	< 0.5	4.9	17.3
OB-102	12	< 1	< 5	32	3	< 2	< 0.5	< 0.2	< 1	< 0.5	1	7.9
OB-103	21	1	20	22	3	< 2	< 0.5	< 0.2	< 1	0.7	1.9	3.4
OB-104	15	1	< 5	49	6	5	0.8	< 0.2	1	< 0.5	2.1	19.3
OB-106	13	1	63	55	3	< 2	< 0.5	< 0.2	< 1	6.8	3.5	19.9
OB-107	20	1	< 5	80	4	< 2	0.6	< 0.2	1	1.7	2.9	22.4
OB-108	26	2	< 5	177	14	< 2	3	< 0.2	5	0.8	2.3	53.1
OB-109	10	1	< 5	16	2	< 2	< 0.5	< 0.2	< 1	0.6	0.5	6
OB-110	16	1	< 5	38	7	2	0.5	< 0.2	1	0.5	1.6	21.8
OB-111	20	1	5	80	7	< 2	0.7	< 0.2	< 1	< 0.5	2.9	33

Analyte Symbol	Ce	Pr	Nd	Sm	Eu	Gd	Tb	Dy	Ho	Er	Tm	Yb
Unit Symbol	ppm	ppm	ppm	ppm	ppm	ppm	ppm	ppm	ppm	ppm	ppm	ppm
Detection Limit	0.1	0.05	0.1	0.1	0.05	0.1	0.1	0.1	0.1	0.1	0.05	0.1
Analysis Method	FUS-MS	FUS-MS	FUS-MS	FUS-MS	FUS-MS	FUS-MS	FUS-MS	FUS-MS	FUS-MS	FUS-MS	FUS-MS	FUS-MS
OB-100	34.3	3.84	14.2	2.3	0.72	1.7	0.2	1.1	0.2	0.6	0.08	0.5
OB-101	31.2	3.28	10.8	1.8	0.55	1.5	0.2	1.3	0.2	0.7	0.11	0.7
OB-102	14.2	1.56	5.6	1.1	0.33	1.1	0.2	1.2	0.2	0.7	0.1	0.7
OB-103	8.3	1.26	5.8	1.8	0.87	2.5	0.4	2.8	0.6	1.9	0.26	1.7
OB-104	36.6	4.27	15.8	2.9	0.82	3	0.5	3.2	0.7	2.1	0.32	2.1
OB-106	33.9	3.7	12.3	2	0.47	1.6	0.2	1.1	0.2	0.6	0.09	0.6
OB-107	40.4	4.37	15.1	2.6	0.57	2.1	0.3	1.6	0.3	0.9	0.13	0.9
OB-108	94.7	10.3	35	6.3	0.73	5.4	0.8	5	1	2.9	0.43	2.8
OB-109	11.5	1.29	4.4	0.9	0.27	1	0.1	0.8	0.2	0.5	0.08	0.5
OB-110	38.6	3.98	13.1	2.2	0.63	2	0.3	1.9	0.4	1.1	0.15	1
OB-111	53.6	5.2	16	2.1	0.53	1.5	0.2	0.9	0.2	0.4	0.06	0.4

Analyte Symbol	Lu	Hf	Ta	W	Tl	Pb	Bi	Th	U
Unit Symbol	ppm	ppm	ppm	ppm	ppm	ppm	ppm	ppm	ppm
Detection Limit	0.04	0.2	0.1	1	0.1	5	0.4	0.1	0.1
Analysis Method	FUS-MS	FUS-MS	FUS-MS	FUS-MS	FUS-MS	FUS-MS	FUS-MS	FUS-MS	FUS-MS
OB-100	0.08	2.4	0.2	1	0.5	5	< 0.4	1.8	0.6
OB-101	0.1	2.7	0.6	1	0.7	11	< 0.4	5.9	1.7
OB-102	0.1	1.6	0.4	< 1	0.2	9	< 0.4	4	0.9
OB-103	0.25	1.5	0.2	< 1	0.2	< 5	< 0.4	0.5	0.2
OB-104	0.32	3.6	0.6	< 1	0.3	< 5	< 0.4	4.6	1.5
OB-106	0.09	1.9	0.4	< 1	0.3	10	< 0.4	6.3	1.7
OB-107	0.13	3.2	0.5	< 1	0.4	11	< 0.4	7.1	1.7
OB-108	0.43	16.5	1.6	3	0.8	10	< 0.4	18.8	3.6
OB-109	0.08	1.4	0.3	< 1	0.1	< 5	< 0.4	5	0.9
OB-110	0.15	2.9	0.6	1	0.2	9	< 0.4	6.8	1.4
OB-111	0.06	4.1	0.7	< 1	0.4	14	< 0.4	10.5	1.9

Appendix IV. Zircon LA-ICMP U-Pb Analysis

Comments	Final207_235	2σ	Final206_238	2σ	Final207_206	2σ	FinalAge207_206	2σ	FinalAge207_235	2σ	FinalAge206_238	2σ	Th/U
OB-031-005 CORE	15.32	0.36	0.5509	0.0077	2848.4	5.6	2848.4	5.6	2834	22	2827	32	0.5074
OB-031-005 RIM	6.62	0.27	0.3034	0.007	2451	17	2451	17	2061	31	1708	33	0.21093
OB-031-007 CORE	15.36	0.35	0.5641	0.0069	2804.7	8	2804.7	8	2838	21	2883	28	0.4529
OB-031-007 RIM	15.44	0.35	0.555	0.0066	2849.3	7.8	2849.3	7.8	2843	22	2845	28	0.44476
OB-031-010 RIM	15.18	0.35	0.5499	0.007	2826.7	6.9	2826.7	6.9	2826	22	2824	29	0.32437
OB-031-010-CORE	12.61	0.39	0.4663	0.0094	2799	18	2799	18	2650	35	2467	43	0.60253
OB-031-011 CORE	15.62	0.38	0.5733	0.0079	2827	12	2827	12	2853	24	2920	32	0.36737
OB-031-011 RIM	15.21	0.35	0.5491	0.0064	2840.6	8.6	2840.6	8.6	2828	22	2821	27	0.40765
OB-031-012	16.34	0.36	0.5921	0.0065	2837.2	6.4	2837.2	6.4	2896	21	2998	27	0.36907
OB-031-014 CORE	14.71	0.34	0.5396	0.0075	2813.4	6.2	2813.4	6.2	2795	23	2781	33	0.76937
OB-031-014 RIM	15.25	0.36	0.5518	0.0069	2830	8.3	2830	8.3	2831	22	2835	29	0.33244
OB-031-016 RIM	15.08	0.36	0.5489	0.007	2820.7	7.3	2820.7	7.3	2819	23	2822	29	0.44458
OB-031-019 CORE	14.81	0.38	0.54	0.0082	2807	11	2807	11	2801	25	2782	35	0.32415
OB-031-019 RIM	15.36	0.36	0.5491	0.0068	2842.6	9.3	2842.6	9.3	2836	22	2821	28	0.42846
OB-031-020 CORE	7.6	2	0.35	0.058	2414	51	2414	51	2180	110	1930	200	0.26235
OB-031-020 RIM	14.95	0.33	0.5411	0.0066	2820.9	6.3	2820.9	6.3	2812	21	2790	28	0.38477
OB-031-022	15.22	0.33	0.5503	0.0059	2829.5	6.2	2829.5	6.2	2829	21	2826	25	0.35229
OB-031-023 CORE	14.7	0.37	0.5354	0.0091	2823.1	7.2	2823.1	7.2	2798	25	2763	39	0.46725
OB-031-023 RIM	15.14	0.34	0.5431	0.007	2843.6	7.9	2843.6	7.9	2823	22	2796	29	0.43905
OB-031-024 CORE	15.32	0.34	0.5504	0.0068	2841.4	7.3	2841.4	7.3	2835	22	2830	29	0.50183
OB-031-024 RIM	15.94	0.35	0.5724	0.0067	2838.1	5.5	2838.1	5.5	2874	21	2919	27	0.40103
OB-031-026 CORE	14.71	0.49	0.53	0.013	2834	17	2834	17	2796	39	2739	56	0.44288
OB-031-026 RIM	15.74	0.39	0.5684	0.0079	2829.9	8.4	2829.9	8.4	2862	23	2901	32	0.22606
OB-031-028 CORE	13.63	0.32	0.4967	0.007	2822	7.8	2822	7.8	2724	23	2599	30	0.47564
OB-031-028 RIM	15.16	0.35	0.5486	0.0065	2825.9	6.7	2825.9	6.7	2825	22	2819	27	0.34995
OB-031-029	15.58	0.35	0.5623	0.0065	2827.2	4.9	2827.2	4.9	2852	21	2876	27	0.33125
OB-031-031 CORE	13.46	0.31	0.5003	0.0067	2780	5.8	2780	5.8	2712	23	2615	29	0.20996
OB-031-031 RIM	14.65	0.32	0.5319	0.0064	2817.6	6.1	2817.6	6.1	2793	21	2749	27	0.34282
OB-031-032 CORE	15.25	0.39	0.5559	0.0085	2816.7	7.6	2816.7	7.6	2832	23	2853	34	0.3191
OB-031-032 RIM	4.65	0.13	0.2398	0.0033	2222	19	2222	19	1757	24	1385	17	0.28311
OB-031-033 CORE	15.07	0.34	0.5491	0.0067	2802.6	6.2	2802.6	6.2	2819	21	2821	28	0.28835
OB-031-033 RIM	15.23	0.34	0.5471	0.0064	2830	5.1	2830	5.1	2829	21	2813	27	0.39715
OB-031-035 RIM	5.8	0.29	0.2833	0.0067	2324	27	2324	27	1944	33	1608	33	0.34764
OB-031-035-CORE	14.87	0.39	0.5381	0.0097	2829	15	2829	15	2805	34	2775	44	0.23868
OB-031-036 CORE	13.49	0.31	0.5054	0.0074	2760.7	6.3	2760.7	6.3	2713	24	2636	33	0.38691
OB-031-036 RIM	13.87	0.31	0.5041	0.006	2815	7.4	2815	7.4	2740	21	2631	25	0.41756

OB-031-037 CORE	13.75	0.31	0.5067	0.0062	2800	6.7	2800	6.7	2733	22	2641	27	0.61889
OB-031-037 RIM	15.48	0.36	0.5556	0.0075	2817.3	9.2	2817.3	9.2	2847	22	2847	31	0.47219
OB-031-038 CORE	15.21	0.34	0.5517	0.0066	2827.2	6.4	2827.2	6.4	2828	22	2835	27	0.32549
OB-031-038 RIM	15.4	0.35	0.5531	0.0068	2840.3	8.3	2840.3	8.3	2840	22	2837	28	0.41358
OB-031-039 CORE	8.69	0.22	0.3417	0.0063	2677.6	9.4	2677.6	9.4	2302	26	1893	31	0.5163
OB-031-039 RIM	13.88	0.36	0.5	0.0093	2825.7	7	2825.7	7	2742	27	2612	42	0.77316
OB-031-040	13.38	0.36	0.4953	0.0095	2768	21	2768	21	2706	36	2593	44	0.42458
OB-031-043 CORE	15.21	0.36	0.5496	0.0075	2814.3	6.7	2814.3	6.7	2827	22	2822	31	0.61383
OB-031-043 RIM	14.79	0.33	0.5364	0.0066	2820.5	7.4	2820.5	7.4	2802	22	2768	28	0.60172
OB-031-045	15.34	0.53	0.558	0.013	2814	16	2814	16	2836	39	2858	58	0.21945
OB-031-046	15.64	0.4	0.556	0.0083	2849	10	2849	10	2855	23	2849	34	0.68441
OB-031-048 CORE	14.65	0.39	0.5309	0.0089	2820	12	2820	12	2792	28	2745	39	0.54047
OB-031-048 RIM	15.33	0.38	0.5515	0.0084	2839.4	9.4	2839.4	9.4	2836	24	2832	35	0.31462
OB-031-049	15.26	0.35	0.5508	0.0071	2821.5	6.3	2821.5	6.3	2831	22	2828	30	0.23228
OB-031-051 CORE	13.35	0.32	0.4846	0.0066	2815	7.3	2815	7.3	2704	23	2548	28	0.84961
OB-031-052 CORE	14.85	0.37	0.5451	0.0087	2811.4	8.7	2811.4	8.7	2804	24	2802	36	0.46851
OB-031-052 RIM	14.57	0.32	0.5276	0.0058	2821.2	6.1	2821.2	6.1	2788	21	2732	25	0.3484
OB-031-054 CORE	14.62	0.34	0.5285	0.0067	2822.5	6.1	2822.5	6.1	2791	21	2735	28	0.61884
OB-031-054 RIM	12.53	0.29	0.4774	0.0071	2735.4	7.8	2735.4	7.8	2644	23	2516	31	0.2199
OB-031-055 CORE	15.09	0.33	0.5443	0.0063	2824.7	5.7	2824.7	5.7	2820	21	2801	26	0.94796
OB-031-058	14.32	0.45	0.535	0.013	2760.7	8.8	2760.7	8.8	2762	31	2757	55	0.38374
OB-031-060 RIM	15.67	0.35	0.5692	0.0064	2826.8	6.6	2826.8	6.6	2857	21	2905	27	0.44784
OB-031-062	15.11	0.33	0.5483	0.0065	2827.7	6.5	2827.7	6.5	2821	21	2818	28	0.34589
OB-031-063	15.27	0.35	0.5486	0.0063	2838.6	8.5	2838.6	8.5	2834	22	2819	26	0.50712
OB-031-065 RIM	14.69	0.33	0.5313	0.0067	2833.6	7.4	2833.6	7.4	2797	23	2751	29	0.54455
OB-031-066	11.68	0.47	0.48	0.014	2616	12	2616	12	2580	35	2527	59	0.3356
OB-031-070	6.69	0.16	0.3108	0.0042	2426.3	9.9	2426.3	9.9	2071	20	1744	21	0.39678
OB-031-072 CORE	15.13	0.34	0.5504	0.0062	2828.3	6.6	2828.3	6.6	2823	21	2826	26	0.87377
OB-031-072 RIM	14.59	0.39	0.5408	0.0092	2785.6	8.1	2785.6	8.1	2785	26	2785	38	0.33095
OB-031-073	14.19	0.33	0.5347	0.0067	2780.7	8.4	2780.7	8.4	2761	23	2761	29	0.63971
OB-031-074	13.87	0.31	0.5077	0.006	2821.6	6	2821.6	6	2740	21	2647	26	0.30944
OB-031-077 CORE	15.06	0.34	0.5498	0.0071	2830.3	6.8	2830.3	6.8	2823	23	2826	29	0.28013
OB-031-077 RIM	11.38	0.26	0.4221	0.0056	2802.9	8.7	2802.9	8.7	2555	22	2270	25	0.79378
OB-031-079	10.22	0.21	0.4331	0.0064	2565.9	9.4	2565.9	9.4	2459	24	2318	30	0.20799
OB-031-080	16.4	0.37	0.5977	0.0071	2833.6	7.5	2833.6	7.5	2900	21	3020	28	0.48899
OB-031-081	15.77	0.35	0.5729	0.0068	2838.1	7.2	2838.1	7.2	2864	22	2919	28	0.76903
OB-031-082 CORE	7.78	0.19	0.3283	0.0054	2602.1	7.7	2602.1	7.7	2208	23	1830	27	0.50997
OB-031-082 RIM	12.63	0.32	0.4632	0.0081	2816.2	7.7	2816.2	7.7	2658	26	2456	36	0.60448
OB-031-083	6.1	0.26	0.2915	0.008	2388	8.5	2388	8.5	1990	24	1649	35	0.20998
OB-031-084 CORE	13.3	0.3	0.5079	0.0059	2760	7.4	2760	7.4	2702	21	2647	26	0.33198
OB-031-084 RIM	16.1	0.36	0.5877	0.0069	2829.9	7.3	2829.9	7.3	2883	21	2979	28	0.43633

OB-031-085	16.08	0.35	0.5843	0.0066	2833.5	5.9	2833.5	5.9	2881	21	2966	27	0.36812
JD-101 1a - 1	15.7	0.37	0.5566	0.011	0.2045	0.004	2858.6	17	2859.5	24	2852	47	0.44306
JD-101 1b - rim	15.958	0.34	0.5626	0.0092	0.20524	0.003	2867.3	16	2874.7	20	2877	38	0.30021
JD-101 2a - 1	14.82	0.32	0.5178	0.0087	0.208	0.004	2890.8	15	2803.1	21	2689	37	0.65687
JD-101 2b - 1 rim	13.264	0.29	0.4865	0.0081	0.19781	0.003	2807.9	18	2698.5	21	2555.3	35	0.58118
JD-101 3 - 1	12.35	0.39	0.4653	0.014	0.1935	0.003	2770.9	19	2629	32	2462	61	0.51959
JD-101 4a - 1	14.67	0.32	0.5139	0.0087	0.20808	0.004	2890.8	15	2793.8	21	2675	38	0.44429
JD-101 4b - rim	12.112	0.27	0.4164	0.0071	0.21209	0.004	2920.7	16	2612.5	21	2244	32	0.856
JD-101 6a - 1	13.95	0.3	0.4925	0.008	0.2058	0.004	2872.6	15	2746.1	20	2582.4	34	0.71289
JD-101 6b - 1 rim	13.4	0.3	0.4832	0.0085	0.20172	0.003	2839.1	22	2708	22	2541	37	0.49252
JD-101 7 - 1	13.678	0.3	0.4987	0.0084	0.20026	0.003	2826.1	19	2727.4	21	2608	37	0.98268
JD-101 9 - 1	15.791	0.34	0.5592	0.0093	0.206	0.004	2876.1	16	2863.9	20	2863	39	0.36434
JD-101 11 - 1	9.78	0.24	0.4059	0.0075	0.17457	0.003	2601.7	24	2417	22	2196	34	0.12592
JD-101 13 - 1	14.39	0.35	0.5111	0.0098	0.20367	0.003	2857.4	20	2774.9	24	2661	43	0.57455
JD-101 14a - 1	12.3	0.32	0.4319	0.0098	0.2058	0.004	2875.1	15	2627	24	2314	44	0.77152
JD-101 14a - 1 rim	15.07	0.65	0.5417	0.022	0.2032	0.003	2850.9	17	2819.4	55	2790	100	0.37736
JD-101 14a - 1 rim	16.35	0.35	0.5688	0.0095	0.20926	0.004	2902.4	16	2897.6	21	2902	39	0.43175
JD-101 15b - 1	16.06	0.35	0.5618	0.0092	0.20833	0.004	2897.7	15	2880.2	21	2874	38	0.36995
JD-101 17 - 1	14.79	0.32	0.5306	0.009	0.20292	0.003	2848.4	20	2801.5	22	2744	39	0.13642
JD-101 19 - 1	15.255	0.33	0.5448	0.0092	0.2054	0.004	2869.8	15	2831.2	21	2803	38	0.57879
JD-101 20 - 1	15.79	0.34	0.5515	0.0091	0.2101	0.004	2903.8	13	2863.5	21	2831	37	0.59517
JD-101 22 - 1	14.68	0.46	0.543	0.016	0.2011	0.004	2833.7	16	2796	35	2795	70	0.69041
JD-101 23a - 1	14.16	0.33	0.5114	0.01	0.2038	0.004	2860.8	15	2759	23	2662	43	0.427
JD-101 23b - 1 rim	15.25	0.33	0.5504	0.009	0.2049	0.004	2865.3	17	2830.7	21	2829	38	0.57532
JD-101 24 - 1	15.129	0.32	0.5328	0.0089	0.20948	0.004	2901.7	17	2823.1	21	2753	37	0.55388
JD-101 27 - 1	14.01	0.36	0.5112	0.01	0.2021	0.003	2845.6	26	2750	27	2661	45	0.47141
JD-101 28 - 1	13.2	0.3	0.4669	0.0084	0.2085	0.004	2896.6	17	2694.8	22	2469	37	0.76917
JD-101 29a - 1	15.67	0.34	0.5572	0.0098	0.20753	0.004	2885.5	20	2856.6	21	2855	41	0.67284
JD-101 29b - 1	15.076	0.33	0.5457	0.0093	0.2039	0.003	2855	15	2819.9	21	2807	39	0.20595
JD-101 32 - 1	15.635	0.34	0.5566	0.0095	0.20576	0.003	2872.8	19	2854.6	21	2852	40	0.44503
JD-101 33 - 1	15.272	0.32	0.5406	0.009	0.2075	0.004	2886.9	16	2832.2	21	2786	38	0.5198
JD-101 35a - 1	11.17	0.3	0.391	0.0092	0.2088	0.004	2896.5	15	2536	27	2127	44	1.92414
JD-101 35b - 1	12.6	0.28	0.4576	0.0082	0.20098	0.003	2833.5	18	2650	22	2432	37	1.06085
JD-101 36 - 1	15.269	0.32	0.5405	0.0091	0.20662	0.004	2880.4	16	2832	20	2785	38	0.49391
JD-101 37 - 1	14.9	0.34	0.5248	0.0098	0.2077	0.004	2885.7	16	2808.3	22	2719	42	0.63108
JD-101 38 - 1	14.21	0.34	0.4956	0.0098	0.2104	0.004	2913.7	18	2763	24	2594	43	0.93262
JD-101 40 - 1	14.859	0.32	0.5232	0.0087	0.20553	0.003	2870.1	17	2806	20	2713	37	0.63211
JD-101 41A - 1	16.07	0.36	0.5641	0.0098	0.2068	0.004	2877.5	16	2880.4	21	2883	40	0.50529
JD-101 41B - 1	14.52	0.33	0.5154	0.0097	0.20476	0.003	2863.6	17	2783.9	22	2679	42	0.52394
JD-101 43 - 1	14.992	0.32	0.5409	0.0088	0.20024	0.003	2831.3	19	2815.4	20	2787	37	0.38566
JD-101 45a - 1	15.32	0.33	0.541	0.0088	0.2046	0.004	2866.5	17	2834.7	21	2788	37	0.54179

JD-101 45b - 1	15.517	0.34	0.5446	0.0094	0.20638	0.003	2876.3	19	2847.4	21	2803	40	0.56164
JD-101 46a - 1	11.88	0.28	0.4083	0.0075	0.2085	0.004	2895.1	20	2595	22	2206	34	1.59483
JD-101 48 - 1	13.833	0.3	0.4845	0.0079	0.2068	0.004	2880.4	15	2738	20	2546.5	34	0.70123
JD-101 50 - 1	8.83	0.29	0.3109	0.0093	0.206	0.004	2874.8	14	2320	32	1745	47	0.49039
JD-101 52a - 1	15.899	0.34	0.5592	0.0092	0.2062	0.004	2874.3	16	2870.6	21	2863	38	0.66596
JD-101 52b - 1	15.8	0.34	0.5498	0.0092	0.2093	0.004	2895.9	14	2864.6	20	2824	39	0.76505
JD-101 53a - 1	15.16	0.34	0.5413	0.0094	0.2042	0.003	2857.3	22	2827.1	23	2788	40	0.7354
JD-101 53b - 1	14.398	0.31	0.5132	0.0085	0.20383	0.003	2856.6	19	2776.9	21	2670.1	37	0.6746
JD-101 54a - 1	15.656	0.33	0.5521	0.009	0.20557	0.003	2869.7	20	2854.5	20	2833	38	0.29136
JD-101 54b - 1	14.75	0.31	0.5131	0.0084	0.2075	0.004	2889.6	17	2798.7	20	2672	37	0.6321
JD-101 55a - 1	15.31	0.35	0.5515	0.0099	0.20157	0.003	2837.6	18	2835.5	23	2831	41	0.30431
JD-101 55b - 1	15.32	0.34	0.5412	0.0092	0.2052	0.003	2864.9	15	2835.1	21	2788	39	0.23846
JD-101 56 - 1	16.15	0.35	0.5693	0.0096	0.2064	0.003	2875.3	16	2885.2	20	2905	39	0.63605
JD-101 57 - 1	13.628	0.3	0.482	0.0081	0.20449	0.003	2862.3	16	2723.8	21	2536	34	0.65267
JD-101 58a - 1	15.09	3.4	0.5376	0.088	0.2044	0.005	2863	33	2820	96	2773	260	0.29055
JD-101 58b - 1	16.042	0.34	0.5626	0.0092	0.20655	0.004	2880.8	15	2879	20	2877	38	0.22437
JD-101 59 - 1	13.25	0.55	0.4882	0.015	0.19716	0.004	2798.8	29	2696	35	2562	62	0.50176
JD-101 60 - 1	16.854	0.36	0.5741	0.0093	0.21316	0.004	2926.9	21	2926.3	20	2924.4	38	0.51536
JD-101 62 - 1	15.738	0.33	0.5576	0.0092	0.20511	0.003	2865.9	16	2861.5	20	2856	38	0.33243
JD-101 63a - 1	15.974	0.34	0.5623	0.0092	0.20618	0.004	2876.3	16	2875.5	20	2876.1	38	0.47003
JD-101 63b - 1	14.63	0.31	0.5163	0.0086	0.2048	0.004	2865.3	18	2790.9	21	2683	37	0.56075
JD-101 64 - 1	16.017	0.34	0.5621	0.0093	0.20681	0.004	2879.1	16	2877.6	21	2875.2	38	0.53932
JD-101 65a - 1	15.775	0.34	0.5586	0.0092	0.20401	0.003	2861	15	2863	20	2861	38	0.38052
JD-101 65b - 1	15.09	0.32	0.5322	0.0086	0.20476	0.004	2863.7	14	2822.3	20	2751.6	36	0.50575
JD-101 66 - 1	15.89	0.37	0.561	0.01	0.2048	0.003	2865.5	18	2869	22	2870	42	0.713
JD-101 67 - 1	14.713	0.31	0.5161	0.0085	0.20588	0.004	2876.1	17	2797.6	20	2682	36	0.58842
JD-101 69 - 1	14.36	0.33	0.4997	0.0092	0.2069	0.004	2882.2	14	2773	22	2616	41	0.65818
JD-101 70 - 1	14.55	0.51	0.5148	0.016	0.2045	0.004	2861.6	19	2785	47	2677	75	0.65281
JD-101 71a - 1	10.03	0.42	0.3811	0.012	0.1899	0.004	2741.5	39	2436	48	2081	58	0.76971
JD-101 71b - 1	12.65	0.3	0.4415	0.0087	0.20738	0.004	2888.2	18	2654	23	2356	39	0.70254
JD-101 73a - 1	12.74	0.29	0.4726	0.0083	0.1945	0.003	2783.1	21	2660	22	2495	36	0.63556
JD-101 73b - 1	15.851	0.34	0.5598	0.0092	0.20377	0.003	2857.2	17	2867.7	20	2867	38	0.40463
JD-101 74 - 1	15.7	0.35	0.5503	0.01	0.2048	0.004	2865	19	2859.4	22	2826	42	0.68443
JD-101 75 - 1	15.789	0.33	0.5556	0.009	0.20404	0.003	2860.2	20	2864	20	2848.4	37	0.23433
JD-101 76a - 1	15.862	0.34	0.5504	0.0092	0.2063	0.004	2873.5	14	2868.2	21	2826	38	0.23178
JD-101 76b - 1	15.636	0.33	0.5467	0.0089	0.20547	0.003	2868.7	18	2854.6	20	2811	37	0.48645
JD-101 79a - 1	16.483	0.35	0.5695	0.0093	0.20724	0.004	2881.5	16	2905	20	2907	38	0.47519
JD-101 79b - 1	15.78	0.36	0.5583	0.0099	0.20193	0.003	2843.9	15	2862.8	22	2859	41	0.8382
JD-101 80 - 1	16.221	0.34	0.5648	0.0091	0.20544	0.003	2870.1	17	2890.4	20	2886	38	0.38479
JD-101 81a - 1	14.11	0.3	0.5025	0.0083	0.20079	0.003	2830.6	18	2756.9	20	2624	36	0.57317
JD-101 81b - 1	17.3	0.37	0.5994	0.01	0.2062	0.004	2874.8	16	2952	20	3027	40	0.68186

JD-101 83a - 1	11.61	0.26	0.4264	0.0072	0.19477	0.003	2787.3	25	2573	21	2289	33	0.38108
JD-101 83b - 1	14.31	0.31	0.5028	0.0085	0.20347	0.003	2851.9	16	2770.1	21	2625	37	0.43062
JD-101 84 - 1	15.286	0.33	0.5306	0.0086	0.20585	0.004	2873.8	16	2833.9	21	2744.8	37	0.76538
JD-101 86 - 1	14.832	0.34	0.5182	0.0092	0.2048	0.004	2863.1	20	2804.3	23	2691	40	0.87555
OB-001-054	11.51	0.25	0.4354	0.0057	0.1918	0.004	2759	26	2565	22	2330	26	0.8851
OB-001-053	15.6	0.56	0.553	0.019	0.2036	0.004	2855	20	2849	47	2847	87	0.35019
OB-001-052 RIM	13.96	0.4	0.488	0.011	0.2082	0.004	2903	27	2750	33	2571	50	0.28501
OB-001-051	13.61	0.31	0.5225	0.0089	0.1882	0.004	2734	19	2723	24	2709	40	0.56931
OB-001-049 CORE	14.02	0.3	0.5313	0.0079	0.1913	0.004	2754	21	2750	22	2746	35	0.62418
OB-001-049 RIM	14.09	0.3	0.5324	0.0066	0.192	0.004	2762	20	2754	20	2750	28	0.63956
OB-001-047	15.9	0.32	0.5599	0.0055	0.2073	0.004	2879	19	2871	19	2868	23	0.49722
OB-001-045	13.9	0.28	0.5422	0.0056	0.186	0.004	2706	22	2744	19	2792	24	0.69813
OB-001-044	17.61	0.42	0.5842	0.0085	0.2187	0.005	2972	19	2966	24	2968	35	0.64333
OB-001-040	14.01	0.29	0.5403	0.0062	0.1883	0.004	2724	21	2749	19	2788	26	0.45045
OB-001-038	13.44	0.28	0.5249	0.0055	0.186	0.004	2708	17	2711	20	2719	23	0.93499
OB-001-035	8.78	0.3	0.3725	0.0086	0.171	0.004	2566	34	2307	30	2037	40	0.41544
OB-001-032	17.15	0.35	0.5823	0.0062	0.2139	0.004	2936	20	2943	19	2958	25	0.13285
OB-001-031	12.59	0.27	0.4951	0.0068	0.1842	0.004	2698	20	2648	21	2592	30	0.50111
OB-001-030 CORE	15.99	0.33	0.564	0.006	0.2042	0.004	2860	17	2876	19	2883	24	1.6779
OB-001-030 RIM	16.41	0.34	0.5803	0.0061	0.2048	0.004	2863	17	2901	20	2949	25	1.11955
OB-001-029 CORE	16.59	0.38	0.5818	0.0075	0.2066	0.005	2879	23	2910	22	2955	31	0.78361
OB-001-029 RIM	16.56	0.33	0.5713	0.0053	0.209	0.004	2897	17	2910	19	2913	22	0.28438
OB-001-026	13.82	0.28	0.5312	0.0054	0.188	0.004	2725	20	2737	19	2748	23	0.62679
OB-001-023	18.04	0.38	0.5971	0.0064	0.2189	0.005	2974	19	2993	20	3020	26	1.09846
OB-001-022 RIM	11.31	0.25	0.4422	0.0057	0.1861	0.004	2707	21	2548	21	2360	26	0.65512
OB-001-019 RIM	13.72	0.29	0.5268	0.0061	0.1892	0.004	2734	18	2729	20	2727	26	0.13875
OB-001-018	13.7	0.3	0.526	0.0063	0.1895	0.004	2737	18	2727	21	2725	26	0.79093
OB-001-016 core	17.71	0.38	0.5852	0.0068	0.2204	0.005	2983	19	2972	21	2969	28	0.55815
OB-001-016 RIM	17.65	0.36	0.5848	0.0057	0.2192	0.005	2978	19	2972	19	2968	23	0.14735
OB-001-015	19.22	0.43	0.6056	0.0065	0.2308	0.005	3060	30	3051	21	3051	26	0.28238
OB-001-014	14.05	0.28	0.5433	0.0053	0.1887	0.004	2729	20	2752	19	2797	22	0.75816
OB-001-013	18.37	0.37	0.6031	0.0059	0.2201	0.004	2984	17	3009	19	3042	24	0.59749
OB-001-012	19.68	0.39	0.6249	0.0063	0.229	0.005	3048	17	3075	19	3129	25	0.58978
OB-001-011 CORE	15.8	0.34	0.5602	0.0072	0.2036	0.004	2860	17	2864	21	2869	30	0.47993
OB-001-011 RIM	14.98	0.35	0.5314	0.0096	0.2046	0.004	2865	18	2813	24	2747	41	0.3805
OB-001-010	15.91	0.33	0.5625	0.0063	0.204	0.004	2856	19	2872	19	2877	26	0.82775
OB-001-009 CORE	16.16	0.34	0.5791	0.0064	0.202	0.004	2844	19	2886	20	2945	26	0.36351
OB-001-009 RIM	18.76	0.42	0.6409	0.0088	0.2123	0.004	2922	20	3031	21	3191	35	0.30332
OB-001-008	13.47	0.7	0.523	0.025	0.1879	0.004	2724	28	2714	77	2710	120	0.68462
OB-012 1 - 1	15.66	0.35	0.5368	0.0089	0.2086	0.004	2900.1	17	2856.3	22	2770	37	0.50955
OB-012 2 - 1	13.12	0.44	0.4658	0.015	0.2024	0.003	2849.1	19	2690	38	2465	67	1.31344

OB-012 3 - 1	16.26	0.35	0.5543	0.0097	0.2109	0.004	2914.8	16	2891.8	22	2843	40	1.06065
OB-012 4 - 1	15.452	0.33	0.5549	0.009	0.20072	0.003	2830.1	16	2843.3	20	2845.4	37	0.6142
OB-012 5 - 1	16.329	0.36	0.5664	0.0099	0.2074	0.004	2884.7	17	2896.1	22	2893	41	0.33873
OB-012 6 - 1	17.47	0.39	0.5816	0.01	0.2162	0.004	2954.5	18	2960.6	22	2955	41	0.51378
OB-012 7 - 1	13.4	0.58	0.508	0.02	0.189	0.003	2735.3	28	2707	52	2656	90	0.55648
OB-012 8 - 1	14.36	0.36	0.5506	0.011	0.19	0.004	2742	19	2772	23	2827	45	0.88
OB-012 10 - 1	15.2	0.34	0.5427	0.0093	0.20168	0.003	2840.3	18	2827.4	21	2795	39	0.46413
OB-012 11 - 1	12.98	0.31	0.4954	0.0097	0.1891	0.003	2737.1	18	2677.3	24	2594	43	0.60206
OB-012 12 - 1	14.74	0.35	0.5163	0.0096	0.2056	0.004	2872	17	2798	23	2683	41	0.28424
OB-012 13 - 1	14.52	0.39	0.5171	0.013	0.2031	0.004	2850	17	2784	30	2686	57	0.4496
OB-012 14a - 1	13.73	0.3	0.5286	0.0089	0.1879	0.003	2716.9	15	2730.7	21	2735	37	0.75643
OB-012 14b - 1	13.682	0.3	0.5261	0.0089	0.187	0.003	2718.9	17	2728.9	21	2726	38	1.00286
OB-012 17 - 1	13.93	0.38	0.4983	0.012	0.2019	0.003	2840.7	18	2746	27	2606	51	0.52778
OB-012 19 - 1	15.367	0.33	0.5371	0.009	0.2058	0.003	2874.2	16	2839.2	20	2771	37	0.43147
OB-012 20 - 1	14.93	0.36	0.5233	0.0099	0.2055	0.004	2871	15	2810.1	22	2713	41	0.33859
OB-012 22a - 1	16.29	0.41	0.5685	0.012	0.20689	0.004	2882.3	15	2892	24	2900	47	0.44684
OB-012 22b - 1	16.001	0.34	0.5629	0.0092	0.2064	0.003	2878.1	18	2877.2	21	2879.3	38	0.21051
OB-012 23 - 1	13.51	0.48	0.5247	0.015	0.1876	0.004	2726.6	29	2715.7	43	2719	70	0.66469
OB-012 28 - 1	5.32	0.53	0.248	0.019	0.15677	0.003	2423	35	1870	64	1428	94	0.24528
OB-012 29 - 1	12.3	0.65	0.4811	0.0097	0.18782	0.005	2725.4	30	2627.2	25	2532	41	0.85533
OB-012 31 - 1	13.4	0.39	0.4879	0.012	0.2021	0.004	2841	20	2708	31	2564	55	0.41772
OB-012 32 - 1	17.45	0.38	0.5828	0.0097	0.221	0.004	2987.3	14	2960.6	21	2960	39	1.43064
OB-012 33 - 1	11.1	0.28	0.4448	0.0093	0.18356	0.003	2684.3	23	2531.2	25	2372	43	0.72
OB-012 34 - 1	11.95	0.49	0.4766	0.015	0.1852	0.004	2696	39	2603	50	2518	70	0.57727
OB-012 37 - 1	11.4	0.3	0.4218	0.0086	0.19781	0.003	2807.9	23	2557	25	2268	39	0.38639
OB-012 38 - 1	12.035	0.26	0.4658	0.0078	0.18855	0.003	2729.5	16	2606.7	20	2465	35	0.38148
OB-012 39 - 1	8.36	0.33	0.3366	0.0087	0.18061	0.004	2659.9	28	2271	30	1870	41	0.218

Appendix V. Zircon LA-ICMP Trace Element Analysis

Sample	Age	Th/U	Al27	Si29	P31	Ca42	Sc45	Ti49	V51	Fe57	Sr88	Y89	Nb93
JD-101-7a	2830	0.8320142	1726.35	153226.63	302.33	606.21	267.87	22.03	1.98	1769.22	9.98	1321.17	2.43
JD-101-7B	2830	0.7674159	634.13	153226.63	2208.35	3621.94	300.74	15.42	0.745	635.54	6.45	1623.05	2.64
JD-101-10	2830	0.6896639	364.65	153226.63	484.64	561.38	287.8	33.81	0.494	302.85	3.89	1148.08	2.57
JD-101-12A	2830	0.811989	442.63	153226.63	225.23	<70.98	290.33	66.21	1.22	691.11	0.784	652.51	1.42
JD-101-12B	2830	0.9091843	398.23	153226.63	408.11	<69.36	347.99	74.12	1.076	411.35	2.3	1776.63	4.98
JD-101-20	2900	0.4395906	24.62	153226.63	261.64	<31.63	436.83	7.73	0.199	26.83	0.258	749.7	1.4
JD-101-30	2830	0.4368107	49.24	153226.63	3108.99	6325.6	399	40.73	6.28	712.89	5.48	712.68	1.383
JD-101-31A	2830	0.2200971	219.92	153226.63	194.39	<96.91	306.42	25.12	0.22	328.55	1.62	823.27	2.66
JD-101-31B	2830	0.683961	435.15	153226.63	358.54	150.49	351.6	6.49	0.114	577.49	0.831	1129.49	0.94
JD-101-60	2930	0.5868343	174.74	153226.63	1873.65	2454.75	308.33	1119.32	2.17	354.24	7.62	1238.85	6.53
JD-101-68	2830	0.6182418	406.35	153226.63	630.94	339.13	342.22	111.57	0.631	1050.58	1.62	1690.44	3.49
JD-101-81	2950	0.5407308	246.42	153226.63	1705.04	1747.8	311.25	24.37	0.19	346.93	2.53	1071.82	3.8
OB-031-72	2865	0.3486127	1037.54	153226.63	164.55	<87.82	265.77	29.85	1.73	1002.32	1.17	430.41	1.98
OB-031-76	2850	0.6552055	2004.35	153226.63	1013.56	1423.7	339.33	44.65	4.52	1756.76	4.82	912.02	3.47
OB-031-77	2820	0.4347595	374.73	153226.63	1137.41	1540.27	285.28	65.2	6.9	267.86	3.17	965.29	3.17
OB-031-38	2850	0.4640167	1753.56	153226.63	4721.25	8236.26	311.1	13.8	5.13	1995.83	4.76	1041.59	2.69
OB-031-37	2820	0.3927843	1703.64	153226.63	1718.04	3393.17	351.22	29.58	2.72	1204.94	15.1	1355.57	4.49
OB-031-37B	2820	0.4994282	1881.38	153226.63	225.14	390.04	298.32	16.73	2.66	1628.3	4.76	503.78	1.58
OB-031-32	2222	0.3254482	3270.03	153226.63	192.45	944.63	284.23	75.9	4.72	3745.48	7.71	773.07	6.26
OB-031-32B	2820	0.30896	758.07	153226.63	396.56	5386.73	331.76	22.67	0.886	2169.57	34.03	1938.49	15.19
OB-031-29	2830	0.4310783	1019.96	153226.63	374.82	597.07	319.71	82.34	6.99	1020.83	3.83	1220.93	6.87
OB-031-12	2850	0.3943218	898.8	153226.63	2403.8	3072.31	313.44	8.53	2	1231.51	4	1397	4.5
OB-031-8	2850	0.6786487	567.1	153226.63	731.61	1146.69	359.34	12.82	1.61	363.8	6.34	1628.58	8.66
OB-031-5	2850	0.5513328	480.41	153226.63	13230.39	18671.9	479.43	8.59	1.76	433.89	8.65	1985.6	4.61
JDA-01	NA	0.3906434	279.68	153226.63	453.51	710.3	389.71	12.87	0.508	228.22	9.35	1906.45	3.17
JDA-02	NA	0.5029854	266.12	153226.63	7204.76	14249.71	380.92	15.41	0.483	128.35	18.06	1864.78	2.33
JDA-03	NA	0.3807144	58.32	153226.63	453.92	156.6	437.47	6.87	0.063	61.5	1.05	1505.52	2.09
JDA-04	NA	0.3853976	246.34	153226.63	1252.95	1664.62	407.01	7.23	0.118	145.48	4.11	1626.49	1.87
JDA-05	NA	0.7343026	4277.99	153226.63	399.2	752.93	302.59	21.21	0.296	555.53	11.73	1215.7	1.48
JDA-06	NA	0.4791963	1764.1	153226.63	868.01	1145.82	386	1043.8	2.17	757.6	8.95	1285.03	3.27
JDA-07	NA	0.5167169	478.85	153226.63	1824.02	2476.19	352.9	10.09	0.543	256.14	14.63	1507.39	1.75
JDA-08	NA	0.3979416	173	153226.63	3219.9	5123.37	321.28	5.54	0.217	128.45	7.53	808.96	1.17
JDA-09	NA	0.4038968	36.55	153226.63	1276.06	1552.99	330.44	3.37	0.073	36.67	2.81	728.62	1.96
JDA-10	NA	0.5156236	429.95	153226.63	9616.77	17019.64	356.44	10.06	0.252	825.37	25.38	1595.19	2.19
JDB-01	NA	0.3178508	182.88	153226.63	275.83	95.21	361.26	7.79	1.1	209.92	3.61	940.82	1.51
JDB-02	NA	0.3438749	92.51	153226.63	221.52	<65.58	382.14	10.79	0.114	146.74	1.06	668	1.29

JDB-03	NA	0.2087667	582.53	153226.63	599.94	138.98	320.89	79.44	5.09	427.14	4.87	1253.35	3.64
JDB-04	NA	0.8475749	89.03	153226.63	201.73	<58.92	309.02	6.56	0.143	93.55	1.07	593.01	0.81
JDB-05	NA	0.3266312	264.92	153226.63	185.06	227.01	292.95	12.29	1.76	568.49	7.25	629.84	1.6
JDB-06	NA	0.4223961	72.09	153226.63	288.62	105.75	380.28	4.88	0.201	163.74	1.04	765.05	0.653
JDB-07	NA	0.5089352	270.45	153226.63	406.77	112.05	420.09	26.59	0.577	636.14	5.95	1348.42	2.45
JDB-08	NA	0.5808031	43.88	153226.63	2510.19	3119.55	277.65	9.63	0.535	250.44	4.32	374.73	0.694
JDB-09	NA	0.5889377	1254.34	153226.63	7388.39	11943.04	399.23	428.33	15.41	3126.36	12.2	1196.27	2.09
OB-001-11	2865	0.6016844	239.81	153226.61	7493.14	13859.75	410.69	20.23	1.437	193.11	10.76	1322.35	1.131
OB-001-12	3048	0.7034367	40.41	153226.61	375.07	<81.62	292.81	2.84	1.8	71.69	0.232	1175.44	0.745
OB-001-08	2724	0.6151126	20.12	153226.61	109.15	<77.77	279.23	6.7	0.186	36.18	0.82	656.14	3.43
OB-001-07	2865	0.7101833	2651.35	153226.61	1914.79	2408.54	326.67	44.79	1.69	1506.47	8.73	2473.01	3.02
OB-001-14	2729	0.9308403	2935.29	153226.61	505.1	97.88	304.29	27.93	2.32	662.12	3.7	1643.66	6.89
OB-001-15	3050	0.2225091	954.44	153226.59	4414.31	8458.82	349.83	6.24	0.791	743.18	8.19	1584.54	2.82
OB-001-19	2734	0.5926812	127.61	153226.63	383	444.61	287.68	9.47	0.491	132.05	0.882	359.39	0.783
OB-001-38	2708	1.2805018	93.86	153226.63	521	620.01	301.72	11.7	0.532	95.6	2.22	1057.18	1.436
OB-001-45	2706	0.7544638	284.38	153226.61	3483.9	2986.15	325.91	18.58	0.499	83.34	2.49	780.51	2.97
OB-001-53	2855	0.6027392	10248.23	153226.61	435.94	230.99	499.94	198.35	29.43	12319.79	5.31	5349.13	2.78

Sample	Zr96	Sn118	Ba137	La139	Ce140	Pr141	Nd146	Sm147	Eu151	Gd157	Tb159	Dy163	Ho165
JD-101-7a	65789.37	0.307	5.42	10.69	72.43	10.03	56.42	37.24	10.46	71.58	16.25	146.45	42.98
JD-101-7B	67118.44	0.233	2.18	10.74	72.22	9.75	55.92	34.57	7.74	66.66	15.98	158.27	50.39
JD-101-10	68327.68	0.245	1.94	8.22	55.19	6.85	39.49	26.12	6.88	50.97	12.15	120.42	36.86
JD-101-12A	76262.73	0.174	0.49	5.13	25.21	3.02	15.93	12.68	2.1	25.85	6.73	65.99	20.38
JD-101-12B	75296.01	0.27	1.13	7.72	62.47	5.71	33.06	24.8	6.27	62.86	16.67	175.42	58.9
JD-101-20	77937.8	0.075	0.119	1.299	16.2	1.44	8.74	5.88	1.41	19.11	5.63	65.5	24.26
JD-101-30	77501.55	0.128	0.337	11.65	39.56	4.06	18.7	5.65	0.768	16.04	4.91	61.38	23.05
JD-101-31A	72008.25	<0.105	1.66	4.14	25.19	3.5	19.72	12.36	3.85	26.73	7.69	77.05	25.84
JD-101-31B	75147.72	0.069	0.616	3.88	24.23	2.94	17.58	14.3	3.53	42.08	11.18	114.92	37.47
JD-101-60	72753.89	0.202	3.06	13.62	71.42	9.02	50.36	23.22	5.97	45.81	10.63	110.53	38.46
JD-101-68	74364.77	0.152	2.68	18.14	98.21	15.27	84.56	56.49	11.43	101.86	22.12	193.53	54.57
JD-101-81	71098.06	<0.083	3.99	13.98	58.59	6.42	36.92	19.61	3.83	41.19	10.09	104.86	34.83
OB-031-72	66925.7	0.265	1.42	0.954	12.68	1.23	10.03	4.2	4.48	10.44	2.68	32.9	13.09
OB-031-76	72919.1	0.443	4.08	8.86	54.38	5.13	35.77	16.53	15.38	37.98	8.39	86.32	29.15
OB-031-77	65670.87	0.6	1.43	9.48	73.92	9.76	56.88	20.56	21.37	36.84	8.18	86.18	29.18
OB-031-38	64917.84	0.448	2.24	6.98	44.59	3.99	24.34	10.04	7.08	25.49	7.05	85.54	31.49
OB-031-37	66395.65	0.721	9.34	8.29	65.63	8.24	53.12	14.99	11.25	36.86	9.66	118.17	43.36
OB-031-37B	64284.03	0.483	3.56	5.34	39.76	4.46	29.79	8.82	2.96	17.26	3.81	43.81	15.51
OB-031-32	67258.05	1.206	5.02	5.18	32.53	3.6	27.87	12.05	15.58	25.57	5.61	61.54	23.62
OB-031-32B	71133.42	0.583	13.76	2.68	31.66	2.48	20.42	10.95	15.09	38.94	12.41	162.86	63.64
OB-031-29	68699.22	0.637	3.5	4.67	47.66	4.69	28.54	10.94	2.44	26.96	8.13	102.4	38.61
OB-031-12	69263.77	0.237	2.23	6.3	38.21	3.82	22.18	8.96	3.16	27.37	8.73	113.79	44.21
OB-031-8	73584.48	0.539	4.97	3.88	53.79	3.42	25.56	13.17	23.01	41.66	12.05	146.94	52.99
OB-031-5	70136.12	0.368	1.83	32.35	135.18	16.66	85.72	23.76	6.84	51.4	14.3	175.99	65.43
JDA-01	73531.69	0.14	23.77	24.35	177.98	32.92	189.49	63.12	13.19	92.53	19.86	192.86	62.4
JDA-02	77680.75	0.135	11.65	82.55	238.57	31.47	161.79	50.92	9.57	75.14	17.6	184.28	61.3
JDA-03	75276.71	0.08	2.73	2.91	29.26	3.16	19.67	11.15	2.65	31.65	9.95	125.64	49.68
JDA-04	75011.85	0.198	17.54	14.94	90.45	14.16	85.69	46.54	9.64	81.95	20.6	192.56	56.72
JDA-05	65609.16	0.13	53.14	40.71	233.95	36.76	166.45	40.79	9.79	59.72	12.83	120.21	38.01
JDA-06	76125.05	0.333	31.62	36.02	147.81	24.66	136.17	58.63	12.13	79.56	16.82	154.9	42.65
JDA-07	75094.18	0.108	23.2	121.31	245.14	26.51	113.38	37.55	7.1	66.5	16.36	164.68	52.32
JDA-08	70443.87	0.137	9.62	43.25	147.79	19.15	81.31	17.79	3.29	30.08	7.1	77.16	25.69
JDA-09	69455.59	0.092	2.9	13.51	45.31	5.04	25.19	7.65	1.48	18.65	5.34	64.16	23.83
JDA-10	72001.06	0.216	27.25	208.31	526.85	63.06	285.38	84.43	12.29	111.6	23.95	209.05	55.67
JDB-01	74431.75	0.165	0.84	6.92	69.34	11.7	68.6	20.7	7.39	34.16	8.7	90.42	28.92
JDB-02	69700.39	0.162	3.02	2.08	16.52	1.44	8.37	6.45	1.84	17.88	5.65	64.62	21.64
JDB-03	72223.85	0.328	3.47	6.9	38.87	6.31	35.72	24.62	7.6	52.85	16.45	168.91	48.57
JDB-04	74101.95	0.099	1.19	3.64	41.55	2.15	13.53	9.51	2.92	22.97	6.56	65.79	19.25
JDB-05	67638.42	0.14	2.4	4.25	27.86	2.47	14.2	8.07	4.54	20.92	5.23	57	19.46
JDB-06	71326.53	0.074	1.87	12.13	23.64	4.24	21.53	11.11	3.51	28.29	7.98	82.13	26.18

JDB-07	72029.85	0.176	2.09	7.25	45.88	6.26	35.3	23.98	9.27	52.8	17.39	187.28	50.49
JDB-08	67519.02	0.091	0.38	19.81	61.9	5.54	24.01	5.64	0.96	12.87	3.34	37.68	12.49
JDB-09	69054.16	0.214	5.53	10.93	47.5	5.62	32.45	18.23	6.44	43.72	11.76	126.34	40.27
OB-001-11	71527.84	0.059	0.77	176.12	290.62	33.75	153.75	55.78	12.58	88.33	20.01	189.83	47.01
OB-001-12	66164.79	<0.081	0.253	0.0348	9.54	0.1646	3.07	4.54	1.007	23.21	7.56	100.87	38.23
OB-001-08	71001.98	0.118	0.364	1.08	48.42	0.571	4.35	4.63	1.337	15.16	4.54	53.2	18.63
OB-001-07	66856.46	0.298	16.76	50.41	133.09	17.27	95.63	59.19	17.7	155.7	36.64	344.61	88.39
OB-001-14	61684.29	1.58	4.73	9.72	125.93	4.67	29.42	21.89	12.37	62.72	16.32	174.41	54.69
OB-001-15	73977.43	0.16	3.93	23.63	79.01	10.61	60.5	30.02	8.38	71.71	17.97	173.91	51.45
OB-001-19	71159.07	0.12	1.028	2.198	20.94	0.845	4.46	3.03	0.898	9.63	2.63	30.59	10.87
OB-001-38	70865.1	0.062	0.602	6.55	85.74	2.9	19.9	17.61	5.55	54.7	12.87	123.8	35.03
OB-001-45	75970.37	0.059	0.294	23.88	105.79	6.1	27.53	13.93	4.01	34.07	8.54	86.45	26.32
OB-001-53	66766.5	0.39	27.89	98.91	296.88	51.05	292.45	234.24	66.89	571.72	129.34	999.44	202.47
OB-001-54	71976.83	0.115	3.79	2.225	34.24	1.223	7.69	6.31	1.96	20.55	5.83	61.21	20.24

Sample	Er167	Tm169	Yb173	Lu175	Hf177	Pb204	Pb206	Pb207	Pb208	Th232	U238
JD-101-7a	170.21	35.05	315.61	61.68	8695.03	3.68	1170.35	257.48	85	559.23	672.14
JD-101-7B	223.57	47.23	429.57	85.39	7704.1	3.19	1055.63	242.14	75.51	364.3	474.71
JD-101-10	161.13	33.9	304.16	61.82	8427.84	3.66	874.02	196.7	67	273.9	397.15
JD-101-12A	82.28	17.79	169.6	32.57	10494.01	4.66	391.71	88.68	18.99	179.75	221.37
JD-101-12B	255.78	53	470.05	88.81	9134.35	2.1	1134.48	260.05	110.51	513.38	564.66
JD-101-20	111.92	24.17	217.88	44.04	9240.74	1.46	591.65	137.71	31.35	116.83	265.77
JD-101-30	111.74	24.61	231.32	47.27	9833.27	1.23	586.16	134.84	32.8	110.5	252.97
JD-101-31A	120.96	26.85	251.14	48.54	11422.8	2.21	1137.34	257.79	23.74	110.13	500.37
JD-101-31B	158.62	31.72	273.33	54.09	8903.95	2.96	525.43	121.11	36.01	158.72	232.06
JD-101-60	176.29	38.18	351.84	72.19	9535.19	5.36	1452.97	322.75	106.7	382.17	651.24
JD-101-68	224.88	45.51	405.63	78.02	9549.15	6.31	920.69	211.9	53.85	294.45	476.27
JD-101-81	158.21	34.49	315.41	63.73	9469.17	28.46	1277.12	303.23	108.48	250.38	463.04
OB-031-72	68.75	16.83	174.13	38.82	8668.24	1.78	644.97	142.27	28.6	92.1	264.19
OB-031-76	126.73	25.94	231.98	43.78	8593.63	1.54	672.98	149.19	57.8	205.04	312.94
OB-031-77	128.31	27.33	243.98	49.15	8394.92	1.63	1318.98	292.82	65.1	228.64	525.9
OB-031-38	150.61	34.3	326.07	66.83	7420.74	<1.81	1286.83	285.91	74.67	238.37	513.71
OB-031-37	207.87	44.03	434.74	72.64	7065.47	<2.29	1389.2	292	78.49	287.09	730.91
OB-031-37B	73.38	15.58	145.4	29.87	7119.2	<2.06	379.87	84.7	24.25	78.61	157.4
OB-031-32	114.57	25.97	258.18	52.37	9050.17	1.25	992.99	204.37	45.74	163.03	500.94
OB-031-32B	308.02	69.67	660.06	119.6	9704.94	4.26	3552.42	662.03	156.08	715.02	2314.28
OB-031-29	189.2	42.07	396.55	79.35	9489.35	1.14	2131.68	470.97	103	393.54	912.92
OB-031-12	218.58	48.62	453.51	93.1	8937.92	2.12	2104.16	462.27	102.32	361.53	916.84
OB-031-8	238.94	48.73	432.55	79.27	9630.69	0.89	1909.14	422.57	158.82	592.63	873.25
OB-031-5	310.87	67.47	608.27	119.92	8694.01	1.39	1941.74	432.62	131.43	436.22	791.21
JDA-01	277.57	57.85	534.24	107.52	9377.29	8.38	1154.94	281	64.67	182.2	466.41
JDA-02	273.05	57.78	527.94	103.88	8724.66	17.54	721.83	186.51	62.45	153.32	304.82
JDA-03	249.35	54.46	516.81	106.85	9784.15	2.35	882.81	213.29	43.86	137.91	362.24
JDA-04	241.4	49.93	452.46	88.61	10397.34	30.25	885.74	237.75	76.24	142.89	370.76
JDA-05	169.47	36.17	342.56	70.35	8082.93	5.19	455.79	113.17	24.42	152.03	207.04
JDA-06	179.11	36.6	303.98	56.45	9430.64	20.28	545.73	142.25	45.79	114.48	238.9
JDA-07	225.45	46.69	414.18	77.42	10008.29	5.45	827.99	185.86	56.39	205.86	398.4
JDA-08	120.01	25.4	228.93	45.95	9218.06	7.15	591.32	138.47	34.5	99.37	249.71
JDA-09	113.45	24.72	232.84	45.06	9387.41	4.16	902.3	205.07	47.04	151.74	375.69
JDA-10	216.39	42.28	358.92	65.85	9465.32	4.76	802.85	184.82	49.57	178.38	345.95
JDB-01	130.58	27.12	249.95	49.48	11069	1.53	637.57	140.4	25.99	94.71	297.97
JDB-02	103.73	22.68	218.34	43.53	9414.95	<1.15	473.81	107.03	20.12	69.7	202.69
JDB-03	199.38	40.1	366.86	69.28	10231.12	2.61	719.46	165.18	21.33	73.06	349.96
JDB-04	81.67	18.02	172.83	36.42	9066.4	<1.22	351.45	74.26	35.75	148.19	174.84
JDB-05	93.41	22.49	251.94	59.78	11220.19	5.24	737.56	162.18	31.53	130.61	399.87
JDB-06	116	24.54	225.21	44.86	9544.42	2.43	375.41	85.35	20	70.16	166.1

JDB-07	203.75	38.53	335.67	56.02	9516.51	1.29	631.17	139.56	41.91	150.37	295.46
JDB-08	56.29	11.79	108.51	21.57	8450.84	1.17	332.7	70.2	23.15	81.87	140.96
JDB-09	175.08	35.11	309.29	59.11	9026.57	8.95	628.52	144.1	52.52	160.78	273
OB-001-11	169.52	30.16	241.97	42.33	8240.04	2.4	397.86	90.04	27.61	120.74	200.67
OB-001-12	182.81	39.38	352.81	68.49	7251.7	<1.23	385.21	96.39	34.03	104.39	148.4
OB-001-08	95.17	23.94	252.07	58.08	9184.05	<1.46	1300.72	268	100.5	375.68	610.75
OB-001-07	315.32	58.23	481.44	85.24	8655.48	6.93	1096.38	245.78	99.61	399.4	562.39
OB-001-14	228.78	47.24	415.5	79.16	6274.99	2.76	1437.42	297.33	162.91	502.57	539.91
OB-001-15	199.28	38.93	343.85	66.04	10519.99	31.6	893.73	235.96	65.11	82.72	371.76
OB-001-19	53.47	12.72	128.99	28.92	8651.6	<1.02	441.77	91.56	30.94	116.45	196.48
OB-001-38	137.52	26.27	220.35	40.41	7847.23	1.2	485.66	98.13	82.34	290.93	227.2
OB-001-45	110.78	22.66	206.13	42.04	8681.3	2.29	349	71.06	33.83	129.3	171.38
OB-001-53	563.58	82.73	583.43	90.36	8023.15	7.67	834.03	182.51	53.08	292.22	484.82
OB-001-54	92.22	20.21	194.24	42.91	8418.68	2.43	463.9	105.36	51.27	196.57	212.05